Fatigue Analysis and Design of Aluminum Partial Joint Penetration (PJP) Welds

by

Ghazaal Ahmadi

A thesis

presented to the University of Waterloo

in fulfillment of the

thesis requirement for the degree of

Master of Applied Science

in

Civil Engineering

Waterloo, Ontario, Canada, 2026

© Ghazaal Ahmadi 2026

Author's Declaration

I hereby declare that I am the sole author of this thesis. This is a true copy of the thesis, including any required final revisions, as accepted by my examiners.

I understand that my thesis may be made electronically available to the public.

Abstract

This study explores the fatigue performance of 6000-series structural aluminum partial joint penetration (PJP) butt joints under cyclic loading. As aluminum alloys become increasingly prevalent in structural applications, understanding the fatigue behaviour of welded aluminum connections, particularly those with geometric discontinuities at the weld root, is essential. Such connections are frequently used in highway accessory structures and pedestrian and multi-use bridges, where significant fatigue damage can occur due to wind- and pedestrian-induced cyclic loading over the service life of the structure.

Combining experimental testing with advanced finite element (FE) analysis methods, in this research weld profiles are modelled, systematically varying key parameters such as the reinforcement height and penetration depth. Along with the notch stress approach for predicting fatigue life of weld details, fracture mechanics principles are employed to determine localized stress intensity factor (SIF) ranges and identify the effects of geometric variations on fatigue life. From this work, the fatigue performance is linked to the connection geometry, and simple relationships are established, which will allow designers to predict this performance using the simple stress-life methods with which they are most familiar.

In this work, two connection geometries are assessed: PJP butt joints and cruciform PJP or fillet-welded attachments. For the first geometry, the effects of weld reinforcement height and lack of penetration (LoP) are characterized. For the second geometry, the analysis results are compared with several formulas in the literature for predicting the fatigue performance of this connection geometry in steel and aluminum structures.

Acknowledgements

First and foremost, I would like to express my deepest and most sincere gratitude to my supervisor, Dr. Scott Walbridge. Your wisdom, kindness, patience, encouragement, and genuine enthusiasm throughout the past two years have been central to both my academic growth and the development of this thesis. Your guidance has shaped not only the technical direction of this research, but also the way I think as an engineer and researcher. You consistently provided thoughtful advice, constructive feedback, and steady support, while also giving me the confidence and independence to grow. I am especially grateful for your generosity with your time, your calm and encouraging approach, and your ability to make every challenge feel manageable. Working under your supervision has been one of the greatest privileges of my graduate studies, and I truly could not have asked for a better supervisor, mentor, and role model.

I am also grateful to the members of the Walbridge Research Group, particularly Thomas Ying, for being such a kind and supportive office mate, and Dr. Hamid Dahaghin. I truly enjoyed the time we spent working together, and I wish you all continued success.

My heartfelt thanks go to Saida Rezaee, my bestie in sun and snow, both on and off campus. I am also thankful to Nora Wie and Maha Forghani for making my journey at the University of Waterloo more enjoyable, welcoming, and friendly.

During my time at this university, I have had the privilege of learning from many excellent professors, some of whom directly or indirectly inspired me to pursue this degree, therefore, my heartfelt thanks to Dr. Nadine Ibrahim for being an amazing inspiration personally and professionally. I would also like to thank my instructors in the EFAS 400 program at Renison University College for their wonderful guidance and support. Special thanks to Kateryna Baranova for being such a wonderful friend during EFAS 400.

I am sincerely thankful to Jaimee Kropf and Dr. Adil Al Mayah for their guidance at the very beginning of my master's program and during its final stages. I am especially honoured to have had you as members of my defence committee. I would also like to thank Dr. Costa Kapsis for

his outstanding support during my time as a teaching assistant for the Building Science and Technology course, and for the honour of having him serve on my defence committee.

Thanks, are also due to the CSA Group, Dr. Liya Li and the Industry Advisory Panel, whose support allowed me to learn far beyond what I expected. I am grateful for the opportunity to benefit from their knowledge and experience, and especially for the financial support they provided for this research.

I would also like to thank the amazing members of the Women in Engineering Graduate Committee and Engineering Outreach. Serving as VP Fundraising and later as President over the past two years has been one of the most meaningful and enjoyable parts of my graduate experience. I am grateful for the friendships, teamwork, and memories we created together.

Finally, and most importantly, I am deeply grateful to my parents, Masouda Jami and Azizullah Ahmadi, and to my brothers, Ahmad, Belal, Ozair, and Shabir. Your unconditional love, endless sacrifices, prayers, encouragement, and belief in me have been the foundation of everything I have achieved. You have supported me through every challenge, celebrated every small success, and given me strength in moments when this journey felt difficult. My parents' resilience, kindness, and dedication have always been my greatest source of inspiration, and my brothers' constant love and support have reminded me that I am never alone. This thesis is not only the result of my own work, but also a reflection of the love, patience, and sacrifices of my family. I would be nothing without you, and I dedicate this achievement to you with all my heart.

Dedication

To the women and girls in Afghanistan who are banned from every primary human right and education,

and

to my family

Table of Contents

Author's Declaration ii

Abstract iii

Acknowledgements iv

Dedication vi

List of Figure x

List of Tables xii

List of Abbreviations xiii

Chapter 1 1

1.1 Introduction 1

1.2 Objectives 3

1.3 Scope 3

Chapter 2 5

2.1 Literature Review 5

2.2 Aluminum Use in Structures 5

2.3 Welding Aluminum 7

2.3.1 International Design Standards 9

2.3.2 Fatigue in Aluminum Structures 11

2.3.3 Defining Fatigue Loads 12

2.3.4 Design Approaches to Fatigue 13

2.4 Partial Joint Penetration Welds 15

2.5 PJP Welds in International Design 18

2.5.1 Fatigue in PJP Aluminum Welds 19
Chapter 3 : Industry Survey 23
3.1 Industry Survey 23
3.2 Highway Accessory Structures 23
3.3 Aluminum Pedestrian Bridges 29
Chapter 4 : Analysis Methods 32
4.1 Analysis Methods 32
4.2 Notch Stress Approach 32
4.3 Fracture mechanics 34
4.4 J-Integral method 37
4.5 Closed Form Solution 40
Chapter 5 : Analysis Results and Discussion 43
5.1 Validation for Weld Toe 43
5.2 Validation for Weld Root 49
5.3 Application 57
5.3.2 Verification of Fisher and Frank formula and CSA formula for butt joint 61
5.3.3 Cruciform Joint 74
5.4 Comparison with previous 81
Chapter 6 : Conclusions and Future Work 83
6.1 Conclusions for PJP Butt Joints 84
6.2 Conclusions for Cruciform Joints 85
6.3 Comparison Between PJP and Cruciform Welds 86

6.4 Practical Design Implications 86
6.5 Future Work 88
References 89
Appendix A 95
Appendix B 110

List of Figure

Figure 1.Examples of weld details in an active-mode bridge structure 1
Figure 2. Aluminum pedestrian bridge in use 5
Figure 3.Hall in Wellington project in Montreal with square HSS K-joints. 8
Figure 4.Partial joint penetration (PJP) groove-welded butt joint (left), load-carrying fillet-welded cruciform joint (right). 9
Figure 5.(a) Double-bevel PJP butt joint, (b) single-bevel groove weld, (c) T-type PJP weld, and (d) flare-bevel-groove (FBG) weld [10]. 9
Figure 6.Aluminum welded joint test data [1] (left) and specimen tested in [3] (right). 12
Figure 7.Fictitious notch rounding [20]. 14
Figure 8. Aluminum K Joint in Pedestrian Bridge 20
Figure 9.Aluminum PJP (left) and FBG (right) weld specimens tested in [9] and [10]. 22
Figure 10. Examples of weld details in highway accessory and active-mode bridge structures. 24
Figure 11.Fabrication of aluminum pedestrian bridge, WSP Conception des passerelles. 25
Figure 12.FE model geometry features for the notch stress approach. 33
Figure 13.LEFM example crack-loading model and key features. 35
Figure 14.Spider-web mesh. 39
Figure 15.Validated specimen geometry and simulation setup, tp=9.5mm 46
Figure 16.FE model for weld toe validation of LEFM application 47
Figure 17.LEFM predictions compared with fatigue test data 49
Figure 18.FE model and crack-tip mesh 51
Figure 19.Degree of penetration Vs SIF 53
Figure 20. PJP Butt joint using notch stress approach 55
Figure 21. SCF at root 55
Figure 22.S-N for tested samples with R = 0.1 vs. notch stress and LEFM results 56
Figure 23.SCF model of butt joints withs several Reinforcement 60

Figure 24. Fisher and Frank validating model 61
Figure 25. Comparison between J-integral vs Lack of penetration- PJP Butt Joint 62
Figure 26. NS vs tp for Butt joint with reinforcement 63
Figure 27.Butt Joint with Reinforcement, Notch stress approach 64
Figure 28. PJP Butt Joint with Reinforcement, J-integral Approach Simulation 65
Figure 29.LEFM calculation at Root for PJP Butt Joint 66
Figure 30.LEFM calculation at Toe for PJP Butt Joint 67
Figure 31.SR/SRt at Root and Toe_ PJP Butt Joint 68
Figure 32. (t_p = 10 mm) Two-dimensional comparison showing the influence of lack-of-penetration ratio on predicted fatigue capacity 70
Figure 33. (t_p = 15 mm) Two-dimensional comparison showing the influence of lack-of-penetration ratio on predicted fatigue capacity 71
Figure 34. (t_p =20 mm) Two-dimensional comparison showing the influence of lack-of-penetration ratio on predicted fatigue capacity 72
Figure 35. (t_p = 25 mm) Two-dimensional comparison showing the influence of lack-of-penetration ratio on predicted fatigue capacity 73
Figure 36. FE Model of Cruciform Joint 75
Figure 37. Cruciform Geometry with variable tp 76
Figure 38.Comparison Table_ governing Kt, governing location, root-to-toe ratio, absolute difference 79
Figure 39. Combined surface comparison between notch stress, (Eq.28), and Frank-Fisher predictions 80

List of Tables

Table 1.Formula description. 37
Table 2.Formula description. 40
Table 3.Recommended weld-toe validation discussion points. 45
Table 4. Parameters used in LEFM analysis. 48
Table 5.Weld root validation parameters. 52
Table 6.Study method. 57
Table 7.Table of Parameters for Notch Stress PJP Butt Joint with reinforcement 58
Table 8.Table of parameters for PJP Butt joint with reinforcement. 58
Table 9. Table of results of fatigue calculations. 67
Table 10. Cruciform joint Parameters. 74
Table 11.Parametric variables used fatigue assessment. 76

List of Abbreviations

AASHTO	= American Association of State and Highway Transportation Officials
CSA	= Canadian Standard Association
SIF	= Stress Intensity Factor
LoP	= Lack of Penetration
BS	= British Standard
FEA	= Finite Element Analysis
LEFM	= Linear Elastic Fracture Mechanics
HSS	= hollow structural section
PJP	= Partial Joint Penetration
ADM	= Aluminum Design Manual
LRFD	= Bridge Design Specifications
HAZ	= Heat Affected Zone

Chapter 1

1.1 Introduction

Aluminum is increasingly becoming a preferred material for highway and bridge structures due to its high strength-to-weight ratio and excellent corrosion resistance [1], [2]. In applications such as highway accessory structures and pedestrian bridges, aluminum can help produce lighter, more durable structures while also reducing transportation and installation costs. However, the long-term performance of aluminum structures can be dependent on the fatigue behaviour of the welds. Fatigue can be defined as the failure of a structural or mechanical component due to damage resulting from the repeated application of load cycles, each of which would not be sufficient to cause structural failure on its own. Given the significance of this potential failure mode under service conditions where cyclic loading is prevalent, this thesis provides a review and investigation of the fatigue behaviour of several aluminum welded connection details commonly used in highway accessory structures and pedestrian (multi-use or "active mode") bridges, such as the one shown in Figure 1.1



Figure 1.Examples of weld details in an active-mode bridge structure

When discussing fatigue, welded areas are of particular concern because the welding process alters the material properties within the heat-affected zone, while also introducing tensile residual stresses and small imperfections such as pores or inclusions [3].

Fatigue test databases have been developed to establish detail categories and design curves for standard welded connections in international design standards [e.g.,4, 5, 6, 7, 8]. However, since aluminum is a relatively newer structural material compared with steel, the available fatigue data for aluminum welded connections remain more limited. As a result, the fatigue design of more complex or non-standard details continues to present challenges, creating an important barrier to the broader use of aluminum and highlighting the need for further study.

The main motivation for this investigation is to address concerns raised in the development of recent editions of CSA S6, *Canadian Highway Bridge Design Code* [4], and CSA S7, *Pedestrian, Cycling, and Multiuse Bridge Design Guideline* [5], regarding the fatigue performance of aluminum welds. For aluminum highway accessory structures, fatigue data are lacking for several commonly used details. This has led to the use of an ad hoc method in which the fatigue strength of an equivalent steel detail is adjusted for aluminum design by a simple factor applied to the fatigue strength. However, where comparable data exist for both materials, the required adjustment factor varies considerably, suggesting this approach may produce results that are either overly conservative or potentially unconservative.

A related issue also arises in the fatigue verification of active-mode bridges, where more economical connection details classified as "statically loaded" may be used only if their fatigue resistance can be shown to exceed a specified limit. For many of these details, however, the necessary databases of fatigue test results are not available, making it difficult for designers to verify whether they are suitable. As a result, engineers are often forced to use more conservative and considerably more expensive connections in their designs.

Consultations with industry practitioners also reveal that uncertainty surrounding weld reliability and fatigue performance remains a major factor limiting the use of partial joint penetration (PJP) welds in aluminum construction. A review of international design standards

further shows that several jurisdictions place fewer restrictions on PJP welds and provide more explicit design guidance for their use. As a result, Canadian engineers may face a competitive disadvantage in international markets when designing aluminum structures.

In response to these concerns, a research project was launched to assess the structural and fatigue performance of aluminum PJP welds, in order to support the development of improved design guidance for cyclically loaded aluminum structures.

1.2 Objectives

The objectives of the research presented in this thesis are as follows:

- To collect, synthesize, and critically review existing experimental and field-based data on the fatigue performance of aluminum welded connections, and to use this information, together with insights from an industry survey, to validate and calibrate two fatigue prediction models employed subsequently in this research.
- To apply the validated modelling approaches to partial joint penetration (PJP) aluminum welded details commonly used in highway accessory structures and active-mode bridge systems, with these details identified and prioritized through consultation with industry experts and survey responses.
- To use the results of this study to compare these details with existing fatigue detail categories, or where appropriate, to propose alternative evaluation methods for aluminum welded components in highway accessory supports and active-mode bridges that are not currently classified in existing design standards.

1.3 Scope

This thesis investigates the fatigue performance of aluminum welded connections, including partial joint penetration (PJP) welds, through a review of existing literature and the use of validated numerical modelling methods. The investigation focuses on typical welded details used in highway accessory structures and active-mode bridges, with the aim of developing or refining fatigue detail categories for these applications. The scope of the work is limited to

linear-elastic numerical modelling, fracture mechanics analysis, available experimental data, and representative weld geometries.

Chapter 2

2.1 Literature Review

A comprehensive review of existing research was carried out to assess the current state of knowledge on the use of PJP welds in aluminum structural systems.

2.2 Aluminum Use in Structures

Aluminum is the third most abundant element in the Earth's crust and the most abundant metal. Despite this, metallic aluminum was not successfully extracted until 1827. It was only after the development of the Hall-Héroult electrolytic process nearly sixty years later that aluminum could be produced economically on a large scale [9].

Since then, aluminum has become an essential material in modern engineering. Its use is especially prominent in the transportation sector, including automotive, rail, aerospace, and marine applications, as well as in architecture, where it is widely used in high-performance façade systems and structural components.



Figure 2. Aluminum pedestrian bridge in use

In structural engineering, aluminum is often preferred when reducing self-weight is a key design objective. Because its density is about one-third that of steel, it is particularly well suited for applications such as curtain walls and large-scale façade systems. Its natural corrosion resistance also makes it attractive for use in marine or chemically aggressive environments. Although the initial cost of aluminum is typically about three times higher than that of steel per unit mass, the weight savings that come from the use of aluminum mean the material cost of an aluminum structure is typically twice that of a comparable steel structure, and life cycle analyses present an even more balanced economic picture. Specifically, recent studies show that aluminum generally requires much less maintenance over its service life, which can often compensate for the higher upfront cost.

Pedestrian (also known as “active mode”) bridges are a good example of this shift toward long-term value (see figure 2). By lowering both the dead load of the structure and the ongoing costs associated with protective treatments such as painting or galvanizing, aluminum has become an increasingly competitive alternative to steel. Research suggests that, over a 50-year service life, aluminum pedestrian bridges can be more economical when total life-cycle or “running” costs are taken into account [10].

Although pure aluminum has several attractive properties, including low density and natural corrosion resistance, it does not provide enough mechanical strength for most structural applications. To overcome this limitation, aluminum is commonly alloyed with elements such as magnesium, manganese, zinc, copper, or silicon. These alloying elements significantly improve strength while also influencing important characteristics such as ductility, corrosion performance, and weldability. As a result, aluminum alloys are organized into a well-established series classification system developed to suit a wide range of engineering applications. The mechanical performance of aluminum alloys depends largely on the mechanisms used to strengthen them. Many structural alloys derive their strength from precipitation hardening, and in some heat-treated tempers, their strength can be more than twice that of the annealed condition. Other alloys rely mainly on work hardening, or strain hardening, to achieve similar levels of performance [11].

A key issue, however, is that both types (i.e., precipitation strengthened and work hardened alloys) are highly sensitive to elevated temperatures. This is especially important in welded construction, where the localized heat generated during welding can weaken the alloy temper. As a result, a heat-affected zone (HAZ) forms around the weld, often with reduced strength and modified fatigue performance. Understanding these metallurgical changes is essential when assessing and designing durable welded aluminum connections [11].

2.3 Welding Aluminum

Most aluminum alloys can be welded without major difficulty (see Figure 2), except for certain ultra-high-strength grades. Even so, welded aluminum structures face an important metallurgical challenge. Structural aluminum alloys usually obtain their strength either through heat treatment or through work hardening, and the high heat input from welding can partially undo these strengthening effects within the HAZ. As a result, the base metal in this region may lose up to 50% of its strength, making the welded joint the weakest part of the structure. This is quite different from structural steel, where conventional welding procedures generally do not reduce the strength of the surrounding base material, and welded joints are often designed to be stronger than the connected members [11].

This loss of strength is mainly caused by the steep thermal gradients created during welding. As noted by Malin, these temperature variations can cause alloying elements to either precipitate too early or dissolve back into the matrix, depending on their distance from the fusion line [12]. The result is a localized softened zone that largely governs load-carrying capacity.

To reduce these effects, solid-state joining methods such as friction stir welding (FSW) have been developed. Because FSW operates at much lower temperatures than conventional fusion welding, it causes less degradation in the HAZ and preserves more of the parent metal's original strength. This process has become increasingly important in high-performance industries such as aerospace, shipbuilding, and automotive manufacturing. In structural

engineering, however, its use is still relatively limited and is mostly confined to specialized applications such as bridge decks [45].



[source: B. Cusson]

Figure 3.Hall in Wellington project in Montreal with square HSS K-joints.

In addition to softening, welding also introduces significant tensile residual stresses due to the different cooling rates of the molten weld metal and the surrounding parent material. These internal stresses play a major role in reducing fatigue resistance [13,14].

From a practical standpoint, partial joint penetration (PJP) and fillet welds (are often preferred over complete joint penetration (CJP) welds because they require less fabrication time and avoid the need for more complex edge preparation (see Figures 2.2 and 2.3).

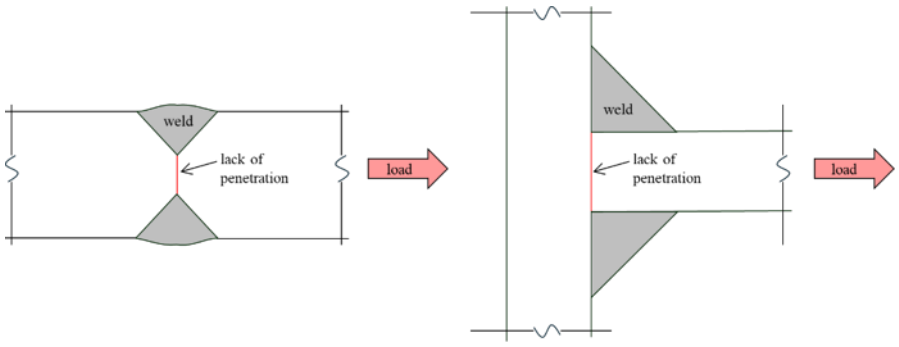

Figure 4.Partial joint penetration (PJP) groove-welded butt joint (left), load-carrying fillet-welded cruciform joint (right).

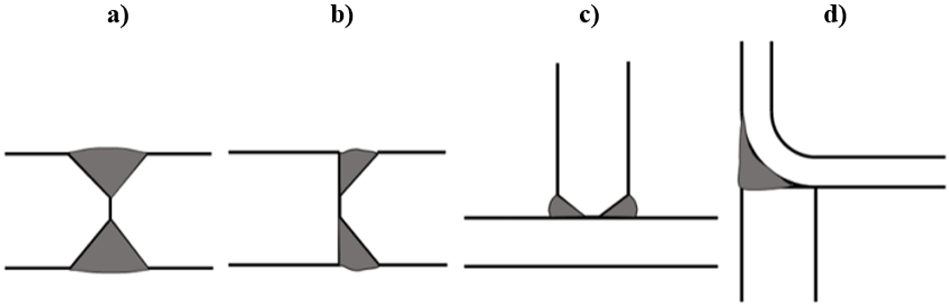

Figure 5.(a) Double-bevel PJP butt joint, (b) single-bevel groove weld, (c) T-type PJP weld, and (d) flare-bevel-groove (FBG) weld [10].

However, PJP welds contain an inherent unfused region at the weld root. This incomplete penetration acts as a severe internal stress concentration, or effectively as a pre-existing crack, which can significantly accelerate fatigue crack initiation. Similarly, although flare-bevel-groove (FBG) connections in HSS members may offer economic advantages, the higher fatigue sensitivity (due to the lack of complete weld penetration) means that they must be designed more conservatively, especially in structures subjected to cyclic loading.

2.3.1 International Design Standards

In the United States, the Aluminum Design Manual (ADM) [15] mainly governs the design of aluminum structures, while bridge design is covered by the AASHTO LRFD Bridge Design

Specifications [16]. In Europe, aluminum structures are designed in accordance with Eurocode 9 [7]. Because aluminum was historically used less often than steel in structural applications, many of the early design provisions were adapted from steel-based rules. However, aluminum behaves differently in several important ways. Its lower modulus of elasticity makes it more prone to local buckling, and its design standards must also account for HAZ softening, a form of metallurgical degradation that is not usually a concern in structural steel. These differences require a more specialized approach to the design of aluminum members and connections, particularly when welding is involved.

Current fatigue design provisions, including those in Eurocode 9 and the recommendations of the International Institute of Welding (IIW) [17], are based mainly on the nominal stress approach, often referred to as the detail category method. This is the simplest method available in practice and defines fatigue resistance using S-N curves that relate stress range to fatigue life for a specified probability of survival, typically 95% or 97.7%. In North America, fatigue categories are usually designated by letters such as Category A, B, or C, whereas European standards identify them by a numerical value corresponding to the fatigue strength, in MPa, at two million cycles. Although this approach is practical and widely used, it is based on far-field nominal stresses and does not explicitly capture local stress concentrations. As a result, it often leads to conservative designs because of the nature of how different connection geometries are placed within the same fatigue classification.

One important application of these provisions is in flare-bevel-groove (FBG) connections for hollow structural sections (HSS), which are commonly used in truss systems and pedestrian bridges. To reduce fabrication costs, these T-joints are often welded without bevelling the edges beforehand, which results in partial joint penetration. While this is an economical and widely used solution, the incomplete penetration leaves an internal root notch that acts as a significant stress concentrator and can reduce fatigue performance. Since the nominal stress method groups details according to similar stress concentration effects, the greater fatigue sensitivity of PJP welds must be carefully considered in their classification to ensure adequate safety over the structure’s service life.

2.3.2 Fatigue in Aluminum Structures

The basis for fatigue design in aluminum structures can be traced back to the guidance developed by the International Institute of Welding, which introduced the use of two-slope *S-N* design curves organized by fatigue classes (FAT) [18]. Each fatigue class corresponds to the characteristic fatigue strength at 2×10^6 cycles. Early aluminum fatigue provisions were often conservative extensions of steel design rules, modified mainly to reflect the difference in elastic modulus [1]. This approach was frequently criticized for being overly simplified and for relying too heavily on small-scale specimen tests (see Figure 2.4), which do not represent the residual stresses present in full-scale structural members.

The move toward modern fatigue standards was largely driven by the work of the European Convention for Constructional Steelwork (ECCS) and the later development of the Eurocodes. These efforts brought together extensive databases from large-scale fatigue tests, providing the experimental basis needed to improve British, North American (The Aluminum Association), and Canadian (CSA) design standards. The IIW also adopts a more conservative position on fatigue damage accumulation, recommending a critical damage index of 0.5 instead of the conventional value of 1.0, and it provides specific guidance on the constant amplitude fatigue limit (CAFL). Although both the ADM and CSA S157 indicate that stresses below the CAFL may be treated as providing infinite life, the IIW notes that this assumption may not hold for aluminum under very high cycle fatigue conditions.

In this research, the term *fatigue* refers typically to high-cycle fatigue, where failure occurs after millions of load cycles while stresses remain within the elastic range. Unlike steel, which often exhibits a distinct fatigue limit below which cracks do not continue to grow, aluminum alloys generally do not have a true fatigue threshold in tests of defect free samples. That said, in structural applications, the crack initiation stage is usually not significant because fabrication processes, especially welding, already introduce small flaws and discontinuities that effectively behave as pre-existing cracks. For that reason, fatigue design in aluminum is concerned primarily with crack propagation rather than crack initiation.

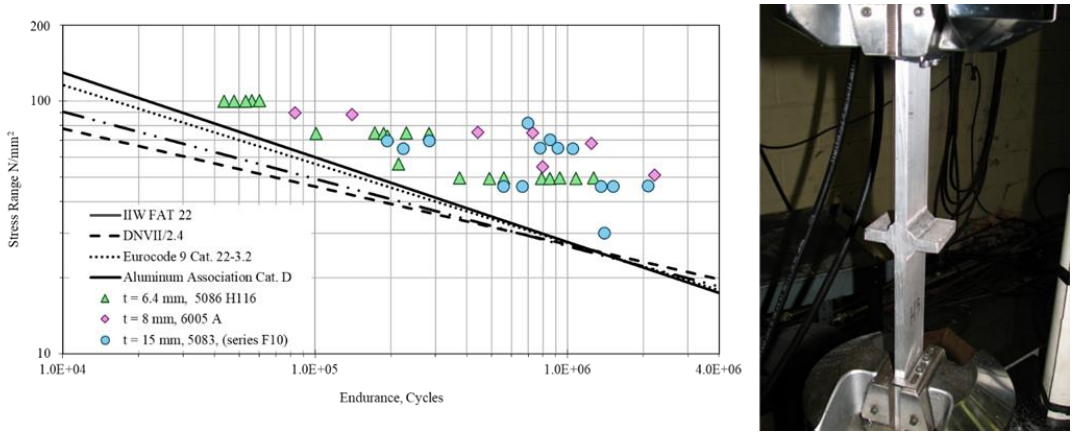

Figure 6.Aluminum welded joint test data [1] (left) and specimen tested in [3] (right).

Because high-cycle fatigue develops with little or no visible deformation, failure can occur suddenly, making it a critical concern in structures such as crane rails, wind-sensitive towers, and pedestrian bridges, all of which may be subjected to millions of load cycles during their service life. In Canada, the design of these structures is governed by CSA S157 [5], and CSA S6 the *Canadian Highway Bridge Design Code* [4]. Understanding how microscopic imperfections develop into fatigue cracks and eventually lead to sudden failure is essential for the safe and effective use of aluminum in modern infrastructure.

2.3.3 Defining Fatigue Loads

Fatigue analysis, like any form of design verification, begins with defining the applied loads. In practice, structures are subjected to cyclic stresses that vary randomly over time. However, for the sake of simplicity, both design methods and experimental studies commonly rely on constant-amplitude (CA) loading. In some cases, variable-amplitude (VA) loading is used to better represent real service conditions, such as traffic loads on bridges or vibrations in machinery. Throughout this study, however, constant-amplitude loading is adopted because it provides a simpler and more broadly applicable basis for evaluating aluminum structures. CA loading is described by the stress range $\Delta\sigma$ in Equation 2.1:

$$\Delta\sigma = \sigma_{max} - \sigma_{min} \tag{2.1}$$

and the stress ratio:

$$R = \frac{\sigma_{min}}{\sigma_{max}} \tag{2.2}$$

Both stresses are taken as positive in tension and are calculated using the relevant section area, such as the weld throat or plate cross section. Under CA loading, $\Delta\sigma$and R in Equation 2.2 remain constant. The stress ratio ranges from 1 to $-\infty$, where $R = 0$ represents full unloading and $R = -1$ represents full stress reversal. In Equation 2.3 and 2.4 relatively the fatigue loading may also be expressed using mean stress and stress amplitude, i.e.:

$$\sigma_m = \frac{\sigma_{max} + \sigma_{min}}{2}, \sigma_a = \frac{\sigma_{max} - \sigma_{min}}{2} \tag{2.3}$$

These relate to $\Delta\sigma$and R through:

$$\sigma_m = \frac{\Delta\sigma}{2}\frac{1+R}{1-R}, \sigma_a = \frac{\Delta\sigma}{2} \tag{2.4}$$

Only the mean stress depends on R. In welded connections, however, welding residual stresses often near yield can dominate the mean stress when considered. As a result, the influence of externally applied mean stress is usually negligible, and fatigue design typically depends only on the stress range $\Delta\sigma$. This simplification may not apply to unwelded components or welds with post-weld treatment where mean stress can affect fatigue life.

2.3.4 Design Approaches to Fatigue

Fatigue failure in welded joints is primarily driven by the growth of cracks that initiate at stress concentrations near plate surface, most commonly at the weld toe or root. These cracks are often assumed to have a semi-elliptical shape, which is important for accurately determining the stress intensity factors (SIFs) needed to predict crack growth rates. Paris and Sih established fundamental relationships between crack growth rates and SIFs for different crack geometries, forming the basis of modern fracture mechanics [19]. However, their work did not fully capture the specific conditions present in welded joints, particularly for shallow cracks, which limits its direct applicability to real welded details.

Fricke later provided a comprehensive overview of fatigue design methods for cracks initiating at weld roots [20]. His work, adopted by the International Institute of Welding (IIW), describes the basis of the effective notch stress approach. This method focuses on the maximum elastic stress at the weld toe or root, where fatigue cracks typically originate. This stress is obtained by finite element (FE) analysis. To avoid unrealistically high stresses caused by sharp geometric discontinuities, the method introduces a fictitious reference radius at the notch. For standard steel and aluminum welds, a radius of 1 mm is commonly used as a representation of the material's microstructural support.

For thin plates (less than 5 mm), however, using a 1 mm radius can artificially reduce the effective cross-section and distort the results. In these cases, a smaller reference radius of 0.05 mm is recommended [20]. (See Figure 2.5 for reference notch example.)

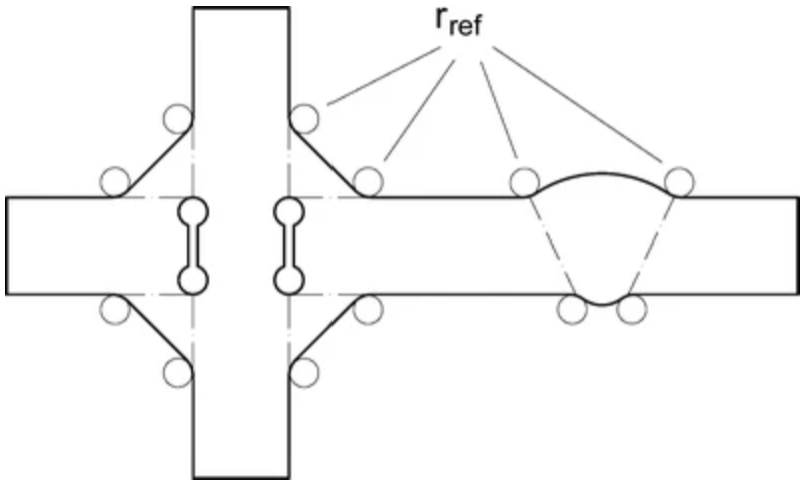

Figure 7.Fictitious notch rounding [20].

Accurate representation of weld geometry is essential when analyzing fatigue cracks that initiate at the weld root. Fricke's guideline distinguishes between idealized weld profiles and measured geometries [20]. In numerical models, weld roots are typically represented using either keyhole-shaped or U-shaped notches. Keyhole-shaped notches generally produce higher stress predictions, especially when the applied load is parallel to the unfused root faces, which

can lead to overly conservative fatigue life estimates. U-shaped notches predict lower stresses but may underestimate the stress within the weld throat.

Fricke also emphasizes that real geometric imperfections, such as undercuts or misalignment, should either be included directly in the model or accounted for through appropriate corrections, since they can substantially increase local stresses. The reliability of the analysis also depends strongly on mesh quality. A very fine mesh is needed near the notch to capture the steep stress gradients accurately. Fricke recommends using at least three quadratic elements along the 1 mm reference radius, with proportionally smaller elements when a 0.05 mm radius is used. Poor mesh quality or abrupt transitions in element size can introduce errors. For large or complex structures, local refinement strategies such as sub-modelling or the use of "super-elements" may be applied, provided stiffness compatibility is maintained between the global and local models. Although three-dimensional analysis is preferred, two-dimensional modelling is acceptable in many situations.

The elastic notch stress obtained from FE analysis is used to predict fatigue life in conjunction with the design S-N curves recommended by Fricke, which depend on both the reference radius and the material. For aluminum welds analyzed with a 1 mm notch radius, the recommended fatigue class is FAT 71. For thin aluminum sheets assessed using a 0.05 mm radius, the recommended fatigue class is FAT 180. These curves are based on the maximum principal stress at the notch. If von Mises stress is used instead, a lower fatigue class should be adopted. The method assumes linear elastic material behaviour and should always be checked against other fatigue assessment approaches.

2.4 Partial Joint Penetration Welds

PJP welds are generally defined in engineering specifications as welds in which the deposited weld metal intentionally penetrates only part of the member thickness. Although they are widely used in steel construction, particularly in applications such as column splices and T-joints where full tensile capacity is not always required, their use in aluminum structures remains relatively limited and has not been studied as extensively.

In tubular truss applications, one common form of PJP weld is the flare-bevel groove (FBG) weld, which is created by placing filler metal within the corner radius of a hollow structural section (HSS). The present study focuses primarily on PJP groove butt welds, which are usually classified as either single-bevel or double-bevel configurations. In practice, double-bevel welds are often preferred in industrial applications because they require less total filler metal to achieve the same effective throat thickness.

By simple trigonometric relations, the weld volume for a single-bevel weld in Equation 2.5, and for a double-bevel weld in Equation 2.6, are:

$$V_w = \frac{1}{2} t_e^2 \cdot \tan(\gamma) L \tag{2.5}$$

$$V_w = \frac{t_e^2}{\tan\gamma} \cdot \left(\frac{L}{2}\right) \tag{2.6}$$

For a groove angle of $\gamma = 60°$, the single-bevel configuration requires approximately 50% more filler metal than the double-bevel configuration.

Most literature on PJP butt welds defines weld penetration using a degree of penetration (DoP) parameter equation 2.7, which is also adopted in this research:

$$\rho = \frac{A_w}{A_g} = \frac{t_e}{t_p} \tag{2.7}$$

Here, ρ denotes the degree of penetration, while A_w and A_g are the weld net-section area and gross plate area, respectively. t_e is the effective throat thickness, and t_p is the plate thickness. Early studies on the strength of PJP welds, most of which were carried out on steel connections, showed that these joints, when designed properly, can develop a net-section strength greater than the nominal ultimate strength of the base metal.

Research by Popov and Stephen (1977) [21], followed by later work from Gagnon and Kennedy (1989) [18], explained this behaviour in terms of lateral restraint. As the penetration ratio (a/t) decreases, the surrounding unloaded material restricts the weld region from contracting laterally due to Poisson's effect. This constrains deformation in the thickness and

width directions, creating a biaxial plane strain condition ($\varepsilon_y = \varepsilon_z = 0$). Under the von Mises failure criterion, the effective ultimate stress in biaxial plane strain becomes:

$$\sigma_{u,eff} = \frac{1-\nu}{1-2\nu}\sigma_u \tag{2.8}$$

where ν is Poisson's ratio (typically 0.30 for steel and 0.33 for aluminum). With $\nu = 0.35$, the predicted net ultimate stress exceeds twice the base-metal ultimate strength. In practice, however, studies have shown a smaller increase, typically on the order of 55%, because ideal plane-strain conditions are difficult to achieve in real structural geometries.

Another study was carried out by Gagnon and Kennedy [54], who tested 75 single-bevel PJP groove welds in structural steel. They established a lower-bound tensile strength as:

$$T_r = A_w\sigma_u \tag{2.9}$$

Based on their experimental data, Gagnon and Kennedy [18] proposed a polynomial expression to more accurately estimate the ultimate strength of a PJP weld as a function of DoP:

$$T_r = (1.55 - 1.16\rho + 0.61\rho^2)A_w\sigma_u \tag{2.10}$$

The exact failure plane in a PJP weld is still debated. Classical failure criteria, such as the von Mises and maximum principal stress theories, predict specific fracture angles under idealized conditions. Experimental observations, however, show that PJP welds often do not fail along these theoretical paths. Instead, failure usually occurs along the fusion face, which is the interface between the weld metal and the base material. Recent work by Reynolds [22] supports this view, showing that the angle of the fusion face is the main factor controlling the failure location. In aluminum structures, this suggests that connection strength is governed primarily by the strength of the HAZ at the fusion interface, which is generally not as strong as the base metal, rather than by the exact groove shape or whether the weld is made with a single- or double-bevel configuration.

2.5 PJP Welds in International Design

The treatment of partial joint penetration (PJP) welds differs considerably among major aluminum design standards. For that reason, this section includes a detailed review of the relevant Canadian, American, and European codes.

The design provisions for PJP welds in aluminum structures show clear differences across these three regulatory frameworks. In Canada, CSA S157 generally discourages the use of PJP welds in joints that are required to resist calculated forces. The standard does not provide specific equations for determining the strength of PJP welds and instead refers to CSA W59.2 [23] for geometric definitions. In most cases, the effective throat must be confirmed through procedure qualification testing. An exception is made for GMAW (MIG) and GTAW (TIG) welds, where the effective throat may be taken as the depth of groove preparation, provided the groove opening angle is at least 60°.

The Canadian Highway Bridge Design Code, CSA S6 [4], takes an even more restrictive approach by explicitly prohibiting the use of PJP welds in any connection subjected to calculated internal forces. This choice is largely driven by the fact that structural elements in highway bridges are much more likely to see significant cyclic loading.

CSA S157 assigns a resistance factor, ϕ, of 0.75 for strength design of groove welds. This value is based largely on the behaviour of complete joint penetration (CJP) welds, where failure usually occurs in the heat-affected zone (HAZ). For PJP welds, however, the reduced net section can shift the governing failure mode to the weld metal itself. Some research therefore suggests that a lower resistance factor of 0.67 would be more appropriate, matching the value used for fillet welds and steel PJP welds in CSA S6 [4].

The American approach, set out in the *Aluminum Design Manual* (ADM) [15], is more direct and generally more permissive in its treatment of PJP welds. Unlike the Canadian requirement for a 60° groove angle, the ADM permits a minimum groove angle of 45° when defining the effective throat. To account for the notching effect created by the unfused root of a PJP weld, the ADM reduces the calculated strength by 40%, using a factor of $0.6\sigma_{wu}$. The ADM applies

this reduction to the lesser of the weld filler strength and the strength of the heat-affected zone. In the AASHTO LRFD bridge specifications [16] the reduction is only applied to the weld metal. This reflects the fact that the weld root, where the stress concentrations are most severe, is made entirely of filler metal [11,16].

European provisions in Eurocode 9 [7] also include explicit equations for strength design of PJP welds, but they note that such welds should generally be limited to secondary or non-load-bearing components. Although the overall mathematical approach is similar to the Canadian net-section check, Eurocode 9 uses different material strength values and partial safety factors. For example, it assumes a considerably lower ultimate strength for 5356 filler metal, around 190 MPa, compared with the 240 MPa commonly used in the North American standards. These differences suggest that there is still not full agreement on the reliability and mechanical behaviour of PJP welds in aluminum, especially with respect to the combined effects of reduced cross-section and the brittle behaviour often associated with the weld root.

2.5.1 Fatigue in PJP Aluminum Welds

Research on the fatigue performance of aluminum PJP welds is still relatively limited, and current understanding is based mainly on two major experimental research programs. The first important study was carried out at the University of Illinois at Urbana-Champaign, where approximately 100 specimens with penetration ratios (ρ) ranging from 45% to 98% were tested [9, 24]. The program used 5083-H116 aluminum plate with 5183 filler metal in plate thicknesses of 9.5 mm and 25 mm in order to examine possible scale effects. To separate the influence of weld surface geometry, half of the specimens were tested with the weld reinforcement left in place, while the other half were machined flush. The tests were conducted at nominal gross-section stress ranges of 82.7 MPa and 131 MPa, with a constant stress ratio of $R = 0$. This study was intentionally designed to mirror earlier investigations of steel PJP welds, allowing for direct comparison between the two materials.

Burk and Lawrence [24] data demonstrated that a single nominal S-N curve is inadequate unless the internal defect size is explicitly considered. Their work supports fracture mechanics

or defect-size-based fatigue assessment, because fatigue life was controlled by the through-thickness lack-of-penetration dimension rather than by nominal stress range alone.



Figure 8. Aluminum K Joint in Pedestrian Bridge

Menzemer [25] conducted full-scale and component fatigue tests, which demonstrated that the lower-bound fatigue resistance of welded aluminum details is governed by the actual welded detail geometry and scatter in crack initiation sites. Rather than proposing a single universal S-N curve, the study used regression and lower confidence limits to evaluate existing design categories, recommending detail-specific adjustment where the test-based lower-bound resistance fell below current design assumptions.

A second major body of data came from German research programs conducted in the late 1990s and early 2000s [26, 27]. These studies also used 5083 base metal and 5183 filler metal, with plate thicknesses of 5 mm and 25 mm and DoP ratios of $\rho = 69\%$ and $\rho = 78\%$. Unlike the Illinois program, all the German specimens were tested with the weld reinforcement retained, since fatigue cracks were consistently observed to propagate through that region. In many cases, the specimens were annealed to relieve residual stresses, which does not reflect the condition of typical as-welded structures. In addition, alloy 5083 is more commonly used in rolled plate for marine applications than the 6000-series alloys that are more typical of the extruded shapes used in building and bridge construction.

Collectively, these research programs show that aluminum PJP welds behave in many ways similarly to steel PJP welds, particularly in the strong influence of weld root conditions and penetration depth on fatigue life. Although the existence of a distinct crack initiation phase is still debated [25, 28], there is broad agreement that fatigue performance is governed mainly by insufficient penetration rather than by the relatively high porosity that can accompany PJP welds. Both programs also found that base metal thickness has little effect on fatigue behaviour, which further supports the conclusion that local weld root geometry is the controlling factor in structural performance.

As shown in Figure 2.6, Gérin's experimental work on aluminum partial joint penetration (PJP) butt welds, where two collinear plates were joined using double-V groove PJP welds and tested under fatigue loading. The macrograph on the left shows the internal lack-of-penetration region at the weld root, which acts as a sharp crack-like defect and controls fatigue behaviour. The specimen photo on the right shows a full fatigue test sample mounted in the loading frame. This work showed that fatigue cracks in these PJP butt welds consistently initiated at the weld root rather than the weld toe, because the incomplete penetration creates a severe internal notch. His program used different plate thicknesses and groove depths, and the fatigue results were interpreted using net-section stress range and LEFM-based crack growth analysis. This makes Gérin's data especially useful for validating root-controlled fatigue models for aluminum PJP butt joints.

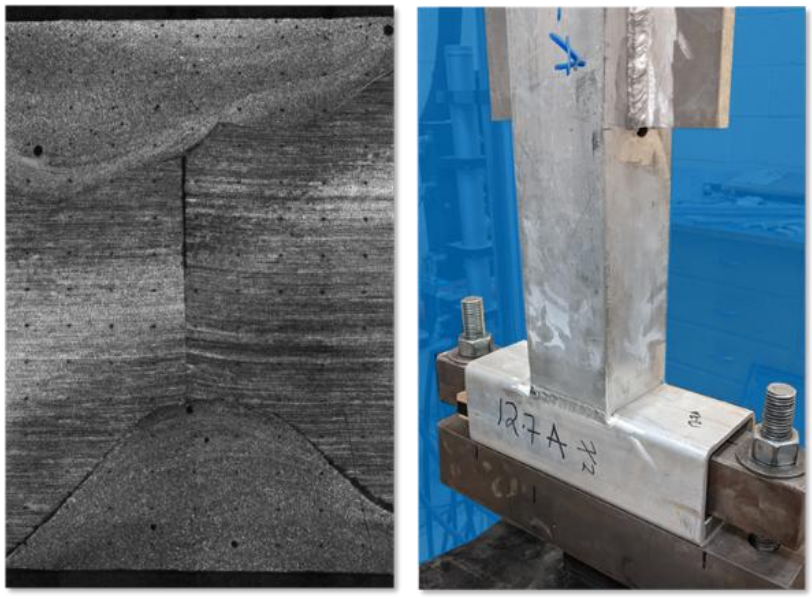

Figure 9.Aluminum PJP (left) and FBG (right) weld specimens tested in [9] and [10].

Despite these advances, important gaps remain in current design guidance. North American standards, including CSA S6 and the *Aluminum Design Manual* (ADM) [15], do not provide specific S-N curves or explicit fatigue design provisions for PJP welds. By contrast, Eurocode 9 and the International Institute of Welding (IIW) [17] do include dedicated design S-N curves, although the IIW notes that fracture mechanics-based approaches may provide greater accuracy for partial penetration joints. Notably, both international standards assign a single fatigue category to aluminum PJP welds regardless of alloy series, reflecting the general view that fatigue performance does not vary greatly between aluminum alloys.

Overall, the available evidence points to the need for further experimental research and for more developed design provisions that reflect the growing use of aluminum in structural applications. A clear understanding of the fatigue behaviour of aluminum welds is essential for designing structures that are both safe and durable.

Chapter 3: Industry Survey

3.1 Industry Survey

This research was conducted by consultations with industry professionals from a range of sectors, including provincial highway authorities, municipalities, consulting firms, and fabrication seven people. They were asked about the welded aluminum connections commonly used in practice, as well as the fabrication and quality control challenges they encounter. The discussions also explored their past experience with fatigue-related design issues and observed failures. In some cases, participants shared photographs and design drawings, which helped provide valuable insight into how aluminum is applied in real-world structures.

3.2 Highway Accessory Structures

Highway accessory structures, such as overhead sign supports and traffic signal arms, play an essential role in maintaining road safety and efficient traffic operations. In Canada, the design and fabrication of aluminum highway accessory structures have been concentrated largely in Quebec, where aluminum is often preferred because of its low weight, corrosion resistance, and proximity to producers. Several examples of aluminum highway accessory structures in Quebec are presented in Figure 3.1.

Laboratory studies on aluminum light poles with shoe base socket connections (see Figure 3.1a) have shown that current design provisions may need to be revised to improve fatigue life predictions [29], [30], [31]. Although the Aluminum Design Manual [6] provides standardized S-N curves for a range of detail categories, these classifications may be too conservative for certain applications. In particular, classifying shoe base socket connections as Category E details may not fully represent their actual fatigue performance, as noted by Azzam and Menzemer [30]. It is also important to recognize that the geometry of shoe base socket connections can vary considerably between manufacturers. Because of this variability, it may be unrealistic to treat all such connections as a single detail category within a nomina1 stress-based design framework. In these cases, fatigue assessment may be more appropriately carried out through experimental testing or by using a suitable local stress-based approach.



Figure 10. Examples of weld details in highway accessory and active-mode bridge structures.

Beyond the research on shoe base socket connections, several published studies have examined the fatigue behaviour of circular HSS connections commonly used in the truss assemblies of highway accessory structures [21], [32]. Owing to the complexity of these connection geometries, fatigue assessment for such structures generally relies on local stress-based methods, such as the hot-spot stress approach.

a. 

b. 

c. 

Figure 11.Fabrication of aluminum pedestrian bridge, WSP Conception des passerelles.

Although relatively few studies have investigated the in-service fatigue performance of highway accessory structures, long-term monitoring efforts have provided useful insight. For

example, monitoring conducted on the Bronx-Whitestone Bridge showed that traffic-induced vibrations can have a significant effect on the fatigue behaviour of light poles [33].

Two of the participants in the industry survey conducted for this report had specialized knowledge of highway accessory structures. Discussions with these experts led to several important observations, which are summarized as follows:

- One of the main factors influencing material selection, particularly the use of aluminum, is the widespread use of de-icing salts in colder Canadian climates. These salts can accelerate corrosion in steel structures, making aluminum an attractive alternative.
- The standard drawings and connection details published by the *Ministère des Transports et de la Mobilité Durable* [34] were identified as the primary reference for the design of highway accessory structures in Quebec. According to the participants, these details are generally adopted with little or no modification.
- The British Columbia Ministry of Infrastructure and Transportation Bridge Standards and Procedures Manual [35] is another useful resource, which emphasizes the importance of accounting for fatigue in the design of overhead sign structures, particularly due to their exposure to dynamic loading from natural wind and traffic-induced gusts. The manual also specifies that vertical deflections caused by galloping and truck-induced wind gusts should be limited to 200 mm for overhead supports.
- Fillet welds were noted as a common feature in the standard details provided in [34]. They are typically used around the ends of tubular sections, while smaller plates attached to the structure are also connected using fillet welds on both sides. These welding practices are considered representative of typical aluminum traffic signal assemblies.
- One standard aluminum connection used in Quebec overhead structures consists of a tube passing through a plate and being connected solely by fillet welds. This detail is well established and, according to the participants, has not caused significant issues in practice. Its use appears to be specific to overhead sign structures in Quebec and is not commonly reported in other provinces or among other manufacturers.

- Cast aluminum footings are also widely used to connect vertical posts to foundations through a welded shoe base socket connection. This detail is commonly found in overhead sign bridge structures, light posts, traffic signal posts, and lateral sign structures. The fabrication process for these members is somewhat specialized. Posts are first produced using 6063-T4 aluminum, and after the cast footing is welded in place, the assembly is heat treated to achieve the 6063-T6 temper. This process increases strength and allows up to 85% of the yield strength to be used in design, although its influence on fatigue performance remains uncertain. While this approach is practical for smaller components, it may not be feasible for larger structures, such as overhead sign supports, because of the size limitations of heat-treatment equipment.
- Another connection type used in Quebec involves welding a tube to a cast aluminum root element and reinforcing the joint with stiffeners on both sides. This detail is used mainly in traffic signal structures and light structures with lattice arms. Its performance has generally been satisfactory, although the favourable behaviour may be due in part to the arm geometry rather than the connection detail alone. Some concerns have nevertheless been raised regarding weld quality. In particular, cases were noted in which manufacturers did not carry out the required post-weld heat treatment, resulting in material inconsistencies and failures near the base of the structure.
- Since the 2019 edition of CSA S6, fatigue design has formally become a requirement for highway accessory structures. However, the participants noted that the 2019 edition did not fully address fatigue loading for all highway accessory structure types. As a result, fatigue design is still not mandatory in Quebec for certain structures that remain outside the scope of the current provisions.
- In Quebec, traffic signal posts are commonly designed with lattice arms rather than single-principal-arm configurations. To date, significant fatigue-related problems have not been observed in these lattice structures. This may be due to the inherent redundancy of lattice systems, along with the use of Stockbridge dampers to reduce vibration and fatigue stresses.

- The participants also noted that older aluminum structures sometimes exhibit weld-related failures that only become apparent during dismantling. Visual inspections often reveal substantial deterioration, especially in structures that are more than 30 years old and were originally designed for lower loading demands. In many cases, the early stages of cracking are never documented because inspection typically occurs only after visible damage has developed. Once such defects are identified, dismantling is generally recommended. Because this process is handled at the regional office level, details of these failures are not always consistently communicated to central authorities. Inconsistent welding practices, particularly with respect to post-weld heat treatment, were identified as an important contributing factor. Around 2008, heat treatment after welding became a formal requirement; before then, compliance varied among manufacturers. This inconsistency appears to have caused material weaknesses, particularly at the base of structures, although these failures are not generally classified as fatigue-related. Improved documentation and analysis of such failures would support better design and inspection practices. In general, the underlying cause is usually either a design error, such as underestimating wind loads or service life, or deficiencies in weld quality and post-weld heat treatment.
- Infrastructure owners were also reported to have concerns about the limited availability of reliable material property data for cast aluminum products, as well as the lack of understanding of how non-standard structures respond to cyclic loading. In practice, this leaves owners with two options: requesting performance testing from manufacturers, which can be costly, or relying on assumptions based on field experience.
- Finally, one documented failure involved a light structure with a straight arm rather than the lattice-arm configuration typically used in Quebec. The structure had a single welded connection between the arm and the cast aluminum root element, using the standard connection detail. The arm was 1.4 m long and supported an LED luminaire. Because some LED luminaires have a flat, plate-like geometry, they can be more vulnerable to wind-induced cyclic loading. According to the participants, this aerodynamic behaviour likely contributed to the fatigue failure observed at the connection.

3.3 Aluminum Pedestrian Bridges

Square HSS joints are commonly used in aluminum pedestrian and active-mode bridge applications. Although Sharp et al. [12] provided design guidance for these joints based on the hot-spot stress approach, research on the fatigue behaviour of aluminum HSS connections remains relatively limited (e.g., [36]). For instance, van Wingerde et al. [37] examined the difficulties associated with calculating stress concentration factors (SCFs) in multiplanar circular and rectangular hollow section connections, primarily for steel structures. Based on extensive numerical and experimental work, they proposed a simplified method that uses correction factors to estimate SCFs. Their approach offers a consistent procedure for evaluating K-connections with gaps in both rectangular and circular hollow sections and extends earlier design methods to account for both uniplanar and multiplanar connections.

Four participants in the industry survey conducted for this report had expertise in the design of active-mode bridges with square HSS joints. Of these, two had direct experience designing such structures in aluminum. Discussions with these individuals highlighted several key observations, which are summarized as follows:

- Aluminum was consistently identified as an attractive material choice due to its low weight and corrosion resistance. These properties reduce transportation and installation demands while also lowering long-term maintenance costs, resulting in a more favourable overall life-cycle cost.
- Several completed projects were referenced, including the Hall and Wellington footbridges in Montreal and the Daigneault Creek aluminum pedestrian bridge in Brossard. Additional examples mentioned included bridges over the Rideau River in Ontario and the Quinchien River in Quebec.
- The Hall and Wellington project (see Figure 2.2) consists of twin active-mode bridges featuring square HSS members connected through welded joints. A defining aspect of this design is the configuration of the primary truss joints, which incorporate both full penetration and fillet welds. The truss system includes vertical and diagonal members, with the diagonals oriented at approximately 45°. Although these diagonal connections are

executed using fillet welds, CSA W59.2 [23] allows welds between members intersecting at angles less than 60° to be classified as partial joint penetration (PJP) welds.

- However, under the current provisions of CSA S6 [4], PJP welds are not permitted in primary structural connections, making this design approach non-compliant. The alternative using full penetration welds with internal backing bars introduces considerable fabrication complexity and cost, in some cases increasing welding costs by up to an order of magnitude compared to fillet welds.
- In contrast, the Daigneault Creek bridge (Figure 3.1c), which was the longest aluminum bridge of its kind in Canada at the time of construction, adopted a different approach. The structure was transported and installed in a single day using a crane with approximately half the capacity and therefore significantly lower cost than would have been required for a comparable steel structure. The truss diagonals in this design were oriented at approximately 60°, meaning the HSS welds would likely have been classified as fillet welds under CSA W59.2 [23].
- From a fabrication standpoint, welding cost is largely governed by the number of passes required. Single-pass fillet welds around thinner sections (up to about 8 mm) are substantially more economical than the multi-pass welds needed for thicker joints (e.g., 10–14 mm). Given the large number of similar joints in bridge trusses, optimizing weld design to minimize the number of passes can result in significant cost savings.
- Gas metal arc welding (GMAW) was identified as the standard fabrication method. This process can be automated using robotic systems with vision-based control, improving both precision and consistency.
- Participants also noted common welding-related challenges. For full penetration welds, lack of fusion during the initial pass is a frequent concern. More generally, defects such as porosity and cracking particularly within the heat-affected zone can occur across all weld types. These issues are typically mitigated through strict quality control procedures and ongoing training of welding personnel.

- No cases of fatigue failure in aluminum active-mode bridges were reported by the participants.
- Finally, it was acknowledged that the limited availability of aluminum-specific fatigue research often necessitates the use of steel-based design guidance (e.g., [37]), with appropriate adjustments. In particular, stress concentration factors (SCFs) derived from such methods are considered applicable to aluminum structures, as they are governed primarily by geometric parameters such as branch-to-chord width ratio, chord wall slenderness, and relative wall thickness which do not significantly change with material. However, it was also noted that fillet welds, while practical for thinner sections, tend to produce higher SCFs. Recommendations from [37], such as avoiding weld starts and terminations in high-stress regions, remain directly applicable to aluminum structures and can help improve fatigue performance.

Chapter 4: Analysis Methods

4.1 Analysis Methods

This chapter describes the approaches used to study how stress is distributed, how cracks begin, and how they grow in structural components with notches. It brings together four main methods: (1) the notch stress approach, (2) fracture mechanics, with the stress intensity factor determined using closed-form equations or by FE analysis along with the J-integral method, and (3) fitted analytical solutions for rapid assessment, which are suitable for inclusion in design codes. Taken together, these methods provide a clear and well-rounded basis for assessing the structural integrity of components with geometric discontinuities.

4.2 Notch Stress Approach

The notch stress approach evaluates fatigue life by obtaining a repeatable measure of the local stress at critical points such as the weld toe or root. It considers microstructural support effects, building on the work of Neuber [28] and later refined by Radaj [38], who introduced the idea of a fictitious radius to better represent stress concentrations. In this method, fatigue resistance is assessed using an effective notch radius while assuming the material behaves in a linear elastic manner. The concept of the notch radius is illustrated in Figure 4.1.

To apply this approach, finite element (FE) analysis is typically used to capture the local stress concentration. However, this requires a much finer mesh and therefore significantly longer computation time compared to the hot-spot stress approach (not employed in this research project), which can limit its practical application. Despite this, the notch stress method has become increasingly popular because of its ability to directly link fatigue strength to local geometric features, making it a powerful tool for engineering analysis. This approach has also been extended to aluminum welded joints by Morgenstern et al. [39].

The notch stress approach can be used to identify areas where stress concentrations are most likely to occur. Features such as grooves, holes, and fillets interrupt the uniform distribution of stress, creating localized regions of higher stress that can significantly reduce fatigue life

and overall structural performance. To evaluate this effect, the nominal stress is first determined based on the applied load and the overall geometry of the specimen. This value is then adjusted using a stress concentration factor, K_t.

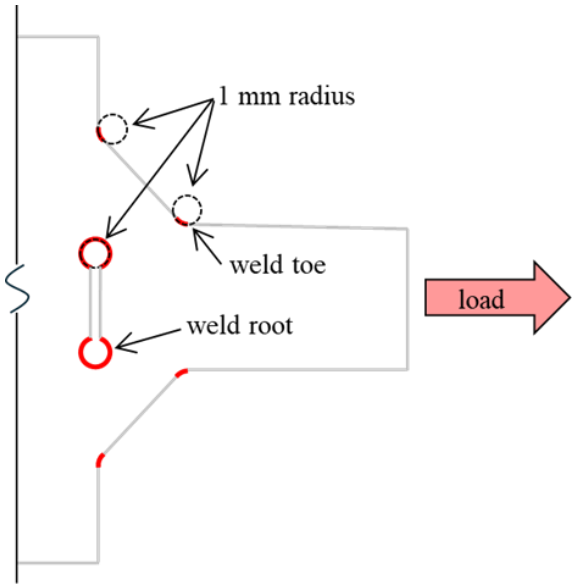

Figure 12.FE model geometry features for the notch stress approach.

Specifically, the local notch stress is computed using the classical relation:

$$\sigma_{notch} = K_t \, \sigma_{nom} \tag{4.1}$$

Here, σ_{nom} represents the far-field stress, which can be obtained either through analytical calculations or numerical simulations. For simple notch geometries, standard charts and equations from elasticity theory are typically used to determine the stress concentration factor, K_t. In contrast, more complex geometries usually require numerical methods to achieve more accurate results. To ensure reliable stress evaluation, the mesh is refined around the notch root so that steep stress gradients are captured accurately. This approach helps pinpoint critical regions where cracks are most likely to initiate. It also provides a solid starting point for further fracture mechanics analysis by establishing the initial stress conditions that drive crack formation.

4.3 Fracture mechanics

Fracture mechanics, particularly linear elastic fracture mechanics (LEFM), has become an important tool for understanding the fatigue behaviour of aluminum welded joints. This approach assumes that a small initial crack or flaw already exists in the structure and that, under cyclic loading, it gradually grows until failure occurs. For this method to predict fatigue life accurately, several factors must be considered carefully, including the initial crack size, the crack shape, and the presence of residual stresses.

The fatigue life of a welded component is generally divided into three stages: crack initiation and crack propagation, followed by ductile or brittle fracture. In smooth, defect-free materials, most of the fatigue life is spent in the initiation stage, where cracks slowly begin to form. In contrast, welded components already contain small, crack-like imperfections from the fabrication process, along with high tensile residual stresses. As a result, most of their fatigue life is dominated by the crack propagation stage rather than initiation. Although the boundary between these two phases is not always clearly defined, this distinction emphasizes the importance of fracture mechanics when evaluating the remaining life of existing structures. Well-established guidelines, such as the International Institute of Welding (IIW) fatigue recommendations [17], provide practical direction on applying fracture mechanics principles. These include evaluating crack growth and stress intensity factors (SIFs), which are key to predicting the fatigue life of welded joints under cyclic loading.

Figure 4.2 highlights the main steps involved in a fracture mechanics analysis. The process begins by calculating the applied stress intensity factor (SIF) range, ΔK_{app}, which depends on the applied stress range, $\Delta\sigma_{app}$, and the crack depth, a. This SIF range can then be adjusted to account for effects such as crack closure and residual stresses, giving an effective SIF range that is used to determine the crack growth rate. To calculate this growth rate, material-specific constants C and m from the Paris-Erdogan crack growth law, along with the threshold SIF range ΔK_{th}, must be known. By evaluating the crack growth rate over a range of crack depths, the total fatigue life can be estimated. This is done by integrating the crack growth rate from the initial crack size, a_i, to a critical size, a_c, typically using numerical methods.

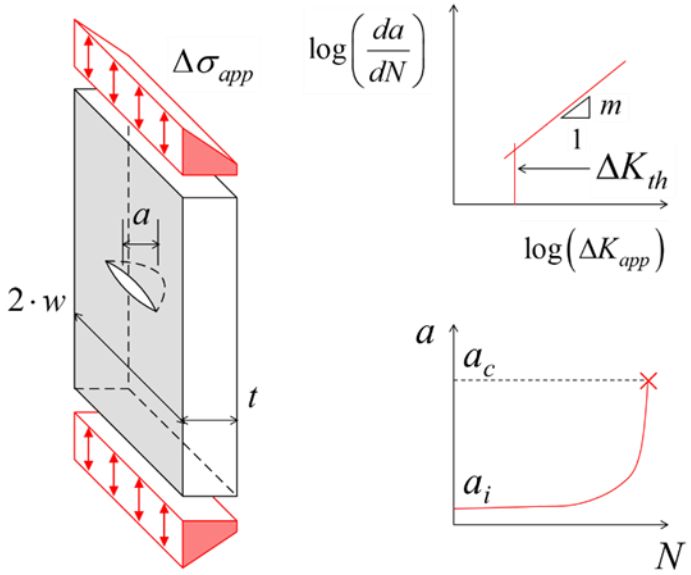

Figure 13.LEFM example crack-loading model and key features.

Coughlin and Walbridge [3], carried out a fatigue testing program to study the behaviour of aluminum welds, focusing on non-load-carrying transverse stiffeners with fillet welds made from *6061-T651* aluminum. The specimens were tested under both constant amplitude and variable amplitude loading, with the variable amplitude loading histories designed to reflect realistic service conditions for highway bridges based on Ontario truck traffic data.

The results showed that the CSA S6 Detail Category C design curve was generally conservative in predicting fatigue performance of the investigated cruciform (transverse stiffener) weld specimens. However, some differences appeared in the high-cycle fatigue range, especially under variable amplitude loading, where a two-slope *S–N* curve was found to provide a better representation of the observed behaviour. To support the fracture mechanics analysis, additional investigations were carried out, including crack shape measurements and material property tests such as tensile, cyclic, and hardness testing. These showed that the heat-affected zone had lower strength than the base metal, while residual stresses measured at the weld toe averaged about *15%* of the base metal yield strength.

Using a validated fracture mechanics model, fatigue life predictions were then performed. The validated model included material properties, assumed initial crack sizes, and stress intensity factors, and it was calibrated using the experimental results. The predictions agreed well with the test data and further supported the use of a two-slope S-N curve. The study also examined the influence of overload events, such as those caused by simultaneous truck crossings, and found that these could significantly reduce fatigue life. In addition, a scale effect study showed that full-scale components generally have shorter fatigue lives than small-scale specimens because of their greater plate thickness and higher residual stresses.

In LEFM, the stress intensity factor, K, in the Equation 4.2 governs crack-tip behaviour and is evaluated using the following expression:

$$K = Y\,\sigma\sqrt{\pi a} \tag{4.2}$$

where a is the crack length and Yis a geometry correction factor accounting for specimen shape and boundary conditions. Crack growth and stability are evaluated by comparing the calculated stress intensity factor, K, with the material's fracture toughness, K_{IC}. If Kexceeds K_{IC}, the crack is expected to grow uncontrollably, leading to failure (i.e., brittle fracture).

In situations where plastic deformation is no longer negligible, the analysis moves beyond linear elastic assumptions and incorporates elastic-plastic fracture mechanics. In these cases, energy-based approaches such as the J-integral method (see Section 4.4), can be used to better capture the material response. Alternatively, strain-based fracture mechanics (SBFM) methods such as those used by Coughlin and Walbridge [3] can be employed.

With fracture mechanics, it is possible to realistically assess how cracks initiate, grow, and eventually lead to failure. This provides a much deeper understanding of fatigue behaviour than can be achieved through simple stress analysis. In this study, the LEFM calculation was combined with FE-based SIF extraction. The FE model, along with the J-integral method, provided the crack-driving force (SIF), while the Paris-Erdogan crack growth law integration was used to estimate the fatigue life or corresponding fatigue stress range.

4.4 J-Integral method

The J-integral method plays a key role in the fracture mechanics approach used in this thesis. It provides a reliable and physically meaningful way to measure the driving force at a crack tip, especially for welded geometries where analytical stress intensity factor (SIF) solutions are not readily available. In the aluminum partial joint penetration (PJP) butt joints studied here, fatigue cracks tend to initiate at the lack of penetration (LOP) region near the weld root. This area has a highly non-uniform stress field due to the geometric discontinuity, making it difficult to analyze using simpler methods. The J-integral addresses this by capturing the overall effect of these complex conditions in a single, path-independent energy parameter.

Originally, the J-integral was developed to describe the energy release rate in nonlinear elastic materials, providing a foundation for analyzing crack growth in situations where linear assumptions no longer hold. For a two-dimensional crack problem in the x–y plane, the J-integral is defined as a counter-clockwise line integral around a contour Γ enclosing the crack tip. This integral can be expressed as follows:

$$J = \int_{\Gamma} \left(w\, dy - T_i \frac{\partial u_i}{\partial x}\, ds \right) \tag{4.3}$$

The various terms in this equation are explained in Table 4.1.

Table 1.Formula description.

Symbol	Description
$w = \frac{1}{2}\sigma_{ij}\varepsilon_{ij}$	Strain energy density in a linear elastic material.
$T_i = \sigma_{ij} n_j$	Traction components acting on integration contour.
u_i	Displacement components.
ds	Differential arc length along contour Γ.
n_j	Outward unit normal vector to the contour.

One of the most important features of the J-integral is its path independence. This means that its value remains the same regardless of the integration contour used, as long as the contour completely surrounds the crack tip. This property is especially valuable in welded structures, where complex geometry makes standard closed-form solutions difficult or impossible to apply. Even in areas with sharp geometric changes, such as weld toes and weld roots, the J-integral can still provide a reliable measure of the energy released at the crack tip. In the LEFM domain, which is relevant for high-cycle fatigue in aluminum, the J-integral becomes equivalent to the strain energy release rate, G. This allows the parameter to be related to the Mode I Stress Intensity Factor, K, in the Equation 4.4 and Equation 4.5 through:

- Plane Stress

$$J = \frac{K^2}{E} \tag{4.4}$$

Plane Strain

$$J = \frac{K^2}{E/(1-\nu^2)} \tag{4.5}$$

where Eis Young's modulus and ν is Poisson's ratio of the aluminum alloy. These relationships enable the conversion of FE-computed J-integral values into equivalent stress intensity factors necessary for fatigue crack growth analysis using LEFM.

In this thesis, the J-integral is calculated using the domain integral method available in the FE analysis software ABAQUS. Rather than evaluating the contour integral directly, this method converts it into a volume integral over a small region of elements surrounding the crack tip. As a result, the calculation becomes more numerically stable and less sensitive to local mesh refinement. To accurately represent the $1/\sqrt{r}$ stress singularity that exists near the crack tip, a spider-web mesh is used. This mesh consists of several concentric rings of structured quadrilateral elements radiating outward from the weld root (see figure 14).

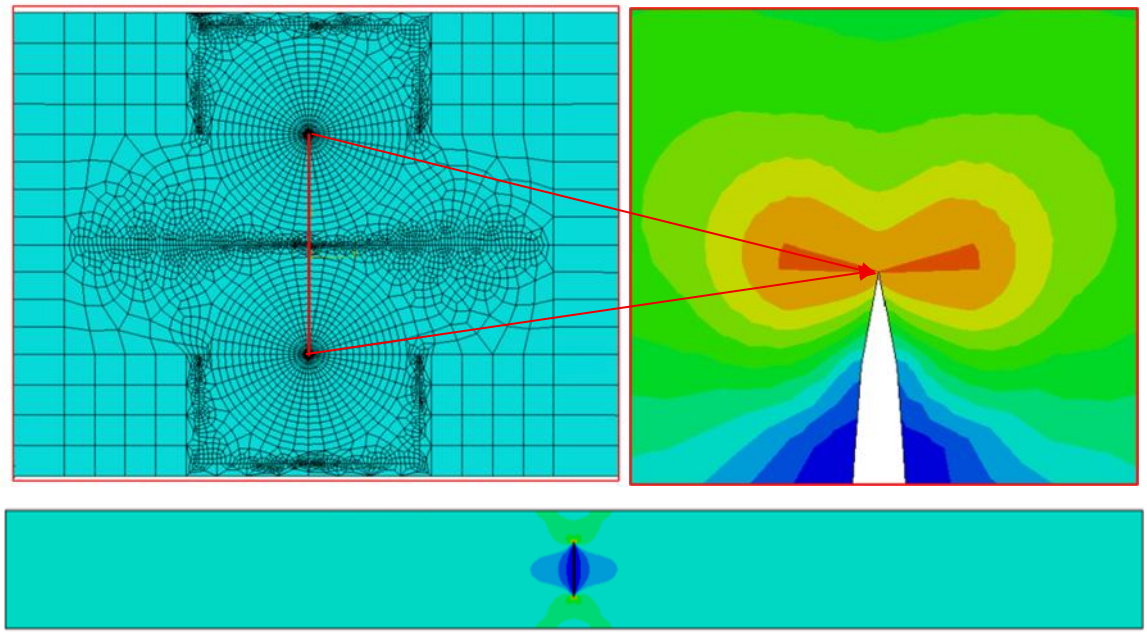

Figure 14.Spider-web mesh.

The J-integral is then calculated over multiple domain contours, and path independence is verified when the values become consistent across successive outer contours. This confirms that the crack-tip stress and strain fields are being captured and that the computed J-integral is physically meaningful.

A major advantage of this approach is that it avoids the extremely fine meshes often needed for displacement-based K-extraction methods, which can be difficult and impractical to apply in welded joint models. For fatigue crack growth modelling, the J-integral must be converted into the stress intensity factor range. This is done using Equation 4.6, ΔK, which serves as the driving parameter in the crack growth law. The conversion is given by:

$$\Delta K = \sqrt{\Delta J \, E'} \tag{4.6}$$

The resulting ΔK is then used in the Paris Law expression:

$$\frac{da}{dN} = C(\Delta K)^m \tag{4.7}$$

In Equation 4.7, C and m are material-specific fatigue crack growth constants.

Table 2.Formula description.

Symbol	Description
s	Range of the J-integral over a loading cycle.
$E' = E$	Effective modulus for plane stress.
$E' = E / (1 - \nu^2)$	Effective modulus for plane strain.

This procedure allows the J-integral obtained from finite element (FE) analysis to be used directly in fatigue life prediction models. As a result, it provides a comprehensive and numerically stable framework for evaluating crack growth in aluminum welded joints.

4.5 Closed Form Solution

In addition to the J-integral method, closed-form solutions are also used in this study to determine the geometry correction factors, or Y-factors (see Equation 4.2), needed to calculate SIFs for different crack configurations without relying on FE analysis. These solutions provide analytical expressions for Y, linking the applied stress, crack size, and structural geometry to the stress intensity factor through the well-known relationship $K = Y\sigma\sqrt{\pi a}$. This approach is especially useful because it allows SIFs to be estimated quickly, reliably, and with minimal computational effort for standard crack shapes and loading cases. More importantly, these Y-factor equations are based on rigorous mathematical, numerical, and experimental work, which has made them widely accepted in fracture mechanics practice and incorporated into engineering codes and reference handbooks.

The simplest Y-factors come from analytical solutions based on LEFM. Early work by Irwin, Westergaard, and Muskhelishvili [40, 41, 42, 43] provided exact mathematical descriptions of how stresses behave near cracks in idealized cases, such as infinite or semi-infinite bodies. A well-known example is the value $Y = 1.12$ for a small through thickness surface crack in a large plate, which comes directly from these classical solutions. This value reflects how the

presence of a free surface increases the stress intensity compared to an internal crack. It also represents a fundamental reference point for verification of more complex Y-factor formulations.

As crack geometries become more complicated such as for semi-elliptical surface cracks, embedded flaws, or cracks in finite plates, exact analytical solutions are no longer possible. In these situations, Y-factors are developed using techniques such as series expansions and asymptotic matching. To do this, researchers create polynomial or rational expressions using variables like a/t, a/W, and $a/c$to approximate the stress field near the crack tip. These expressions are carefully formulated so that they remain consistent with known limiting cases, such as the infinite plate solution for very small cracks, the through-thickness condition as $a/t \rightarrow 1$, or the edge-crack solution when a crack approaches a free surface. Although these closed-form expressions are not exact solutions, they are built to reflect the correct physical behaviour over a wide range of crack shapes and geometries.

The most accurate and commonly used Y-factor formulas, such as the Newman–Raju equations [44], are developed from extensive finite element analysis (FEA). In these studies, thousands of numerical simulations are carried out to determine stress intensity factors for different combinations of crack depth, crack shape, plate thickness, and loading conditions. The resulting K-values are then used to build smooth, continuous equations that closely represent the numerical data. In this way, many closed-form Y-factor equations are not purely analytical in origin but are instead curve-fitted expressions based on highly detailed numerical models. Even so, they are still treated as analytical formulas in practice because they can be applied directly without the need for additional simulations.

Finally, some Y-factor expressions are improved through experimental calibration, so they better reflect real structural behaviour. Experimental methods such as crack opening displacement measurements, full-field photoelastic studies, and fracture testing are often used to validate or refine analytical and numerical Y-factor equations. This is particularly important in design codes and standards, where the formulas must remain both reliable and conservative across a wide range of practical applications. Experimental data are also valuable for

confirming that the equations capture actual physical behaviour, especially in situations involving shallow surface cracks or welded structures with non-ideal geometry.

In summary, the closed-form Y-factors used in fracture mechanics are developed through a combination of analytical derivations, polynomial approximations, large finite element databases, and experimental validation. Together, these approaches ensure that the resulting formulas are mathematically sound, physically meaningful, and accurate enough for engineering use. For this reason, closed-form Y-factor solutions remain the preferred method for calculating stress intensity factors in many practical cases where the geometry is standard and does not require problem-specific numerical analysis.

Chapter 5: Analysis Results and Discussion

This chapter presents and interprets the validation and application of the fatigue assessment procedures used for aluminum welded joints, with specific emphasis on partial joint penetration (PJP) butt joints. The discussion is divided into two validation stages and two application stages. The first validation stage concerns weld-toe fatigue, which represents a conventional external fatigue-critical location in welded aluminum details. The second concerns weld-root fatigue, which is the controlling mechanism for PJP butt joints because the incomplete penetration creates an internal crack-like defect at the weld root.

The chapter is written around one central logic chain: geometry controls the local crack-driving force, the crack-driving force controls crack-growth rate and fatigue life, and the resulting fatigue capacity is normalized against a common design reference. This logic allows the FE, LEFM, and effective notch stress analyses, as well as empirical equations proposed by Frank and Fisher [13, 14] and the CSA [45] to be compared on the same basis.

5.1 Validation for Weld Toe

The weld-toe validation was performed to demonstrate that the numerical and analytical fatigue procedures can reproduce the fatigue response of a conventional welded aluminum detail before being applied to the more specialized PJP weld-root problem. Weld toe cracking is a common fatigue mechanism because the weld toe forms an abrupt geometric transition between the weld reinforcement and the base plate. This transition creates a local stress concentration that increases the cyclic stress range near the surface and promotes crack initiation. In toe-controlled details, the fatigue problem is often dominated by local notch severity rather than by a pre-existing internal crack. Therefore, the validation must confirm two aspects: first, the finite element model should locate the maximum local stress or notch stress near the weld toe; second, the predicted fatigue strength or life should follow the experimental trend for toe-governed welded specimens. Agreement in only one of these aspects is insufficient. A model can produce a high local stress at the toe but still provide the wrong fatigue life if the stress definition, notch radius, or fatigue curve is inconsistent.

$$\mathrm{SCF} = {}^{\sigma_{max}}/_{\sigma_{nom}} \tag{5.1}$$

The stress concentration factor, *SCF*, provides a measure of local stress amplification. In the effective notch stress formulation Equation 5.2, the same idea is applied with an elastic notch factor, K_t, which amplifies the nominal stress range to obtain local notch stress range:

$$\Delta\sigma_{notch} = K_t \, \Delta\sigma_{nom} \tag{5.2}$$

The effective notch stress method is particularly useful for weld toe fatigue because it captures the elastic stress increase caused by weld profile, toe angle, and toe radius.

For the LEFM analysis of weld toe fatigue, an initial surface crack assumed at the weld toe. The crack grows under cyclic loading. The fatigue life is obtained by integrating crack growth from an initial crack size to a final crack size. In Equation 5.3, when *Y(a)* is not constant, numerical integration is required. When *Y* is assumed to be constant for a first screening calculation, the fatigue life can be written in a closed form.

$$N_f = \int_{a_i}^{a_f} \frac{da}{C\left[Y \, \Delta\sigma \sqrt{\pi a}\right]^m} \tag{5.3}$$

This expression shows why fatigue life is sensitive to both stress range and initial crack size. Since stress range appears to the power ***m*,** even a moderate increase in $\Delta\sigma$ can sharply reduce N_f. Similarly, the initial crack size controls the lower limit of the integration and affects the amount of crack growth available before failure. The weld-toe validation provides an important baseline for the rest of the chapter. If the model can correctly represent a toe-controlled welded detail, then the finite element mesh, loading condition, material properties, and fatigue constants are reasonably consistent. This does not automatically validate the PJP butt-joint root calculation, because the root mechanism is different, but it does establish that the general modelling procedure is credible for welded aluminum fatigue assessment.

Table 3.Recommended weld-toe validation discussion points.

Validation check	Expected evidence	Use
Crack location	Maximum local stress or notch severity occurs at weld toe for toe-governed specimens	Confirms that the model reproduces the observed toe-controlled mechanism
Stress trend	Higher applied stress range predicts lower fatigue life	Confirms basic fatigue sensitivity
Mesh adequacy	Local stress or $\frac{K}{J}$ output stabilizes with mesh refinement	Reduces risk of numerical artifact
Life comparison	N_{model}/N_{test} within acceptable scatter or conservative side	Supports use of the method for further parametric studies

The expected conclusion from the weld-toe validation is that the adopted modelling approach can capture local stress amplification and fatigue-life trends for conventional welded aluminum details. This validation is necessary but not sufficient for PJP Butt joints. The key limitation is that weld toe fatigue involves an external geometric notch and possible crack initiation, whereas PJP root fatigue begins from an existing internal lack-of-penetration flaw. This section presents a validation of the modelling approaches for predicting the fatigue performance of welded aluminum connections (i.e., FE notch stress analysis and LEFM via the J-integral method) against two benchmark datasets representative of the governing crack locations: the weld toe in fillet welded cruciform joints [3] and the weld root in PJP butt joints [20]. With that basis established, fatigue design relations are developed for aluminum and then applied to a parametric study of the connection details of interest. The outputs are design S-N curves and normalized capacity surfaces (SR / SRC) over plate thickness and LoP ratio, which are used to compare conservatism and identify the governing failure location. In the first step of this

validation, the objective is to confirm that the application of LEFM, together with calibrated input parameters, reproduces the S-N behaviour of a toe-controlled cruciform coupon (i.e., transverse fillet welded attachment). The non load-carrying cruciform specimen tested in [3] was adopted for this purpose (transverse stiffener, double fillet welds). In [3], this specimen was tested under constant amplitude loading at three stress ratios, R (= σmin / σmax). The specimen geometries for various thicknesses and test setup are shown in Figure 15.

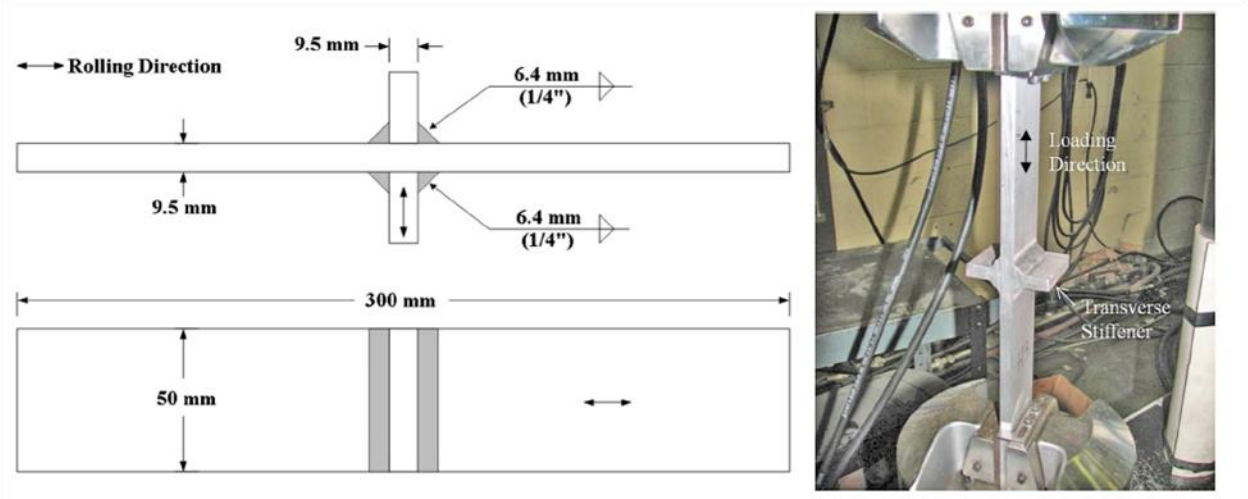

Figure 15.Validated specimen geometry and simulation setup, tp=9.5mm

Analysis was performed in Abaqus/Standard using a 2D plane-strain model with quarter symmetry about the plate mid-lines, as shown in Figure 16. The base plate and attachment were meshed with quadratic plane-strain elements (CPE8 family).

A crack was introduced at the weld toe on the plate surface and advanced in discrete depth steps from an initial flaw, a0 = 0.025 mm, to an engineering limit near half of plate thickness.

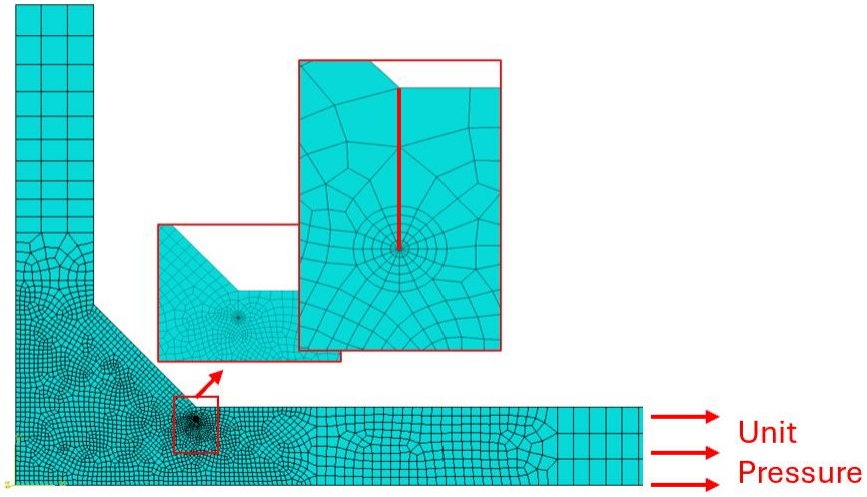

Figure 16.FE model for weld toe validation of LEFM application

A unit remote pressure of 1.0 MPa was applied at the free end to generate a library of J-integral values $J(a)$. These were converted to Mode I stress intensity factors (SIFs) using the standard plane-strain relation:

$$K_I = \sqrt{\frac{J \cdot E}{1-\nu^2}} \tag{5.4}$$

For a target stress range, ΔS, and ratio, R, nominal linear scaling was used to obtain $\Delta K(a)$.

In practice, weld toe cracks typically develop as semi-elliptical surface cracks rather than purely two-dimensional flaws. To account for this, a crack shape or aspect ratio (a/c) was used to relate the surface half-length c to depth a. Shape effects were then included by multiplying the 2-D SIFs by (Y_s /1.12), where:

$$Y_s = 1 + 0.12 \cdot (1 - 0.75 \cdot a/c) \tag{5.5}$$

and 1.12 is the infinite-plate edge-crack factor already embedded in the FE solution. Residual stress was incorporated through an effective R-ratio (R_{eff}) using a constant mean field of $\sigma_{RS} = 0.15 \cdot \sigma_y$ through a Walker mean-stress correction [48]. The Walker model is expressed as:

$$\Delta K_{eff} = (1 - R_{eff})^{1-\gamma} \Delta K, \qquad R_{eff} = \frac{\sigma_{min} + \sigma_{RS}}{\sigma_{max} + \sigma_{RS}} \tag{5.6}$$

where γ is the Walker exponent, which calibrated against test data and is equal to 0.5. Fatigue life was obtained by integrating the Paris-Erdogan crack growth law [32] at the deepest point from a_0 to a_f:

$$N = \int_{a_0}^{a_f} \frac{da}{C \cdot (\Delta K_{eff}^n - \Delta K_{th}^n)} \tag{5.7}$$

A long-crack threshold ΔK_{th} = 30 MPa·√mm was applied in the low-growth regime. Paris constants (C, n) were taken from the wrought-aluminum envelope. The integral was evaluated with adaptive crack size increments; $K(a)$, the Walker scaling, the threshold, and the shape update were applied at each step.

Table 4. Parameters used in LEFM analysis.

Parameter	**Value**	**Unit**
σ_y	95	MPa
σ_u	240	MPa
σ_0	165	MPa
C	$7.97 \cdot 10^{-14}$	(MPa, mm)
n	3.96	-
ΔK_{th}	$56.7 - 72.3 \cdot R > 21$	MPa·√mm

Predicted S-N curves for the three stress ratios are compared with the test data in Figure15. As can be seen in this figure, the model reproduces both the slope and level of the measured trends. The overall agreement supports the accuracy of the LEFM procedure for toe-controlled aluminum cruciform details.

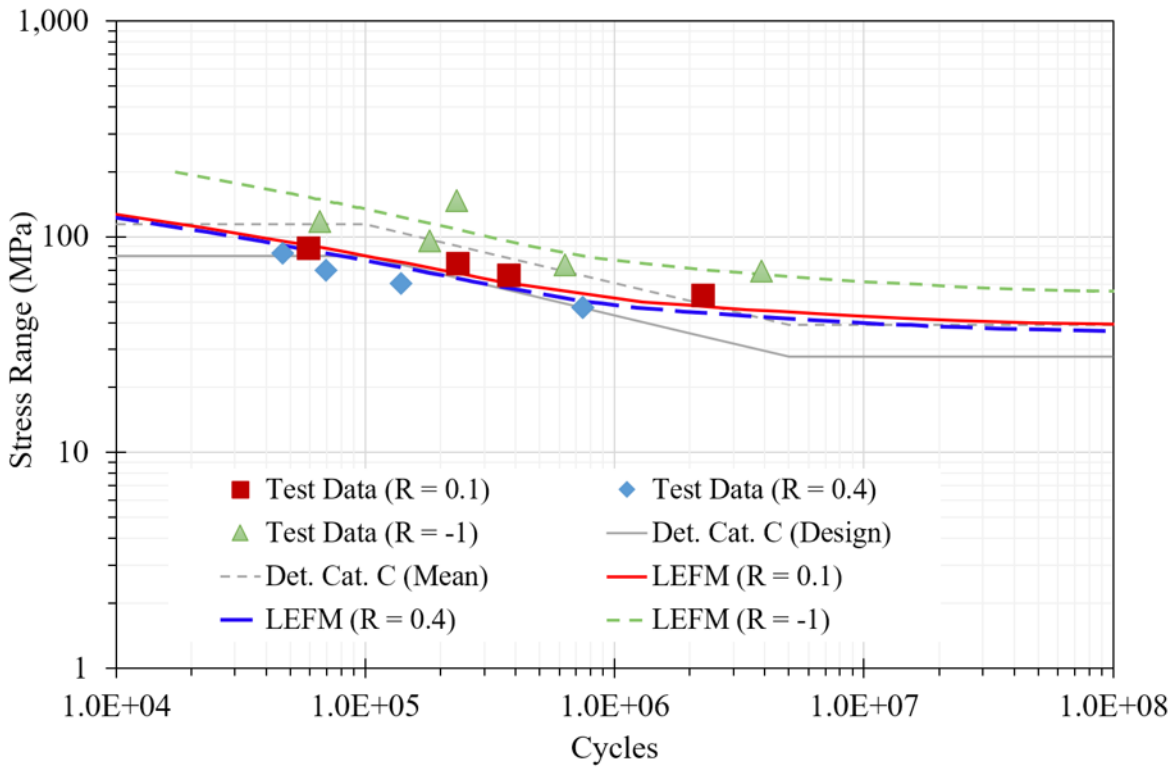

Figure 17.LEFM predictions compared with fatigue test data

5.2 Validation for Weld Root

The weld root validation was required because PJP butt joints are typically not governed by the same fatigue mechanism as toe-critical fatigue details. In PJP butt joints, the unfused root region or lack of penetration normally acts as an initial crack-like defect. The lack of penetration is idealized as an initial crack with size a_i, and the crack is assumed to grow under

cyclic loading until it reaches a final or critical crack size a_f. The fatigue life is then estimated by integrating the crack growth law between the initial and final crack sizes.

$$\Delta K = Y \Delta\sigma \sqrt{\pi a} \tag{5.8}$$

$$\Delta K(a) = K_{ref}(a) S_R \tag{5.9}$$

where Y is the geometry correction factor, $\Delta\sigma$ is the applied stress range, and a is the crack size and C and m are material crack growth constants. The number of cycles to failure is obtained by integration of the Paris-Erdogan crack growth law:

$$N_f = \int_{a_i}^{a_f} \frac{da}{C\left[Y \Delta\sigma \sqrt{\pi a}\right]^m} \tag{5.10}$$

This equation shows that the fatigue life of a PJP butt joint is strongly controlled by the initial lack of penetration, the applied stress range, and the geometry correction factor. A larger initial root defect increases ΔK, accelerates crack growth, and reduces fatigue life.

For FE model validation, the J-integral method was used to obtain the energy release rate around the crack tip. Under linear elastic conditions, the J-integral can be converted to an equivalent stress intensity factor, for plane strain using Equation 4.5. The FE analysis procedure therefore provides an independent method for calculating the crack driving force at the weld root. The J-integral values are converted into equivalent SIFs, and the resulting ΔK values are used to estimate fatigue life through Equation 5.8.

The root validation compares the predicted fatigue lives with available PJP butt-joint fatigue data from Gerin [20]. The validation is based on parameters such as plate thickness (t_p), effective throat (t_e), penetration ratio $(\rho = t_e/t_p)$, normalized lack of penetration ratio $(2a_i/t_p)$, net-section stress range ($\Delta\sigma_n$), initial crack size (a_i), final crack size, geometry correction factor, initial stress intensity range, test life, predicted life, and model-to-test validation ratio.

The validation confirms that PJP root fatigue behaviour can be reasonably represented by treating the lack of penetration (LoP) as an initial crack. This is physically consistent because the root discontinuity already provides a crack-like stress concentration before cyclic loading begins. In contrast with weld toe fatigue, where crack initiation may occupy part of the fatigue life, PJP root fatigue is dominated to a much greater extent by crack propagation from an

existing defect. For PJP butt joints, the initial flaw is not a small random imperfection; it is a direct consequence of the joint geometry. This subsection verifies root-controlled cracking in a PJP groove-welded butt joint against the test program reported by Gerin [20]. A representative PJP geometry and notation (plate thickness t, groove depth S, and degree of penetration ρ) are shown in Figure 5.4. The specimens consisted of two collinear plates joined with double-V PJP welds; the groove angle was 45° and the preparation depth, with various plate thicknesses t. To match Gérin's convention, results are expressed in terms of the net-section stress range $\Delta\sigma$ (i.e., the load divided by the reduced net section area at the weld), and the validation focuses on the R = 0.1 and t = 9.5 mm test data.

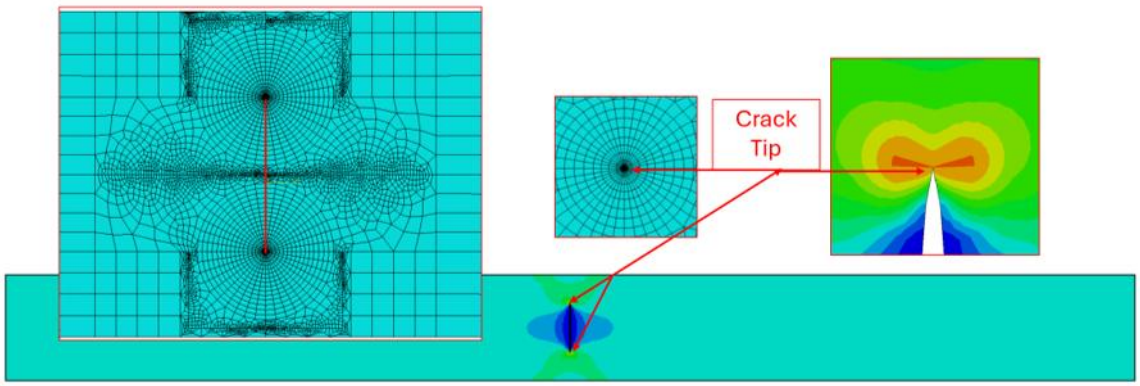

Figure 18.FE model and crack-tip mesh

Analysis was carried out in ABAQUS/Standard using a 2D plane-strain model of the full specimen. The plates were meshed with quadratic plane-strain elements (CPE8 family). An edge/embedded crack was inserted at the weld root along the joint centerline with initial depth a0 = 2.5 mm, obtained directly from the degree of penetration ρ0 for t = 10 mm. The region around the crack tip used quarter-point singular elements with concentric refinement rings to capture the $(1 / \sqrt{r})$ field. A representative tip mesh is shown in Figure 5.6. A mesh-sensitivity study was also performed to confirm stability of J and K as mesh size was varied. Linear-elastic material with nominal properties for aluminum (E = 70 GPa and ν = 0.33) was assumed. It should be noted that the weld and HAZ were not distinguished in the model, as their elasticity

and Poisson ratio were assumed to be the same as the base metal. The analysis parameters are listed in Table 5.

Table 5.Weld root validation parameters.

Symbol	Value	Unit
(t_p)	9.5	mm
$\left(\frac{2a_i}{t_p}\right)$	0.0 to 0.6	–
$(2a_i)$	$\left(\left(\frac{2a_i}{t_p}\right)t_p\right)$	mm
(a_i)	$\left(\frac{\left(\frac{2a_i}{t_p}\right)t_p}{2}\right)$	mm
(t_e)	$(t_p - 2a_i)$	mm
(ρ)	$\left(\frac{t_e}{t_p}\right)$	–
(R)	0.1	–
$(\Delta\sigma_n)$	Variable	MPa
(K_t)or SCF	From FE model	–
(J)	Abaqus J – integral	$\frac{N}{mm}$
(E)	70,000	MPa
(ν)	0.33	–
(E')	$\left(\frac{E}{1-\nu^2}\right)$	MPa
(K)	$\left(\sqrt{\{JE'\}}\right)$	$MPa\sqrt{mm}$
(ΔK)	Calculated	$MPa\sqrt{mm}$
$\left(\Delta K_{\{th\}}\right)$	From threshold $\frac{\text{relation}}{\text{table}}$	$MPa\sqrt{mm}$
(C)	$\left(7.97 \times 10^{\{-14\}}\right)$	consistent with (ΔK)
(m)	3.64	–
(FAT)	71	MPa
(N_f)	Calculated	cycles

$(N_{\{test\}})$	test data[20]	Cycles

For the PJP coupons, 2·w = t and the half-crack length a is measured from the root end. The FE (J-integral) method (FEM) vs. analytical comparison in Figure 19, shows good agreement across the practical range of the degree of penetration ρ (= a / w), confirming that the J-integral-to-K conversion provides an accurate crack-tip driving force for the root-controlled models.

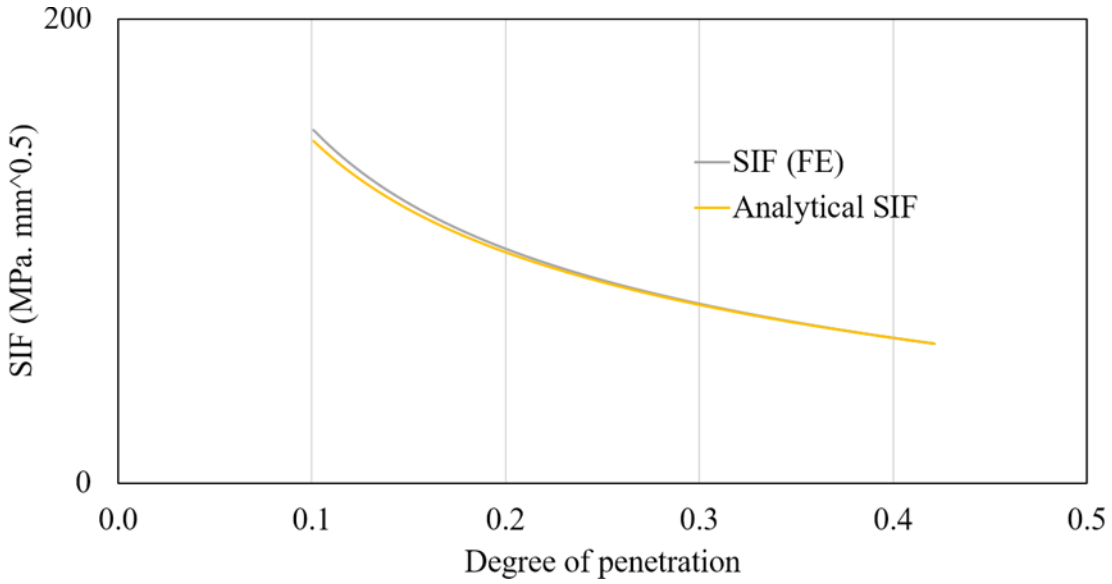

Figure 19.Degree of penetration Vs SIF

To account for the dependence of fatigue growth on stress ratio *R* a closure-based correction at the SIF level was applied. The effective SIF is defined in Eq. (5.11) where *U* is the Newman crack-opening factor in McClung's SIF formulation. The opening ratio is also expressed in Eq. (5.13):

$$\Delta K_{eff} = U\Delta K \tag{5.11}$$

$$U = \frac{1 - \frac{K_{op}}{K_{max}}}{1 - R} \tag{5.12}$$

$$\frac{K_{op}}{K_{max}} = C_0 + C_0 R + C_1 R^2 + C_2 R^3 \tag{5.13}$$

with coefficients:

$$C_0 = 0.255\left[\cos\left(\frac{\pi}{2}\frac{K_{max}}{K_0}\right)\right]^{\left(\frac{1}{3}\right)} \tag{5.14}$$

$$C_1 = 0.202\left(\frac{K_{max}}{K_0}\right)$$

$$C_3 = 2C_0 + C_1 - 1$$

$$C_2 = 1 - C_0 - C_1$$

and (with Y omitted from K0 to avoid double counting geometry). is obtained using the FE model from the J-integral value at . An SIF threshold ΔKth from Table 4.2 is used where noted. These ingredients are then employed in the Paris-Erdogan crack growth law. Along with this approach for validation of the LEFM implementation for weld root analysis, a companion set of FE models was developed for analyzing the same PJP butt joint, under the same loading conditions, using the notch stress approach as in figure 20. Specifically, a 2-D plane-strain model was established with 1-mm keyholes at the two roots and a unit remote tension applied.

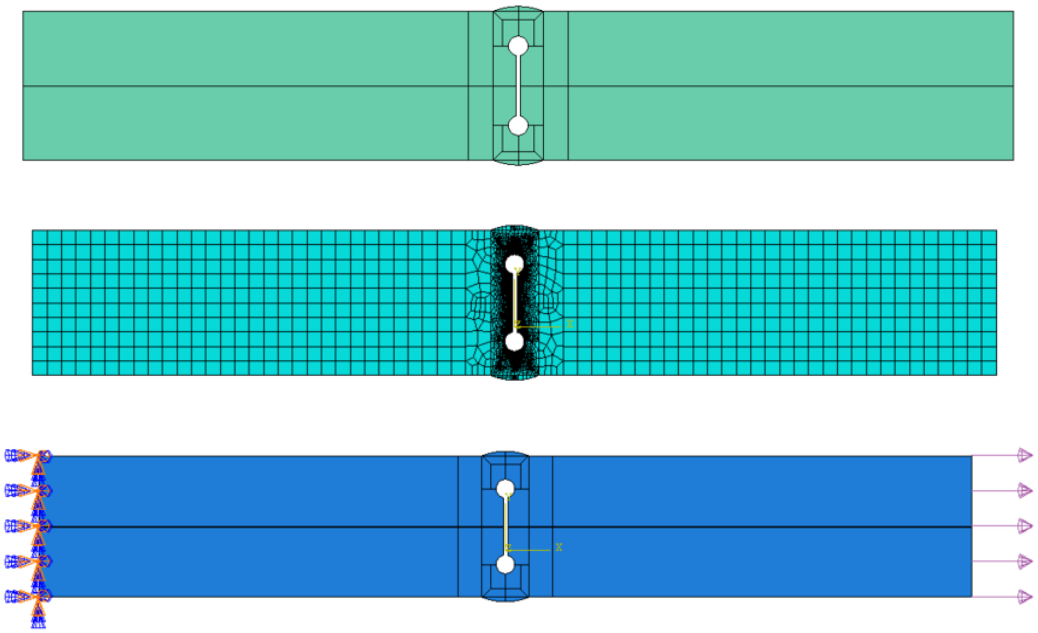

Figure 20. PJP Butt joint using notch stress approach

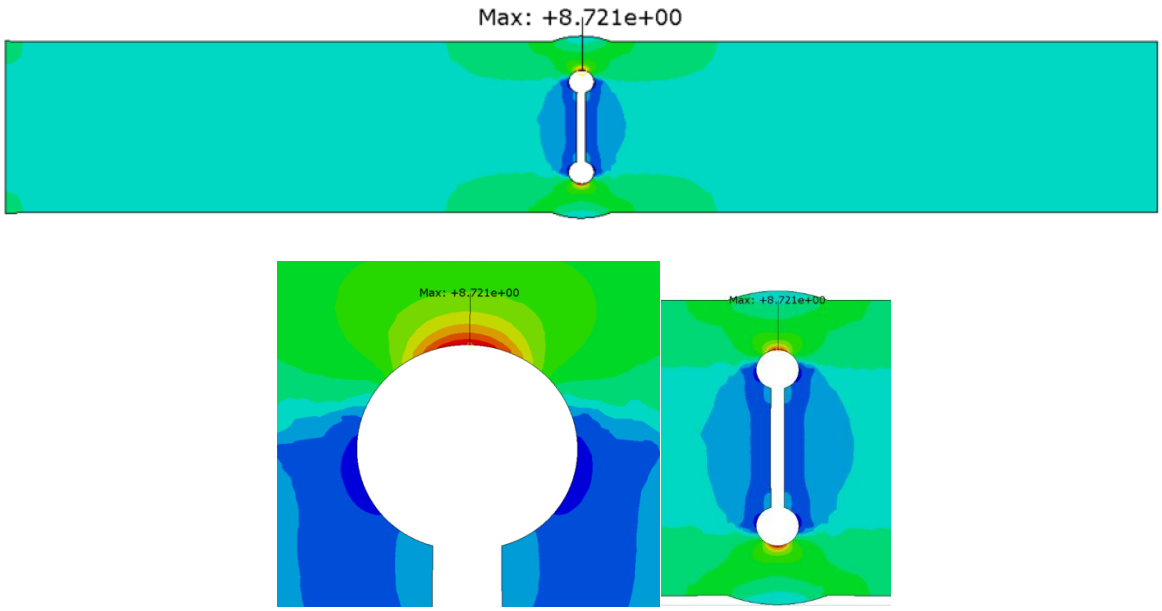

Figure 21. SCF at root

The output of this analysis was a root stress concentration factor (SCF) K_t^{root} (see Figure 21.). Using the FAT = 71 MPa S-N curve, with a slope of m = 3.64, based on [8] for the notch stress approach, the fatigue life, Nf, for any nominal stress range, ΔS, can be calculated as:

$$N_f = N_C \left(\frac{FAT}{K_t^{root} \Delta S}\right)^m, N_C = 2 \cdot 10^6 \quad (5.15)$$

Figure 22 compares this notch-stress design line with the LEFM prediction and Gérin's test data expressed in terms of net-section stress range Δσ. The LEFM curve tracks the data across the life range, whereas the notch-stress line intersects the trend near N ≈ 105 cycles and is non-conservative at short lives and increasingly conservative at long lives due to its fixed slope of m = 3.64 and the surrogate (rounded) root representation.

In this figure, additional notch stress curves are added for predictions made using CSA S6 Detail Category B, rather than the FAT 71 curve normally used for notch stress analysis. This suggests that the use of CSA S6 Cat. B for notch stress analysis of weld root failures may be reasonable and appropriate.

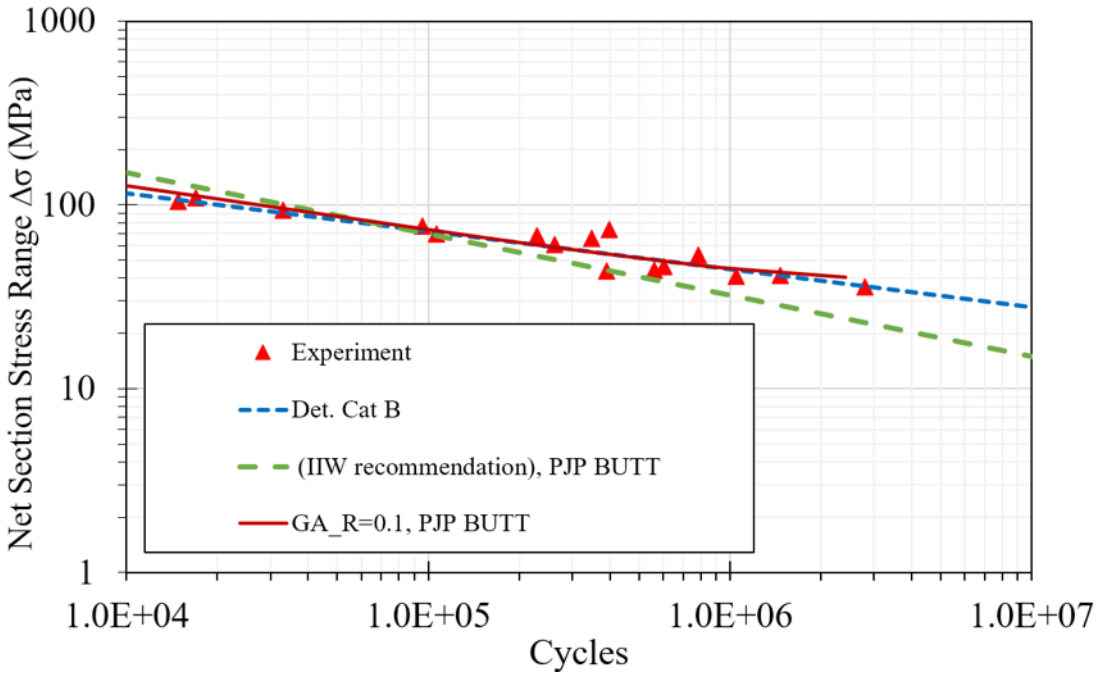

Figure 22.S-N for tested samples with R = 0.1 vs. notch stress and LEFM results

5.3 Application

After validating the weld toe and weld root procedures, the methods were applied to representative aluminum welded joints. The purpose of this application was to evaluate how fatigue resistance changes with joint geometry, plate thickness, penetration depth, and lack-of-penetration ratio. Two joint types were considered: the PJP Butt joint and the cruciform joint.

5.3.1.1 Weld Reinforcement Study

The PJP Butt joint was assessed mainly using the validated weld root fracture mechanics approach. The cruciform joint was assessed using the validated weld toe or structural stress approach, depending on the governing crack initiation location. This application stage is important because validation alone only shows that a method can reproduce known data; application demonstrates how the method can be used as a design tool for geometries relevant to aluminum infrastructure. The unfused root behaves as a crack-like flaw, and increasing lack of penetration increases the crack-driving force. Therefore, LEFM and Abaqus J-integral methods provide a rational basis for PJP butt-joint fatigue assessment. The validation also establishes the boundary between validation and comparison. Agreement with PJP experimental data or independent *J/K* output validates the method. Agreement with another fitted formula only verifies consistency with that formula.

Table 6.Study method.

Study method	Primary quantity	Fatigue mechanism	Use
Effective notch stress	Kt and local notch stress	Toe or root stress concentration	Identify governing location and fatigue capacity
LEFM / J-integral	ΔK, J, crack-growth life	Root crack propagation	Validate root-controlled fatigue response

CSA Report Fitted Equation	In and SR/SRC	Root-defect severity	Compare with report-based analytical surface
Frank-Fisher	SR/SRC expression	Penetration-based empirical trend	Simplified comparison with previous work

The PJP butt joint represents the primary application of the root fatigue assessment method. In this joint, incomplete penetration creates a root discontinuity that behaves as an initial crack. As a result, fatigue resistance is governed mainly by the size of the unfused region and the stress range acting across the effective or net section (see figure 23).

Table 7.Table of Parameters for Notch Stress PJP Butt Joint with reinforcement

Symbol	**Parameter**	**Value**	**Unit**
t_p	Plate thickness	10, 15, 20, 25	mm
h	Reinforcement height	0.1, 0.2, 0.5, 1.00	mm
m	Paris-law exponent	3.64	-
C	Paris-law coefficient	1.0×10^{-13}	Consistent Paris-law units
γ	S–N curve constant	8.94×10^{11}	-
r	Notch radius	1	mm

Table 8.Table of parameters for PJP Butt joint with reinforcement.

Symbol	**Parameter**	**Value**	**Unit**
tp	Plate thickness	10, 15, 20, 25	mm

Symbol	Parameter	Value	Unit
S	Applied stress	1	MPa
L	Specimen length	100	mm
E	Young's modulus	70,000	MPa
2a	weld depth	5	mm
ν	Poisson's ratio	0.33	-
a_i	Initial crack length	2.5	mm
θ	Weld angle	45	degree

The geometry of the PJP butt joint is described using the plate thickness t_p, the effective throat or penetration depth t_e, and the initial lack-of-penetration size $2a_i$. The penetration ratio is defined as:

$$\rho = \frac{t_e}{t_p} \tag{5.16}$$

The normalized lack-of-penetration ratio is:

$$x = \frac{2a_i}{t_p} \tag{5.17}$$

The initial half-crack size can be calculated from the normalized lack-of-penetration ratio as:

$$a_i = 0.5\left(\frac{2a_i}{t_p}\right)t_p \tag{5.18}$$

The fatigue life of the PJP butt joint was calculated using the LEFM-based crack growth relationship.

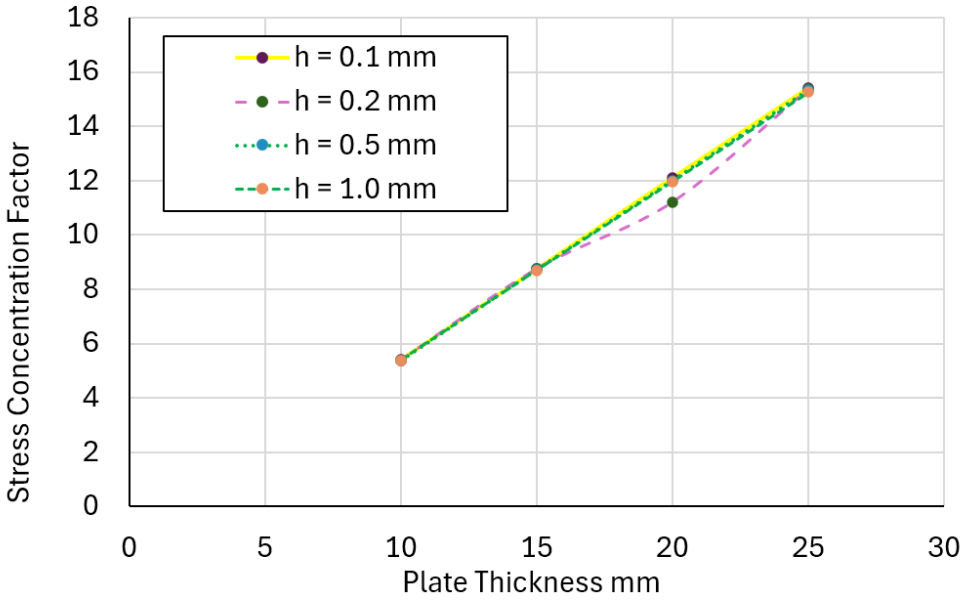

Figure 23.SCF model of butt joints withs several Reinforcement

The unfused root behaves as a crack-like flaw, and increasing lack of penetration increases the crack-driving force. Therefore, LEFM and Abaqus J-integral methods provide a rational basis for PJP butt-joint fatigue assessment. The validation also establishes the boundary between validation and comparison. Agreement with PJP experimental data or independent *J/K* output validates the method. Agreement with another fitted formula only verifies consistency with that formula.

$$N_f = \int_{a_i}^{a_f} \frac{da}{C\left[Y\,\Delta\sigma\sqrt{\pi a}\right]^m} \tag{5.19}$$

where $\Delta\sigma_n$ is the net-section stress range. The use of net-section stress is important because the effective load-carrying area is reduced by incomplete penetration. As the lack-of-penetration ratio increases, the effective section decreases, the stress intensity factor increases, and the predicted fatigue life decreases.

5.3.2 Verification of Fisher and Frank formula and CSA formula for butt joint

The normalized fatigue capacity was expressed using the ratio $\frac{S_R}{S_R^C}$, where SR is the predicted fatigue stress range for the PJP butt joint and $S_R^C$is the reference fatigue stress range associated with the relevant design or comparison curve in Equation 5.20. This normalization allows the parametric results to be compared across different thicknesses and defect sizes. The parametric analysis considered combinations of plate thickness and lack-of-penetration ratio.

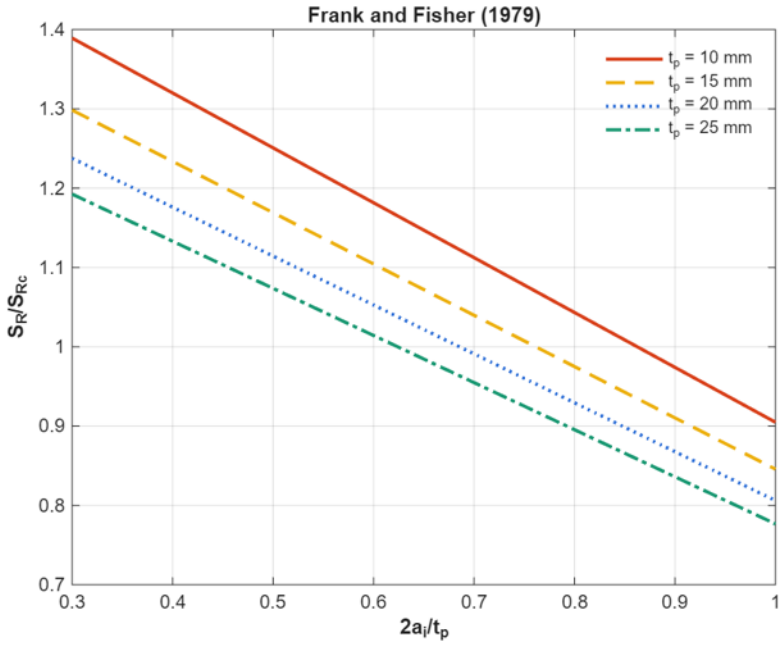

Figure 24. Fisher and Frank validating model

The application results show that the lack-of-penetration ratio is the governing geometric parameter. As $x = \frac{2a_i}{t_p}$ increases, the normalized fatigue capacity decreases. This trend is predicted by all methods that include root severity, including LEFM, CSA Report formulation 5.24, and the modified Frank-Fisher expression. The physical explanation is direct: increasing x increases a_i, decreases the remaining effective throat, increases ΔK at the same stress range, and therefore reduces the allowable stress range for the same target fatigue life.

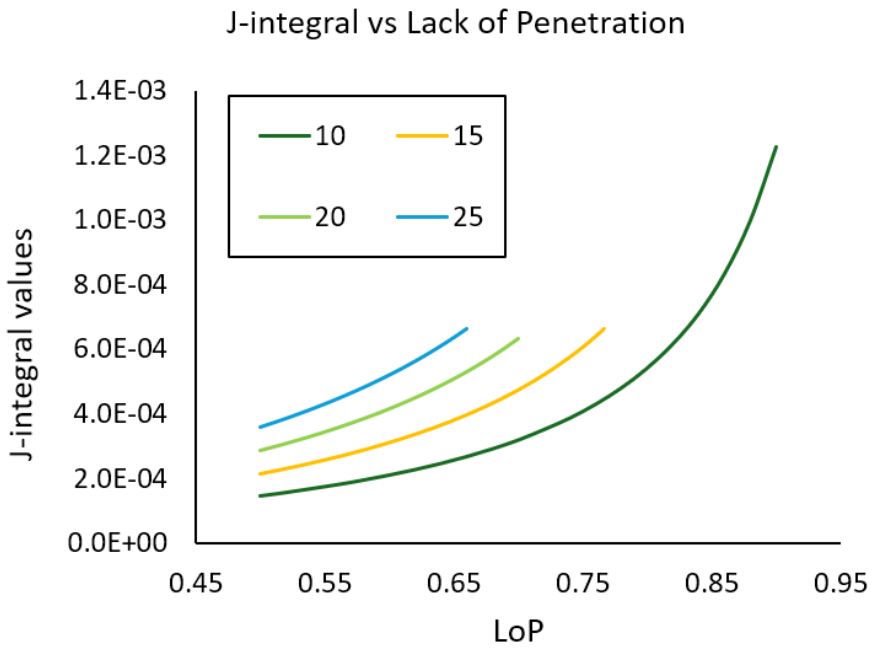

Figure 25. Comparison between J-integral vs Lack of penetration- PJP Butt Joint

The effect of plate thickness is more subtle (see figure 25, 26). For a fixed normalized lack-of-penetration ratio, a thicker plate produces a larger absolute crack size because $a_i = 0.5xt_p$. This can increase the crack-driving force. At the same time, thickness may affect geometry correction, constraint, and stress distribution. Therefore, thickness appears in the design surface, but the dominant trend remains controlled by x. The design implication is that penetration quality should be treated as a primary fatigue design variable rather than as a secondary fabrication detail. The Abaqus/LEFM application provides the most physically transparent assessment because it calculates crack-driving force from the modeled butt-joint geometry. If $K_{ref}(a)$ in Equation 5.4 is extracted at several crack sizes, then Equation 5.6 provides a rigorous crack-growth capacity calculation. If only one K value is available for each initial crack size, the result should be described as an approximate capacity estimate and should

be checked against additional crack sizes or experimental data before being converted into a design recommendation.

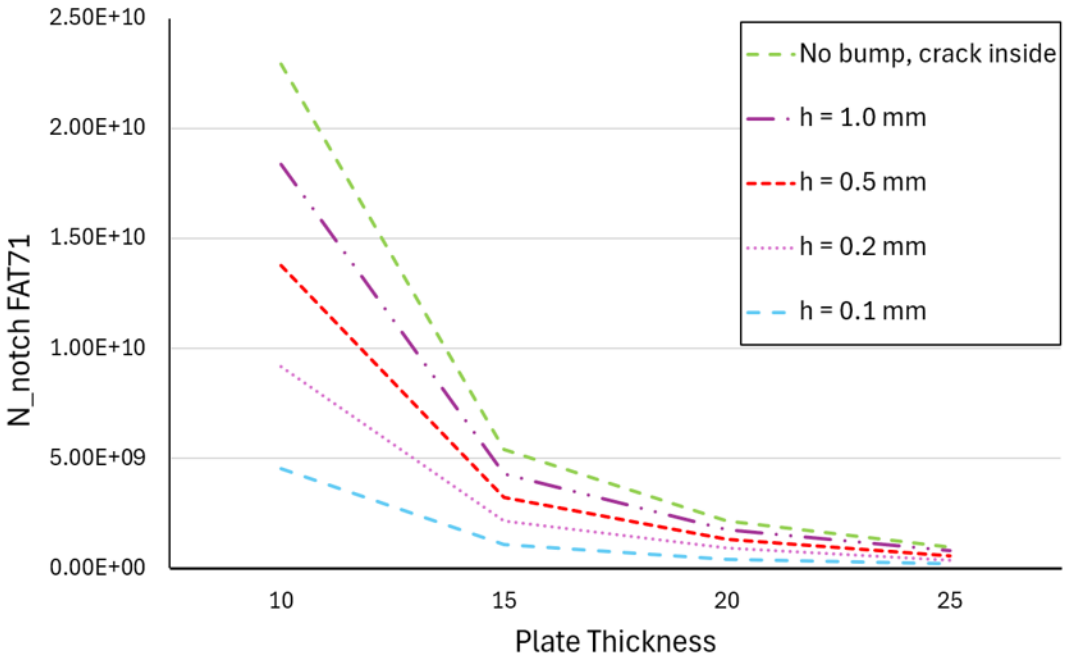

Figure 26. NS vs t_p for Butt joint with reinforcement

However, for PJP butt joints, the root is a real crack-like flaw, so notch stress alone does not fully represent crack propagation. The effective notch stress application provides a local elastic severity measure at the weld root or weld toe. It is useful for comparing local stress amplification between geometries.

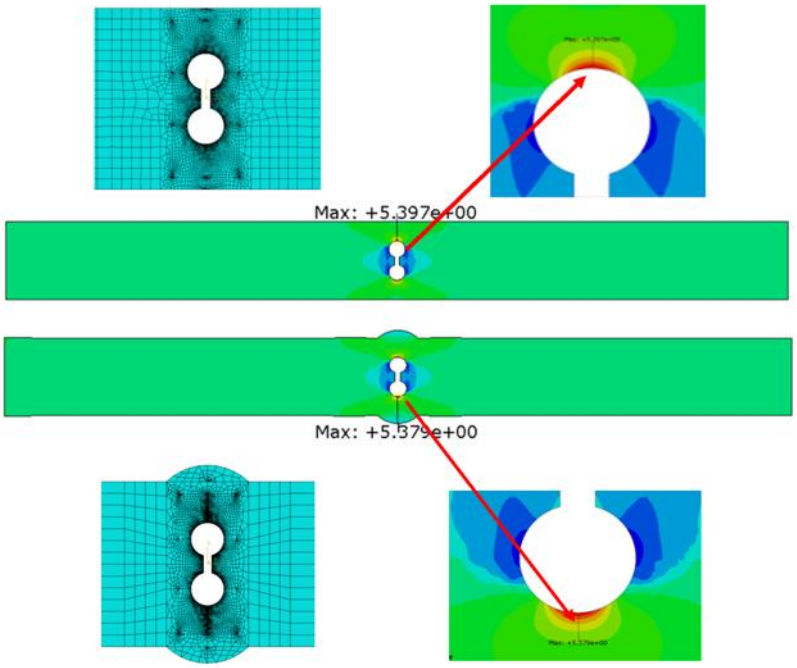

Figure 27.Butt Joint with Reinforcement, Notch stress approach

The Equation 5.24 and Frank-Fisher Equation 5.25 comparisons provide design context. They are useful because they give smooth $\frac{SR}{S_R^C}$ curves and surfaces that can be compared against LEFM or Abaqus-derived points. However, they must not be treated as independent validation data. If markers lie exactly on the CSA Report Equation 5.24 [45] curve, this is expected when the markers were generated from the same equation. That result verifies calculation consistency, not physical validation. A real butt-joint geometry effect must enter through independently calculated *Y(a), J, K,* or experimental PJP data (see figure 26).

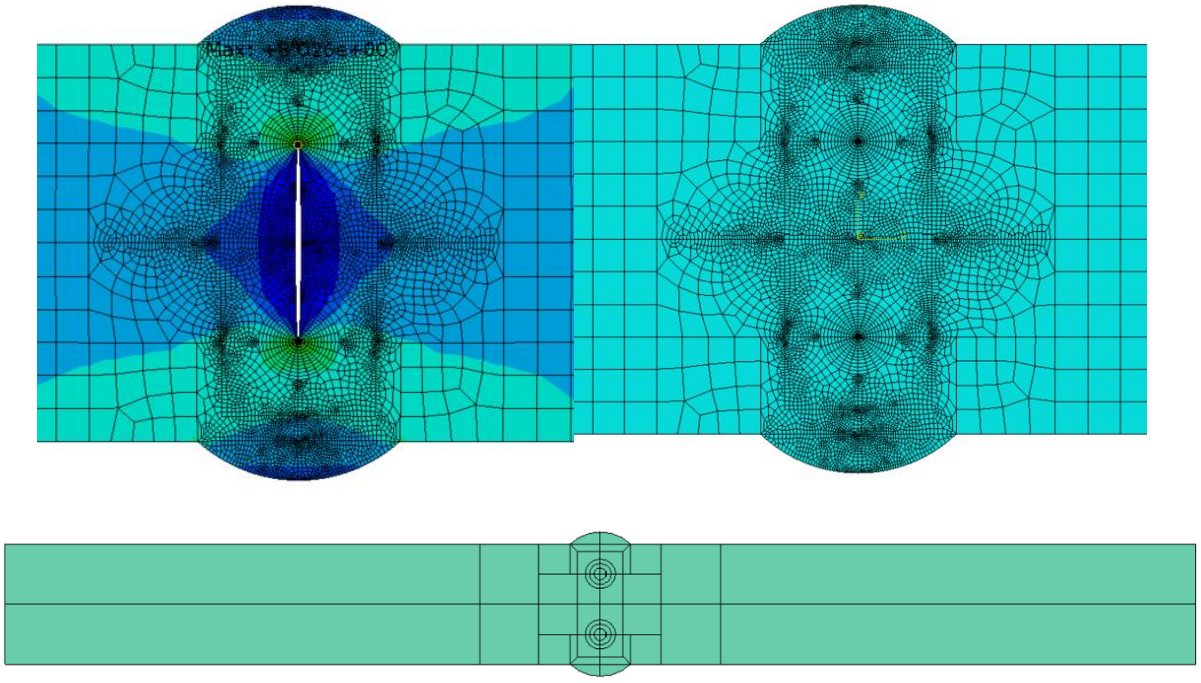

Figure 28. PJP Butt Joint with Reinforcement, J-integral Approach Simulation

The results show that normalized fatigue resistance decreases as the lack-of-penetration ratio increases. This trend is expected because a larger unfused root region corresponds to a larger initial crack. Since ΔK is proportional to $\sqrt{a}$, even moderate increases in initial crack size can significantly increase the crack driving force. The influence of plate thickness is more complex. When the defect size is normalized by plate thickness, the direct thickness effect is partly reduced. However, thickness can still affect the stress intensity factor through geometry correction factors, crack shape, constraint conditions, and the assumed final crack size. Therefore, the PJP butt joint results should be interpreted using both normalized defect size and actual plate thickness.

The key outcome of the PJP butt joint application is that root fatigue is highly sensitive to incomplete penetration. This confirms that PJP Butt welds should not be evaluated only using nominal weld strength or gross-section stress. Instead, the lack of penetration must be explicitly

included in the fatigue assessment. The main conclusion for the PJP Butt joint is that root-fatigue behaviour is controlled by the severity of the incomplete penetration (see figure27, 28).

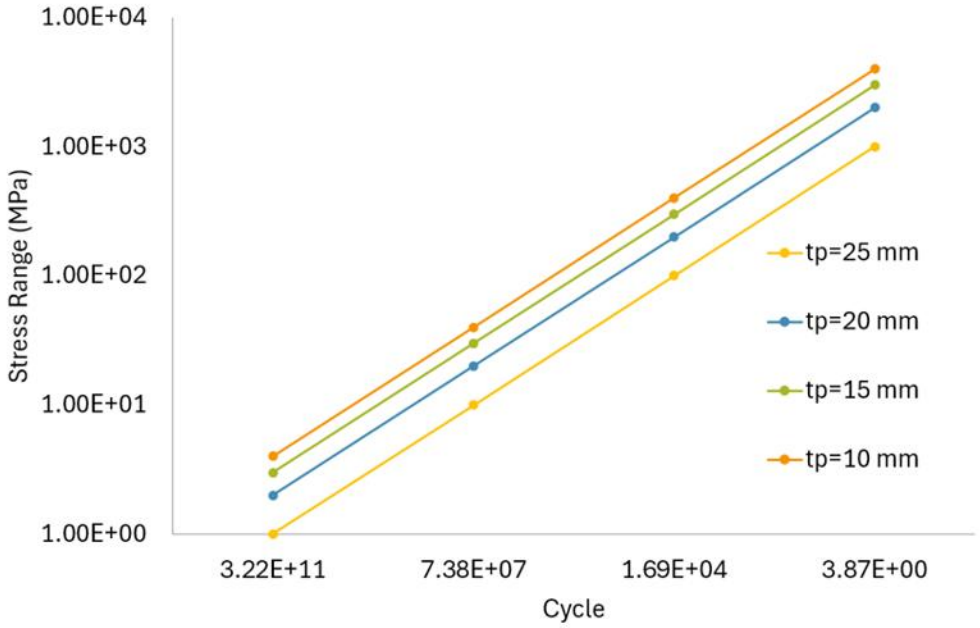

Figure 29.LEFM calculation at Root for PJP Butt Joint

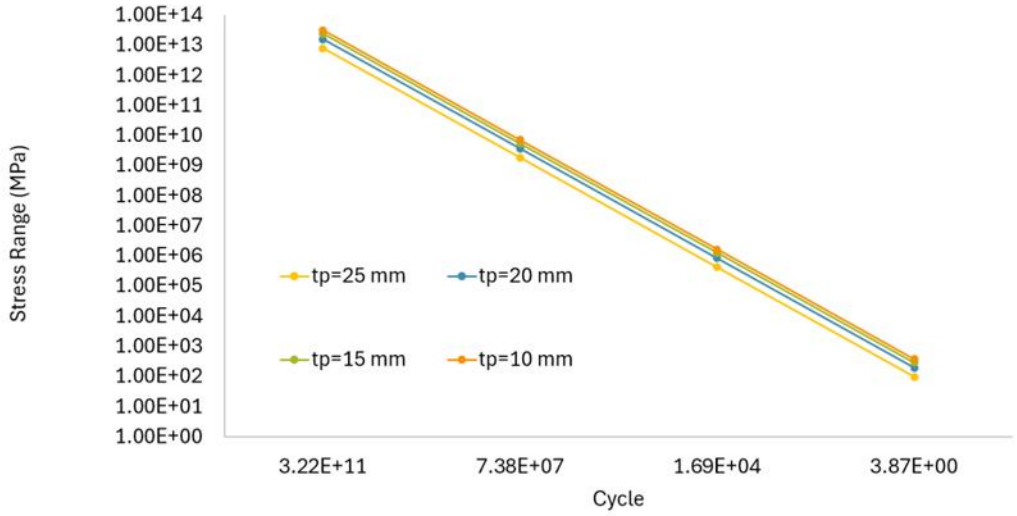

Figure 30.LEFM calculation at Toe for PJP Butt Joint

The root and toe stress-life calculations were performed to convert the LEFM-based crack-growth predictions into conventional S-N relationships suitable for fatigue design interpretation. Reference crack-growth lives calculated at a unit stress range were scaled using the Paris-law exponent to generate stress-life curves for each plate thickness. These curves were evaluated at a target life of two million cycles to determine the corresponding root and toe fatigue strengths. The root-to-toe strength ratio was then used to identify the governing fatigue location and quantify the relative severity of root cracking (see figure 27). For all investigated thicknesses, the root fatigue strength was substantially lower than the toe fatigue strength, indicating that the weld root controlled the predicted fatigue performance.

Table 9. Table of results of fatigue calculations.

Thickness, tp (mm)	**Toe strength (MPa)**	**Root strength (MPa)**	**Root/Toe ratio**
10	64.66	24.97	**0.3861**
15	64.90	26.46	**0.4078**
20	64.99	26.84	**0.4129**
25	65.04	27.01	**0.4153**

The normalized capacity surfaces are useful for design interpretation because they translate detailed crack-growth mechanics into a practical capacity index as in figure 29. Nevertheless, the final design use of these surfaces requires calibration against independent PJP experimental data or a larger set of Abaqus-derived crack-growth calculations.

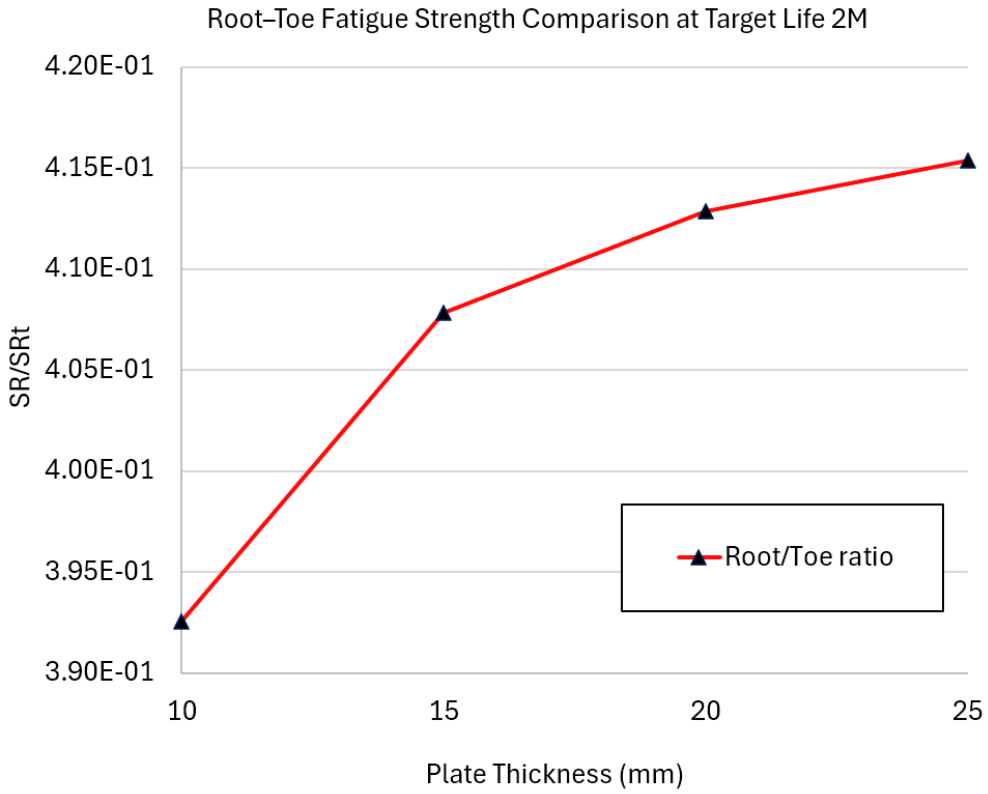

Figure 31.SR/SRt at Root and Toe_ PJP Butt Joint

The ratios range from approximately 0.39 to 0.42 (see figure 25, 30, and table 9). Consequently, the predicted root fatigue strength is only about 39% to 42% of the predicted toe strength. The weld root therefore controls the fatigue performance for all four thicknesses. The toe strength changes very little with thickness, whereas the root strength increases slightly but remains substantially lower.

The stress-intensity factors obtained from the Abaqus J-integral analysis were consistently higher than those calculated using the analytical LEFM solution. This difference is mainly due to the more realistic representation of the structure in the finite element model. The analytical LEFM approach assumes an idealized Mode I crack under uniform tensile loading and uses a simplified correction for finite specimen width. In contrast, the Abaqus model captures additional effects that occur in the actual welded joint, including stress concentrations at the PJP weld root, stress redistribution in the remaining ligament, crack-tip constraint, and possible local bending or mixed-mode loading.

As the crack grows, the gap between the Abaqus and analytical results becomes larger. This trend suggests that the influence of the remaining ligament becomes increasingly important as the crack length approaches the plate thickness. Because the Abaqus model accounts for these effects, it predicts higher stress-intensity factors, which in turn lead to faster crack growth rates according to the Paris law, shorter fatigue lives, and lower normalized SR/SRC capacities compared with the analytical LEFM predictions. The analytical LEFM method predicts a higher normalized capacity than the J-integral, FF, and CSA methods because its simplified geometry factor underestimates the crack-driving force for the actual PJP weld-root geometry. It is therefore less conservative and should be validated or calibrated against the J-integral or experimental results before being used for design (see figure 32).

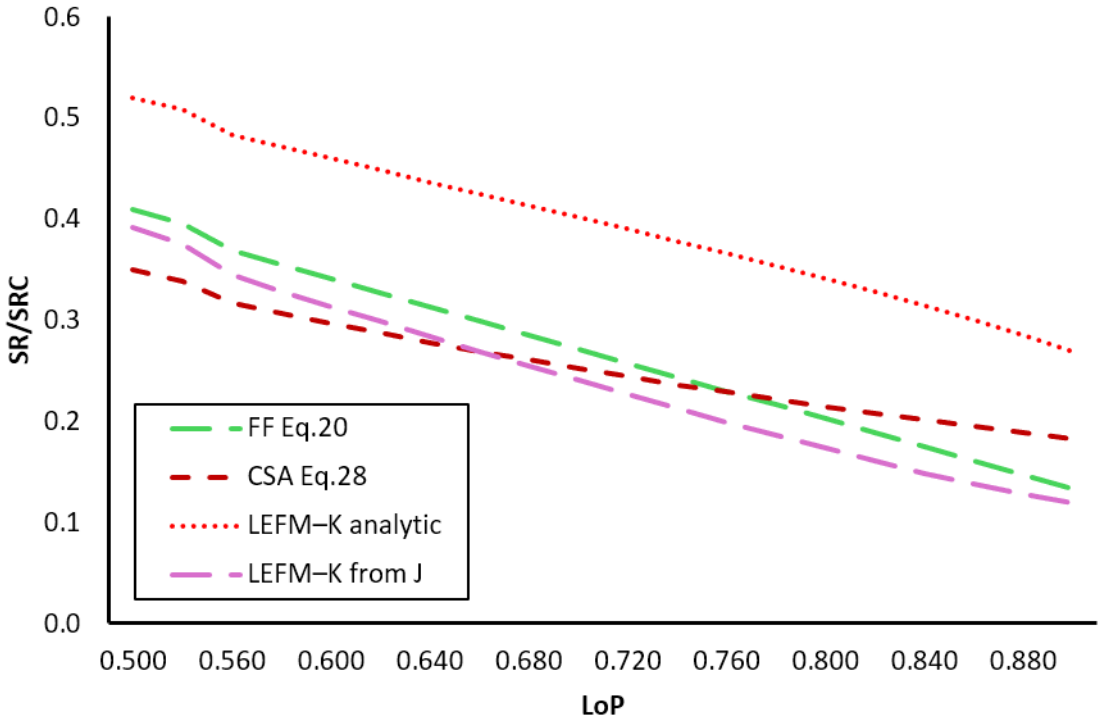

Figure 32. (t_p = 10 mm) Two-dimensional comparison showing the influence of lack-of-penetration ratio on predicted fatigue capacity

Because the finite-element model represents the PJP geometry and the remaining ligament more realistically, the Abaqus-derived (K) values increase more rapidly as the crack grows. For example, for the 10 mm plate, the Abaqus stress-intensity factor was approximately 14% higher than the analytical result at (a=2.5) mm, 31% higher at (a=3.3) mm, and more than twice the analytical value at (a=4.4) mm. The increasing separation indicates that the simplified analytical solution becomes less representative as the crack approaches the final ligament condition.

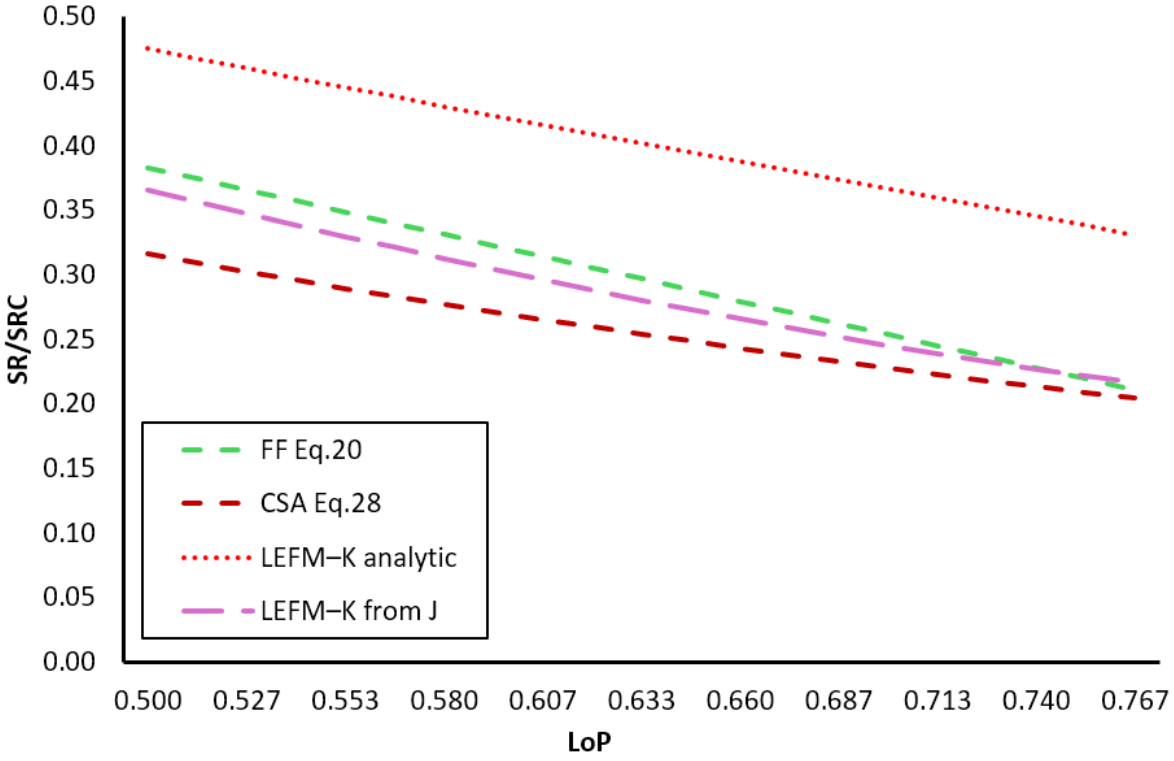

Figure 33. (t_p = 15 mm) Two-dimensional comparison showing the influence of lack-of-penetration ratio on predicted fatigue capacity

The higher Abaqus stress-intensity factors result in faster predicted crack growth according to the Paris law. Therefore, the Abaqus (J)-integral method produces shorter fatigue lives and lower ($\frac{S_R}{S_R^C}$) values than the analytical LEFM method. This explains why the analytical curve can appear higher in the normalized-capacity graphs even though the Abaqus curve is higher in the stress-intensity-factor graph. A higher (K) represents a more severe crack-driving condition and consequently a lower allowable fatigue stress range.

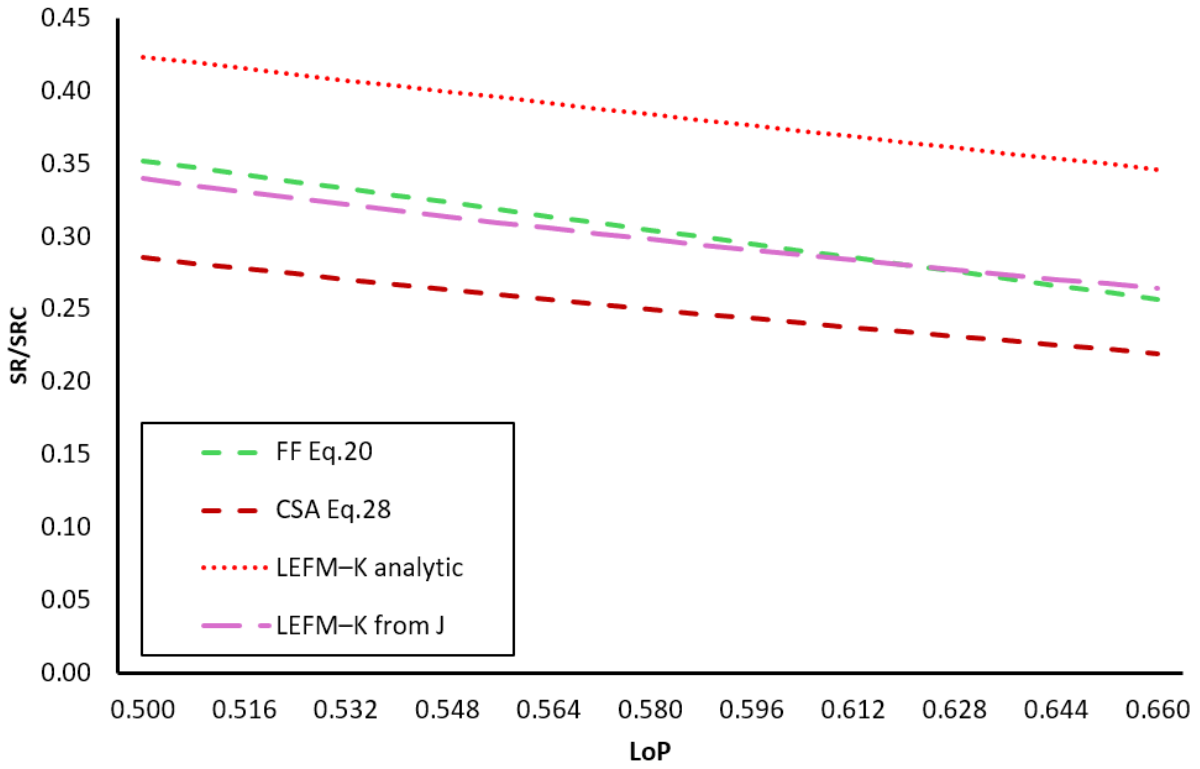

Figure 34. (t_p =20 mm) Two-dimensional comparison showing the influence of lack-of-penetration ratio on predicted fatigue capacity

CSA Report Equation 28 generally produced lower normalized fatigue capacities than the analytical LEFM method and provided a conservative estimate for most of the investigated PJP butt-joint configurations. It also remained below the Abaqus (J)-integral results for all evaluated 15, 20, and 25 mm plate cases and for the 10 mm plate up to approximately ($\frac{2a_i}{t_p}$ = 0.66). This agreement indicates that Equation 28 appropriately represents the adverse influence of plate thickness and incomplete penetration without requiring a detailed fracture-mechanics model.

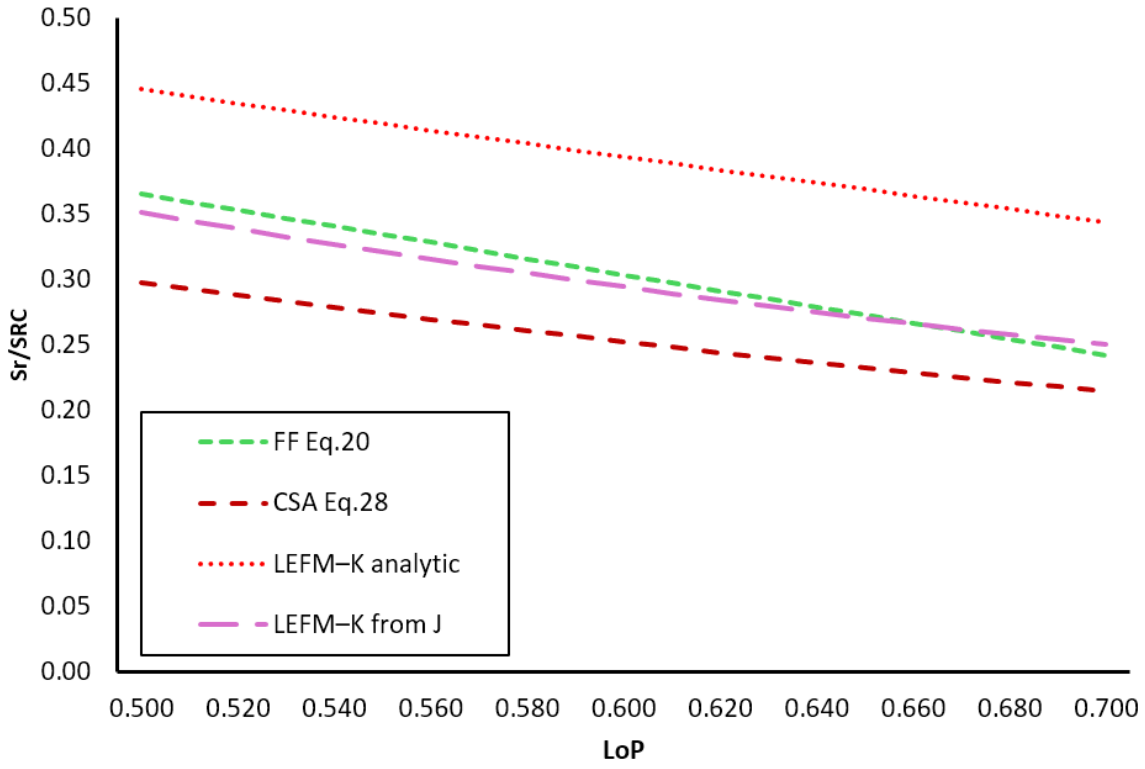

Figure 35. (t_p = 25 mm) Two-dimensional comparison showing the influence of lack-of-penetration ratio on predicted fatigue capacity

The key outcome of the PJP butt joint application is that root fatigue is highly sensitive to incomplete penetration (see figure 31, 32, 33, 34, 35). Equation 28 is therefore recommended within the investigated range where it provides a conservative lower-bound estimate, while geometry-specific Abaqus analysis remains preferable for very large lack of penetration, unusual weld geometries, or critical structural details.

Overall, CSA Report Equation 28 offers the most practical balance between simplicity, conservatism, and engineering applicability for the investigated PJP butt joints. The Abaqus (J)-integral approach should be retained as the more detailed verification method for cases where the remaining ligament is small or where the consequences of fatigue failure are significant.

5.3.3 Cruciform Joint

Cruciform joints are important comparison cases because they can experience either toe-controlled or root-controlled fatigue depending on weld size, penetration, attachment stiffness, and loading arrangement.

Table 10. Cruciform joint Parameters.

Parameter	**Symbol**	**Value**	**Units**
Target fatigue life	Nf	2000000	cycles
Notch FAT class	FAT	71	MPa at Nref
Reference life	Nref	2000000	cycles
Notch stress slope	mNS	3	
Category/Reference gamma	gamma	8.94E+11	
Reference slope	m	3.64	
Paris/material constant	C	7.97E-14	
Reference stress range	SRC	35.6682898	
Notch life factor	ScaleN	1	

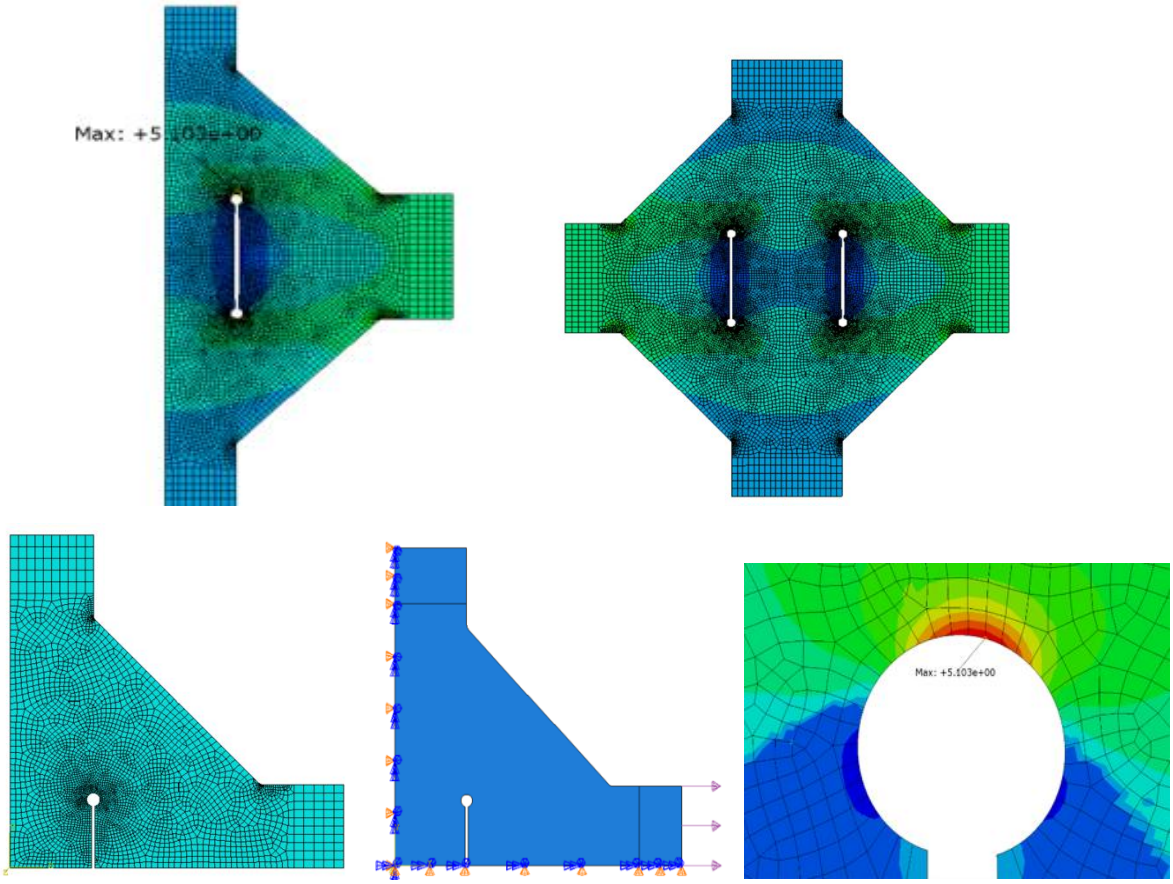

Figure 36. FE Model of Cruciform Joint

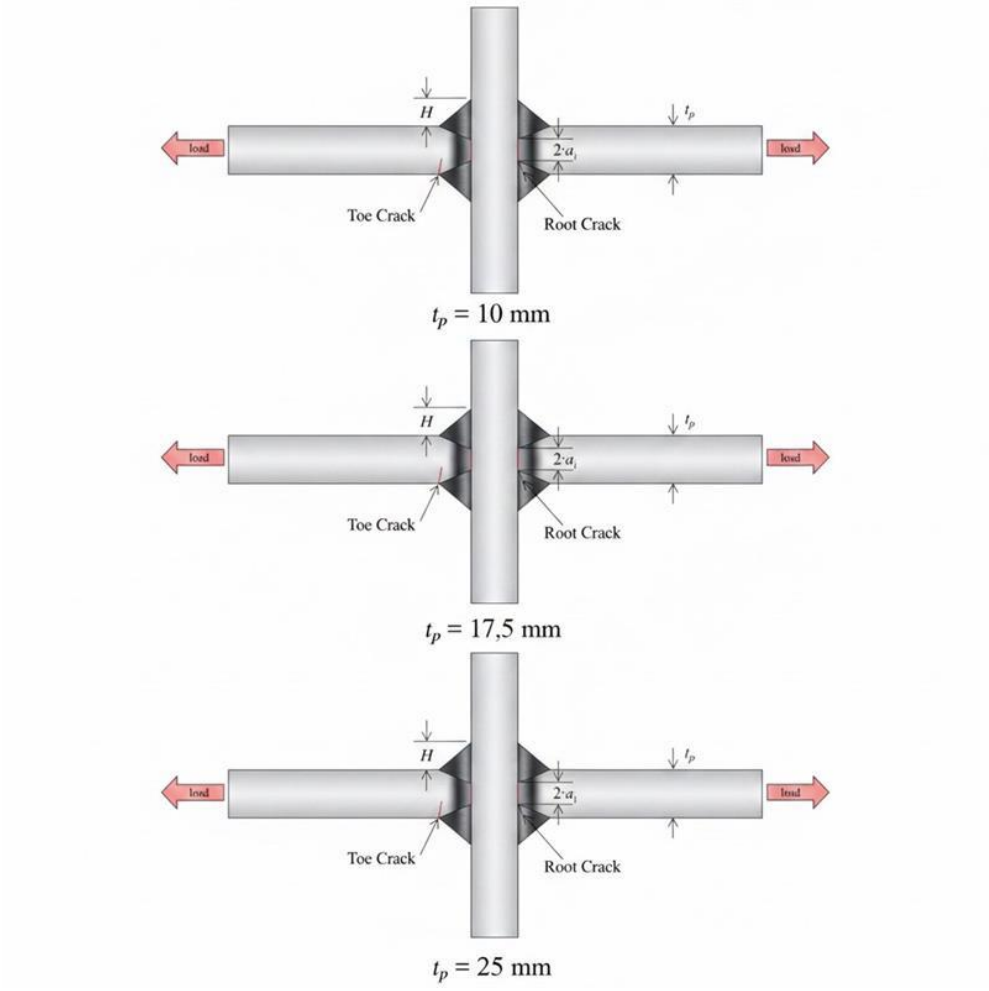

Figure 37. Cruciform Geometry with variable t_p

Table 11.Parametric variables used fatigue assessment.

Parameter	**Values or definition used in the application**	**Result**
t_p	10, 17.5, and 25 mm	Controls absolute crack size and thickness correction

Parameter	Values or definition used in the application	Result
$x = \frac{2a_i}{t_p}$	Typically, 0.4 to 1.0 for the calibrated CSA fitted-expression range	Dominant lack-of-penetration severity variable
$\frac{H}{t_p}$	H/t_p or selected H values such as H = tp mm	Represents weld height variable in fitted comparisons
N_f	2 × 10^6 cycles	Reference life for SR/SRC comparison
C, m	Paris-law constants used consistently across LEFM and fitted comparisons	Controls crack-growth rate and stress-range sensitivity
$\frac{S_R}{S_R^C}$	Normalized capacity ratio	Common output for method comparison

For root-controlled cruciform joints, fatigue cracking initiates at the weld root (see Figure 33). The local weld profile and notch radius strongly influence stress concentration. The effective notch stress method is therefore well suited for this case because it explicitly captures local elastic stress concentration at the root and toe. The fatigue assessment can be performed by comparing the effective notch stress range with an appropriate notch fatigue resistance curve (see table 10, 11).

For root-controlled cruciform joints figure 33, the fatigue mechanism becomes closer to PJP butt-joint behaviour because an unfused root region can act as an internal crack-like flaw. In this case, LEFM becomes more appropriate because it directly includes initial crack size and crack-growth rate. However, the stress field in a cruciform joint is still not identical to the

stress field in a PJP butt joint. The cruciform joint includes transverse attachment stiffness, weld leg geometry, load transfer effects, and possible toe/root interaction. These features can change Y(a), J, and K compared with a straight butt joint. For cruciform joints, the following procedure was applied. The fatigue study is as follows:

$$\Delta\sigma_{\mathrm{Notch}} = \mathrm{K_t}\Delta\sigma_{\mathrm{nom}} \tag{5.21}$$

and capacity ratio is approximately the ratio of a reference stress concentration to the actual notch stress concentration, meaning higher local stress concentration reduces fatigue capacity:

$$\frac{\mathrm{S_R}}{\mathrm{S_R^C}} \approx \frac{\mathrm{K_{ref}}}{\mathrm{K_t}} \tag{5.22}$$

The stress concentration factor K_t is obtained from finite element analysis by extracting the surface stress near the weld toe and applying the selected extrapolation method, a higher $\mathrm{K_t}$leads to greater local stress, resulting in reduced capacity. In contrast, a lower $\mathrm{K_t}$reduces stress concentration and therefore increases capacity.

$$\mathrm{I_n} = \exp\left[-5.9871 - 2.4975\left(\frac{2\mathrm{a_i}}{\mathrm{t_p}}\right) + 0.2146\left(\frac{2\mathrm{a_i}}{\mathrm{t_p}}\right)^2 + \frac{6.4101}{\sqrt{\mathrm{t_p}}}\right] \tag{5.23}$$

$$\frac{\mathrm{S_R}}{\mathrm{S_R^C}} = 0.71\left(1 + \frac{2\mathrm{H}}{\mathrm{t_p}}\right)\left(\frac{\mathrm{I_n}}{\gamma\mathrm{C}}\right)^{1/\mathrm{m}} \tag{5.24}$$

$$\frac{\mathrm{S_R}}{\mathrm{S_R^C}} = \frac{0.71 - 0.65\left(\frac{2\mathrm{a_i}}{\mathrm{t_p}}\right) + 0.79\left(\frac{\mathrm{H}}{\mathrm{t_p}}\right)}{0.64 \cdot \left(\mathrm{t_p}\right)^{1/6}} \tag{5.25}$$

This study is critical for interpreting Equations 5.24 and 5.25. These equations are useful because they combined a fitted crack-growth or capacity trend into a simple normalized design expression. However, if the fitted expression was developed for an incomplete-penetration cruciform or transverse attachment detail, it should not be presented as direct PJP butt-joint validation. It is presented as a guiding principle that helps assess whether the PJP butt-joint results follow a reasonable trend.

The cruciform application therefore serves two purposes. First, it confirms that the validated methods can be applied to a broader class of aluminum welded details. Second, it helps separate mechanism-based interpretation from equation-based curve fitting. If the cruciform formula and PJP butt-joint LEFM results are close over part of the parameter range, this indicates trend compatibility. It does not prove that the fatigue mechanisms are identical.

Root Kt							
tp (mm)	0.4	0.5	0.6	0.7	0.8	0.9	1
25	3.5286	3.8710	4.0910	4.4090	4.5730	4.7990	5.1030
17.5	3.0044	3.2170	3.5470	3.7170	3.9610	4.1560	4.5540
10	2.3626	2.5659	2.7601	2.9900	3.2490	3.3620	3.6350

Toe Kt							
tp (mm)	0.4	0.5	0.6	0.7	0.8	0.9	1
25	3.8540	3.6670	3.7919	3.7813	3.7766	4.1550	4.0650
17.5	3.1540	3.1453	3.3129	3.3195	3.4814	3.4551	3.6801
10	2.6650	2.6560	2.7820	2.7899	2.8946	2.9475	3.0770

Figure 38.Comparison Table_ governing Kt, governing location, root-to-toe ratio, absolute difference

Figure 35 the result from Abaqus Kt**,** the root governs 16 of the 21 cases, while the toe governs 5 cases. Toe control occurs mainly at the lower $2a_i/t_p$values, while the root becomes increasingly dominant as the lack-of-penetration ratio increases.

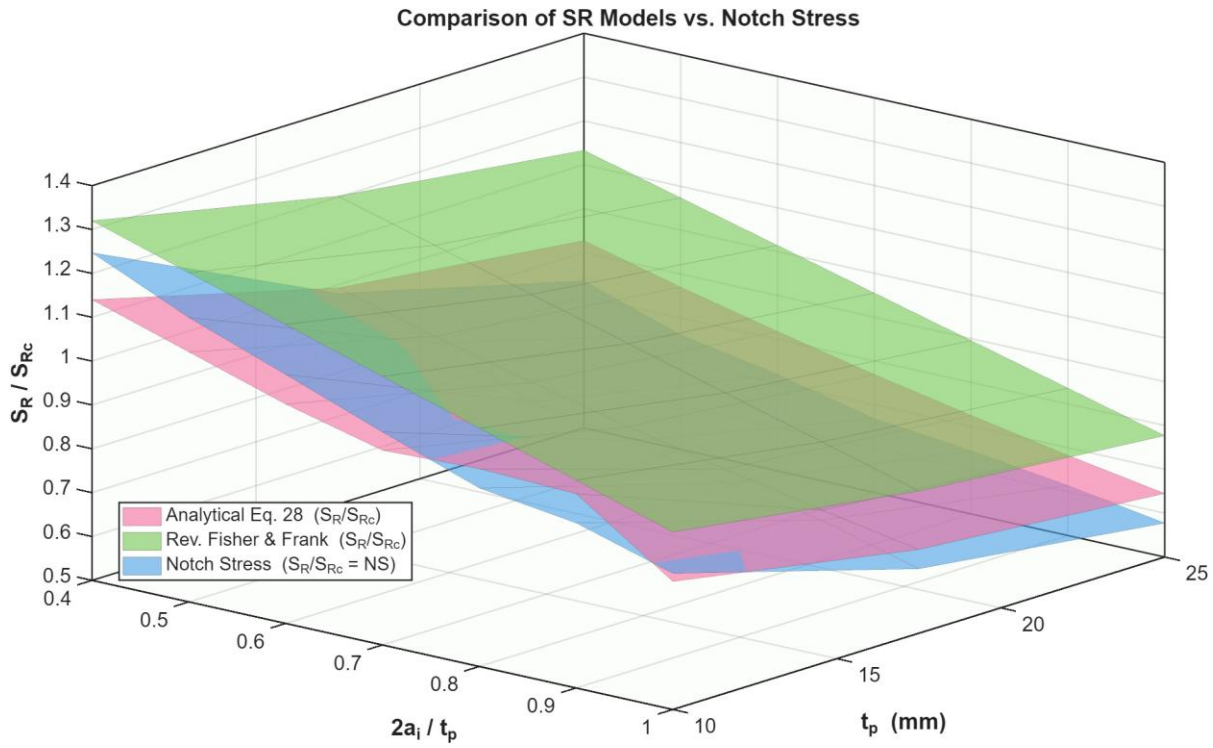

Figure 39. Combined surface comparison between notch stress, (Eq.28), and Frank-Fisher predictions

The combined surface comparison shows that the methods generally agree on the direction of the main trend: increasing lack of penetration reduces fatigue capacity. This trend agreement is important because it shows that all methods recognize the severity of the root flaw. However, the vertical separation between surfaces is equally important. Different methods represent different assumptions. Notch stress reflects local elastic stress severity. LEFM reflects crack-growth mechanics. CSA Report Equation *5.24* represents a fitted capacity surface. The Frank-Fisher Equation 5.25 represents an empirical penetration-based comparison. Therefore, differences in absolute capacity should be interpreted as differences in method conservatism and calibration, not automatically as errors.

This is a calculation-consistency check, not physical validation. A genuine difference between a butt joint and a cruciform joint will appear only when the calculation uses geometry-sensitive

quantities that are independent of the fitted formula, such as *Y(a), J, K,* or experimental fatigue lives.

5.4 Comparison with previous

The results of this study are consistent with previous research showing that fatigue assessment of welded aluminum details is highly dependent on the assumed crack initiation location, stress definition, and joint geometry.

The comparison supports the use of finite element analysis combined with appropriate stress extraction to identify the critical location which is root. Therefore, weld root fatigue, previous PJP studies have shown that incomplete penetration is the dominant fatigue parameter. The lack of penetration behaves as an initial crack, and fatigue life is also controlled by crack propagation rather than by crack initiation. This supports the use of LEFM and J-integral methods for PJP Butt joints.

Compared with nominal stress design methods, the fracture mechanics method provides a more physically meaningful assessment because it directly includes the initial root defect size. Nominal stress approaches may classify the joint using a general fatigue detail category, but they cannot explicitly account for variations in penetration ratio or lack-of-penetration size.

Cruciform formulations are often calibrated for a different weld geometry and crack path, while PJP butt joints are governed by an unfused root defect.

Therefore, the comparison with previous works leads to the following conclusions LEFM is more appropriate for PJP weld root fatigue PJP Butt joints should be assessed using methods that explicitly include lack of penetration. Cruciform-based formulas may be useful for comparison but should not be directly adopted for PJP Butt joints without validation. Finite element analysis must be supported by careful stress extraction, mesh evaluation, and, where possible, experimental validation.

Overall, the present work extends previous fatigue assessment approaches by combining weld root validation, and parametric application to PJP Butt and cruciform joints. This provides a

more complete framework for evaluating welded aluminum details where both external toe cracking and internal root cracking may be critical.

Chapter 6: Conclusions and Future Work

This thesis investigates the fatigue behaviour of aluminum welded details with particular attention to partial joint penetration (PJP) butt joints and cruciform-type welded connections assessed using analytical, fracture mechanics, and notch stress approaches. The main objective is to evaluate whether simplified fatigue design relationships can reasonably capture the fatigue capacity reduction caused by lack of penetration, plate thickness, and local weld-root stress concentration. The results are presented using normalized fatigue capacity ratios, (S_R/S_R^C), where (S_R) represents the predicted fatigue stress range of the investigated detail and (S_R^C) represents the reference Detail Category C fatigue resistance.

The results show that the weld root can be the critical region for both types of details. In PJP butt joints, the unfused region at the center of the weld behaves like a preexisting crack. Because of this, fatigue life is mainly controlled by the time required for propagation of a crack that already exists in the form of a lack of full penetration. Similarly, for cruciform welded connections, the notch stress approach shows that the local weld-root geometry creates severe stress concentration, which can significantly reduce fatigue resistance.

The normalized plots clearly show that fatigue capacity decreases as the lack-of-penetration ratio $(\frac{2a_i}{t_p})$ increases. This trend was observed consistently in both the 2D dimensional comparison plots and the 3D dimensional capacity surfaces. In practical terms, this means that as the unfused root becomes larger relative to the plate thickness, the joint becomes more vulnerable to fatigue cracking. Plate thickness also affects the results, but the lack of penetration ratio is the stronger controlling parameter.

Effectively, the normalized capacity plots are useful because they provide a clear visual way to judge whether a welded detail performs above or below the reference Category C fatigue boundary. In this study, the PJP Butt joint results remained below the Category *C* limit, showing that these details should be treated conservatively in fatigue design.

6.1 Conclusions for PJP Butt Joints

The PJP butt-joint results indicate that the investigated joints are root-critical and should not be assumed to behave as Category *C* details. In the attached plots, all calculated ($\frac{S_R}{S_R^C}$) values fall below the Category C boundary of *(1)* This means that the fatigue resistance of the PJP Butt joints is lower than the reference Category *C* resistance for the investigated range of plate thicknesses and lack of penetration ratios.

The comparison between Equation *5.24* and the modified Frank and Fisher Equation *5.25* relationship shows the same general trend; the fatigue capacity decreases as ($\frac{2a_i}{t_p}$) increases. This behaviour is expected because a larger lack of penetration ratio represents a larger initial crack-like defect at the weld root. As this initial defect increases, the stress intensity at the root also increases, which reduces the allowable fatigue stress range.

The results also show that plate thickness influences the normalized fatigue capacity. For the same lack of penetration ratio, thinner plates generally show higher capacity ratios, while thicker plates show lower values. This suggests that fatigue assessment of PJP Butt joints should not be based only on the penetration ratio. The combined effect of plate thickness and lack of penetration must be considered. Increasing lack of penetration and plate thickness generally reduce the normalized fatigue capacity, while detailed finite-element fracture mechanics predicts a more severe response than the idealized analytical solution as the remaining ligament becomes small.

Within the range investigated, CSA Report Equation (28) *5.24* provides a practical and generally conservative basis for assessing PJP butt joints. Its use is recommended for routine design and preliminary evaluation, supported by geometry-specific (J)-integral analysis for large LoP ratios, thin remaining ligaments, unusual geometries, or fatigue-critical applications. This combined approach provides a rational balance between practical design simplicity and the need for accurate assessment of crack-driven fatigue behaviour.

From a design point of view, this is an important finding. A PJP butt joint contains an inherent root flaw, therefore, fabrication quality, weld inspection, and realistic assumptions about achieved penetration are essential when PJP butt joints are used in fatigue sensitive aluminum welds.

6.2 Conclusions for Cruciform Joints

The cruciform notch stress results show the combined surface plot at *(N_f = 2,000,000)* cycles, the results indicate that the root is the dominant fatigue critical location. This result is reasonable because the notch stress approach directly captures the local stress concentration at the weld root. Instead of relying only on a simplified nominal stress equation, it considers the local geometry of the weld root and the stress amplification caused by the notch. For welded details such as cruciform joints, where the local geometry strongly affects fatigue behaviour, this method provides a more direct and conservative assessment.

The combined plot also shows that the analytical Equation *5.24* surface gives intermediate results, while the Frank and Fisher surface gives the highest capacity ratios. This separation between the three surfaces shows that the selected fatigue assessment method has a major influence on the predicted fatigue capacity.

In practical design, this means that simplified equations may be suitable for preliminary comparison, but a local stress method may be more appropriate when the detail is fatigue-critical or when no standard detail category is available.

The notch stress approach is especially useful for complex welded connections because it can represent the local root stress concentration more realistically than a nominal stress method. This conclusion is based on the comparison between the weld toe and weld root stress concentration factors obtained from the finite element models. For most of the investigated geometries, the exceeded $K_{t,root}$, indicating that the maximum local stress occurred at the weld root. Therefore, fatigue cracking is expected to initiate from the weld root in most cases.

The cruciform results follow the same overall trend as the PJP Butt joint results; increasing lack of penetration reduces fatigue capacity. This confirms that root condition is also prone to fatigue and important factors in the fatigue performance of aluminum welded details.

6.3 Comparison Between PJP and Cruciform Welds

The PJP Butt joint and cruciform notch stress results show similar trends, but they should not be interpreted as identical problems. The PJP Butt joint behaves more like a center cracked plate, where the lack of penetration forms a crack like defect between two welded regions.

The cruciform detail has a different geometry, load path, and local stress field. Therefore, even if the plots show similar decreasing trends, a cruciform based equation should not be directly applied to a PJP Butt joint without careful calibration. The cruciform joint results indicate that the root is the dominant fatigue critical location. The common feature between the two cases, increasing $(\frac{2a_i}{t_p})$ reduces $(\frac{S_R}{S_R^C})$, which means the fatigue capacity decreases as the root defect becomes larger in butt joints and partially in cruciform joints. The difference is in how each method represents the stress field. The analytical methods simplify the behaviour through fitted or closed form equations, while the notch stress method captures the local root stress concentration more directly.

This explains why the notch stress surface is almost same as the analytical surfaces in the combined comparison plot. The notch stress method is more sensitive to the local weld geometry and therefore gives a more conservative prediction.

The PJP Butt joint should be discussed mainly as a fracture mechanics root crack problem, while the cruciform detail should be discussed as a local notch stress problem. Both approaches are useful, but their results must be interpreted within the application of each method.

6.4 Practical Design Implications

The results of this study have several important implications for fatigue design of aluminum welded structures.

First, PJP butt joints should not be automatically treated as Category *C* details when fatigue loading is important. The calculated capacity ratios remain below the Category *C* boundary, which indicates that either a lower fatigue category or a fracture mechanics-based evaluation should be used.

Second, the lack of penetration ratio ($\frac{2a_i}{t_p}$) should be treated as a key fatigue design parameter. As this ratio increases, fatigue resistance decreases. Therefore, design drawings and weld procedures should not only specify the nominal weld size, but should also ensure that the actual effective throat can be achieved and verified. Equation 28 is particularly suitable for preliminary design, routine engineering assessment, and conservative screening of PJP details within the range represented by this study. Its relative simplicity makes it more practical for design-office applications than a full Abaqus (J)-integral analysis. It also produced more conservative results than the analytical LEFM and Frank–Fisher methods throughout the investigated cases.

Third, the cruciform joint response should be described as predominantly root governed with limited toe governed transition cases. This finding confirms that the presence of lack of penetration does automatically produce root-controlled fatigue failure. The governing fatigue location depends on the relative severity of the weld root and stress concentration fields. Additionally, because the method depends strongly on local modelling assumptions, it should be used with proper mesh refinement, consistent notch geometry, and an appropriate fatigue curve.

Fourth, the comparison between Equation *5.24*, Frank and Fisher Equation *5.25*, and the notch stress approach shows that simplified analytical equations are useful for identifying trends and performing preliminary design checks. However, for fatigue-critical aluminum welded details, these simplified methods should be supported by local stress analysis or fracture mechanics assessment.

6.5 Future Work

- The following is a list of suggested opportunities to continue this research:
- Future research should include additional experimental testing and advanced 3D dimensional finite element modelling to validate the predicted toe and root-controlled fatigue behaviour of aluminum PJP butt and cruciform joints.
- Further calibration is particularly needed for thin and thick plates with large LoP ratios, where the Abaqus method predicted a more rapid reduction in capacity than Equation 28. Establishing a verified transition limit between simplified Equation 28 assessment and detailed fracture-mechanics analysis would improve the practical design application of the results.
- The notch stress and LEFM approaches should also be further compared against full scale weldment details so that their applicability can be clearly defined for the pedestrian bridge and highway accessory design.
- Finally, future work should aim to establish a larger fatigue database, and reliability-based calibration is needed to develop simplified design charts or equations suitable for inclusion in structural design standards such as CSA S6 and S7.

References

[1] Maddox, S. J. (2003). Review of fatigue assessment procedures for welded aluminium structures. International Journal of Fatigue, 25(12), 1359-1378.

[2] Walbridge S, de la Chevrotière A. Opportunities for the use of Aluminum in Vehicular Bridge Construction. Aluminium Association of Canada Report, MAADI Group, Montreal. 2012.

[3] Coughlin, R., & Walbridge, S. (2012). Fatigue testing and analysis of aluminum welds under in-service highway bridge loading conditions. Journal of Bridge Engineering, 17(3), 409-419.

[4] CSA (Canadian Standards Association). (2025). Canadian highway bridge design code. CAN/CSA S6:25.

[5] CSA. (2023). Pedestrian, cycling, and multiuse bridge design guideline. CAN/CSA S7:23.

[6] AA (Aluminum Association). (2020). Specification for Aluminum Structures.

[7] CEN (European Committee for Standardization) (2006). Eurocode 9: Design of aluminium structures – Part 1-3: Structures susceptible to fatigue.

[8] Hobbacher, A. (2004). Recommendations for fatigue design of welded joint and components. IIW (International Institute of Welding) Doc. XIII-1965-03/XV-1127-03.

[9] Gérin, L. (2020). Partial Joint Penetration Welds in Aluminum Structures (Master's thesis, University of Waterloo).

[10] Abdelbadie, A. (2023). Fatigue Testing and Analysis of Aluminum and Steel Partial Joint Penetration (PJP) Welds for Bridge Applications (Master's thesis, University of Waterloo).

[11] Beaulieu, D. (2006). *Design of aluminium structures* (C. Marsh, Trans.). Presses de l’aluminium.

[12] Sharp, M. L., Nordmark, G. E., & Menzemer, C. C. (1996, November). Hot-Spot Fatigue Design of Aluminum Joints. In Materials for the New Millennium (pp. 1027-1036). ASCE.

[13] Menzemer, C. C., & Fisher, J. W. (1993). Fatigue design of welded aluminum structures. Transportation Research Record, (1393).

[14] Frank, K. H., & Fisher, J. W. (1979). Fatigue strength of fillet welded cruciform joints. Journal of the Structural Division, 105(9), 1727-1740.

[15] Kissell, J. R., & Ferry, R. L. (2002). *Aluminum structures: a guide to their specifications and design*. John Wiley & Sons.

[16] Barker, R. M., & Puckett, J. A. (1987). *Design of highway bridges based on AASHTO LRFD bridge design specifications*.

[17] Janosch, J. J. (2008). International Institute of Welding work on residual stress and its application to industry. *International journal of pressure vessels and piping*, *85*(3), 183-190.

[18] Gagnon, D. P., & Kennedy, D. L. (1989). Behaviour and ultimate tensile strength of partial joint penetration groove welds. *Canadian Journal of Civil Engineering*, *16*(3), 384-399.

[19] Paris, P. C., & Sih, G. C. (1964). *Stress analysis of cracks* (No. NASA-CR-58751).

[20] Fricke, W. (2013). IIW guideline for the assessment of weld root fatigue. Welding in the World, 57, 753-791.

[21] Sharp, M. L., & Nordmark, G. E. (1977). Fatigue strength of welded tubular aluminum truss. *Journal of the Structural Division*, *103*(8), 1619–1629.

[22] Ye, N., & Moan, T. (2002). Fatigue and Static Behaviour of Aluminum Box-Stiffener Lap Joints. International Journal of Fatigue, 24(5), 581-589.

[23] CSA. (2018). Welded Aluminum Construction. CAN/CSA W59.2.

[24] Burk, J. D., & Lawrence Jr, F. V. (1976). Effects of Lack-of-Penetration and Lack-of-Fusion on the Fatigue Properties of 5083 Aluminum Alloy Welds.

[25] Menzemer, C. C. (1992). Fatigue behavior of welded aluminum structures. Lehigh University.

[26] Maddox, S. J. (2008). Status review on fatigue performance of fillet welds. *Journal of offshore mechanics and Arctic engineering*, *130*(3).

[27] Paris, P. & Erdogan, F. (1963). A Critical Analysis of Crack Propagation Laws. Journal of Basic Engineering, 85(4), 528–533.

[28] Neuber, H. (1946). Theory of notch stresses: Principles for exact stress calculation (Vol. 74). JW Edwards.

[29] Kaczinski, M. R., Dexter, R. J., & Van Dien, J. P. (1998). *Fatigue-resistant design of cantilevered signal, sign and light supports* (Vol. 412). Transportation Research Board.

[30] Azzam, D., & Menzemer, C. C. (2006). Fatigue behavior of welded aluminum light pole support details. Journal of Structural Engineering, 132(12), 1919-1927.

[31] Azzam, D., & Menzemer, C. C. (2007). Fatigue life assessment and comparison of two types of bridge-mounted welded aluminum light pole support structures. Bridge Structures, 3(1), 81-90.

[32] Bédard, S. (2000). Behavior of aluminum aerial signaling structures subjected to cyclic stresses. Master's thesis, École Polytechnique de Montréal.

[33] Hodgson, I. C., & Connor, R. J. (2003). Field instrumentation and analysis of prototype and existing light poles on the Bronx-Whitestone bridge (No. 03-17). Lehigh University.

[34] Québec Ministry of Transport and Sustainable Mobility (MTMD). (2025, December 22). *Documentation relating to structures*. www.transports.gouv.qc.ca/fr/projets-infrastructures/structures/documentation-structures/Pages/documentation-structures.aspx.

[35] Ministry of Transportation and Transit. (2025, February 27). Volume 1 - Supplement to CHBDC S6:19 - Province of British Columbia. https://www2.gov.bc.ca/gov/content/transportation/transportation-infrastructure/engineering-standards-guidelines/structural/standards-procedures/volume-1.

[36] Kalač, Š., Mensinger, M., Radlbeck, C., Zejnelagić, N., Đuričić, Đ., & Lučić, D. (2023). Experimental and Theoretical Research on Welded Aluminum K-Joints. Engineering Proceedings, 43(1), 18.

[37] van Wingerde, A. M., Packer, J. A., & Wardenier, J. (2001). Simplified SCF formulae and graphs for CHS and RHS K-and KK-connections. Journal of Constructional Steel Research, 57(3), 221-252.

[38] Radaj, D. (1990). Design and analysis of fatigue resistant welded structures. Woodhead Publishing.

[39] Morgenstern, C., Sonsino, C. M., Hobbacher, A., & Sorbo, F. (2006). Fatigue design of aluminium welded joints by the local stress concept with the fictitious notch radius of r_f = 1 mm. International Journal of Fatigue, 28(8), 881-890.

[40] Irwin, G. R. (1957). *Journal of Applied Mechanics, 24*(3), 361–364.

[41] Westergaard, H. M. (1939). *Journal of Applied Mechanics, 6*, A49–A53.

[42] Muskhelishvili, N. I. (1953). *Some basic problems of the mathematical theory of elasticity: Fundamental equations, plane theory of elasticity, torsion and bending* (J. R. M. Radok, Trans.; 3rd ed.). P. Noordhoff.

[43] Tada, H., Paris, P. C., & Irwin, G. R. (2000). *The stress analysis of cracks handbook* (3rd ed.). ASME Press.

[44] Newman Jr, J. C. (1984). A crack opening stress equation for fatigue crack growth. *International Journal of fracture*, *24*(ISSN: 0376-9429).

[45] Ahmadi, G., Dahaghin, H., Li, L., & Walbridge, S. (2026, March). *Fatigue design of aluminum highway accessory structures and active mode bridges*. Canadian Standards Association

[46] Tveiten, B. R. W., Berge, S., & Wang, X. (2011, January). Fatigue assessment of aluminum ship details by hot-spot stress approach. In International Conference on Offshore Mechanics and Arctic Engineering (Vol. 44359, pp. 549-558).

[47] Zhao, X.-L., HeDesign Guideker, J.A., Puthand RectangularekHollow SectionWeWelded Joints van Winderde, A.M., and YYeomans, N.F. (2001), CIDECT 8: Design Guide for Circular and Rectangular Hollow Section Welded Joints Under Fatigue Loading, TUV-Verlag, Koln, Germany.

[48] Foley CM, Peronto JL, Fournelle RA. Fatigue life prediction and variability of new and existing welded CHS Y-joints. Engineering Journal. 2006 Mar 31;43(1):57-64.

[49] Gitter, R. (2008). Design of aluminium structures: selection of structural alloys. Eurocodes: Background and Applications, Brussels, Belgium.

[50] Partanen T, Niemi E. (1999). Hot spot S-N curves based on fatigue tests of small MIG welded aluminium specimens. Welding in the World, 43(1):16–22.

[51] Jaccard, R. (1990). Fatigue crack propagation in aluminium, IIW Document XIII-1377.

[52] Jaccard, R., Kosteas, D., and Ondra, R. (1995). “Background document to fatigue design curves for welded aluminium components.” Doc. XIII-1588-95, International Institute of Welding (IIW), Villepinte, France.

[53] Kosteas, D. (1988). Estimating residual stresses and their effect in welded aluminum components in fatigue. In Analytical and experimental methods for residual stress effects in fatigue. ASTM International.

[54] Kosteas, D., & Gietl, B. (1996). A comparative analysis of existing test data on welded aluminium tubular joints. Fatigue & Fracture of Engineering Materials & Structures, 19(6), 731-738.

[55] CSA Group. (2017). Strength design in aluminum. CAN/CSA-S157-17.

[56] van Wingerde, A. M., Packer, J. A., & Wardenier, J. (1995). Criteria for the fatigue assessment of hollow structural section connections. Journal of Constructional Steel Research, 35(1), 71-115.

[57] Sanders, R. E., & Marshall, G. J. (2023). Aluminum: Technology, Industry, and Applications. ASM International.

[58] Fricke, W. (2003). Fatigue analysis of welded joints: state of development. Marine structures, 16(3), 85- 200.

[59] Coughlin, R. (2010). Fatigue of aluminum welds in Canadian highway bridges (Master's thesis, University of Waterloo).

[60] Maddox, S. J. (1975). An analysis of fatigue cracks in fillet welded joints. International Journal of Fracture, 11, 221-243.

[61] Ranjan, R., & Jha, S. K. (2024). Experimental investigation and optimization of impact strength during low frequency vibration assisted shielded metal arc welded joints. *Welding international*, *38*(5), 347-365.

Appendix A

PJP Butt Joint Normalized SR/SRC Results

Table A.1. Frank and Fisher – t*p* = 10 mm

t_p (mm)	$2a_i/t_p$	S_R/S_R^C
10	0.5000	0.702673
10	0.5200	0.678946
10	0.5600	0.631493
10	0.5800	0.607766
10	0.6000	0.584040
10	0.6200	0.560313
10	0.6400	0.536586
10	0.6600	0.512860
10	0.6800	0.489133
10	0.7000	0.465407
10	0.7200	0.441680
10	0.7400	0.417953
10	0.7600	0.394227
10	0.7800	0.370500
10	0.8000	0.346774
10	0.8200	0.323047
10	0.8400	0.299320
10	0.8600	0.275594
10	0.8800	0.251867
10	0.9000	0.228140

TableA.2. Frank and Fisher – t*p* = 15 mm

t_p (mm)	$2a_i/t_p$	S_R/S_R^C
15	0.5000	0.656757
15	0.5133	0.641973

t_p (mm)	$2a_i/t_p$	S_R/S_R^C
15	0.5267	0.627188
15	0.5400	0.612404
15	0.5533	0.597620
15	0.5667	0.582836
15	0.5800	0.568052
15	0.5933	0.553268
15	0.6067	0.538484
15	0.6200	0.523699
15	0.6333	0.508915
15	0.6467	0.494131
15	0.6600	0.479347
15	0.6733	0.464563
15	0.6867	0.449779
15	0.7000	0.434995
15	0.7133	0.420211
15	0.7267	0.405426
15	0.7400	0.390642
15	0.7533	0.375858
15	0.7667	0.361074

Table A. 3. Frank and Fisher – t*p* = 20 mm

t_p (mm)	$2a_i/t_p$	S_R/S_R^C
20	0.5000	0.626010
20	0.5100	0.615441
20	0.5200	0.604872
20	0.5300	0.594303
20	0.5400	0.583734

t_p (mm)	$2a_i/t_p$	S_R/S_R^C
20	0.5500	0.573165
20	0.5600	0.562596
20	0.5700	0.552027
20	0.5800	0.541458
20	0.5900	0.530889
20	0.6000	0.520320
20	0.6100	0.509751
20	0.6200	0.499182
20	0.6300	0.488613
20	0.6400	0.478044
20	0.6500	0.467475
20	0.6600	0.456906
20	0.6700	0.446337
20	0.6800	0.435768
20	0.6900	0.425199
20	0.7000	0.414630

Table A. 4. Frank and Fisher – t*p* = 25 mm

t_p (mm)	$2a_i/t_p$	S_R/S_R^C
25	0.5000	0.603156
25	0.5080	0.595010
25	0.5160	0.586863
25	0.5240	0.578717
25	0.5320	0.570570
25	0.5400	0.562423
25	0.5480	0.554277
25	0.5560	0.546130

t_p (mm)	$2a_i/t_p$	S_R/S_R^C
25	0.5640	0.537984
25	0.5720	0.529837
25	0.5800	0.521691
25	0.5880	0.513544
25	0.5960	0.505398
25	0.6040	0.497251
25	0.6120	0.489105
25	0.6200	0.480958
25	0.6280	0.472812
25	0.6360	0.464665
25	0.6440	0.456519
25	0.6520	0.448372
25	0.6600	0.440226

Table A. 5. CSA Report CSA Eq.28 t*p* = 10 mm

t_p (mm)	$2a_i/t_p$	S_R/S_R^C
10	0.5000	0.350026
10	0.5200	0.338668
10	0.5600	0.317090
10	0.5800	0.306844
10	0.6000	0.296943
10	0.6200	0.287375
10	0.6400	0.278128
10	0.6600	0.269192
10	0.6800	0.260555
10	0.7000	0.252207
10	0.7200	0.244138

t_p (mm)	$2a_i/t_p$	S_R/S_R^C
10	0.7400	0.236339
10	0.7600	0.228799
10	0.7800	0.221510
10	0.8000	0.214464
10	0.8200	0.207651
10	0.8400	0.201065
10	0.8600	0.194696
10	0.8800	0.188538
10	0.9000	0.182584

Table A. 6. CSA Report Eq.28 – t*p* = 15 mm

t_p (mm)	$2a_i/t_p$	S_R/S_R^C
15	0.5000	0.316024
15	0.5133	0.309148
15	0.5267	0.302428
15	0.5400	0.295861
15	0.5533	0.289442
15	0.5667	0.283168
15	0.5800	0.277037
15	0.5933	0.271043
15	0.6067	0.265185
15	0.6200	0.259459
15	0.6333	0.253862
15	0.6467	0.248390
15	0.6600	0.243042
15	0.6733	0.237814
15	0.6867	0.232703

t_p (mm)	$2a_i/t_p$	S_R/S_R^C
15	0.7000	0.227707
15	0.7133	0.222823
15	0.7267	0.218048
15	0.7400	0.213380
15	0.7533	0.208816
15	0.7667	0.204355

Table A. 7. CSA Report Eq. 28 – t*p* = 20 mm

t_p (mm)	$2a_i/t_p$	S_R/S_R^C
20	0.5000	0.297347
20	0.5100	0.292481
20	0.5200	0.287699
20	0.5300	0.282997
20	0.5400	0.278376
20	0.5500	0.273833
20	0.5600	0.269368
20	0.5700	0.264979
20	0.5800	0.260664
20	0.5900	0.256423
20	0.6000	0.252253
20	0.6100	0.248154
20	0.6200	0.244125
20	0.6300	0.240164
20	0.6400	0.236270
20	0.6500	0.232442
20	0.6600	0.228679
20	0.6700	0.224979

t_p (mm)	$2a_i/t_p$	S_R/S_R^C
20	0.6800	0.221342
20	0.6900	0.217766
20	0.7000	0.214250

Table A. 8. CSA Report Eq. 28 – t*p* = 25 mm

t_p (mm)	$2a_i/t_p$	S_R/S_R^C
25	0.5000	0.285239
25	0.5080	0.281499
25	0.5160	0.277809
25	0.5240	0.274170
25	0.5320	0.270581
25	0.5400	0.267041
25	0.5480	0.263548
25	0.5560	0.260104
25	0.5640	0.256707
25	0.5720	0.253355
25	0.5800	0.250050
25	0.5880	0.246789
25	0.5960	0.243573
25	0.6040	0.240401
25	0.6120	0.237271
25	0.6200	0.234184
25	0.6280	0.231139
25	0.6360	0.228136
25	0.6440	0.225173
25	0.6520	0.222250
25	0.6600	0.219367

Table A. 9. LEFM Analytical – t*p* = 10 mm

t_p (mm)	$2a_i/t_p$	S_R/S_R^C
10	0.5000	0.520359
10	0.5200	0.507900
10	0.5600	0.483619
10	0.5800	0.471730
10	0.6000	0.459967
10	0.6200	0.448298
10	0.6400	0.436690
10	0.6600	0.425111
10	0.6800	0.413527
10	0.7000	0.401900
10	0.7200	0.390191
10	0.7400	0.378352
10	0.7600	0.366331
10	0.7800	0.354065
10	0.8000	0.341477
10	0.8200	0.328472
10	0.8400	0.314923
10	0.8600	0.300666
10	0.8800	0.285464
10	0.9000	0.268969

Table A. 10. LEFM Analytical – t*p* = 15 mm

t_p (mm)	$2a_i/t_p$	S_R/S_R^C
15	0.5000	0.474993
15	0.5133	0.467385

t_p (mm)	$2a_i/t_p$	S_R/S_R^C
15	0.5267	0.459874
15	0.5400	0.452449
15	0.5533	0.445101
15	0.5667	0.437821
15	0.5800	0.430600
15	0.5933	0.423430
15	0.6067	0.416303
15	0.6200	0.409209
15	0.6333	0.402141
15	0.6467	0.395089
15	0.6600	0.388044
15	0.6733	0.380997
15	0.6867	0.373938
15	0.7000	0.366857
15	0.7133	0.359742
15	0.7267	0.352581
15	0.7400	0.345361
15	0.7533	0.338068
15	0.7667	0.330685

Table A. 11. LEFM Analytical – t*p* = 20 mm

t_p (mm)	$2a_i/t_p$	S_R/S_R^C
20	0.5000	0.445205
20	0.5100	0.439848
20	0.5200	0.434543
20	0.5300	0.429286
20	0.5400	0.424074

t_p (mm)	$2a_i/t_p$	S_R/S_R^C
20	0.5500	0.418902
20	0.5600	0.413767
20	0.5700	0.408666
20	0.5800	0.403595
20	0.5900	0.398551
20	0.6000	0.393530
20	0.6100	0.388529
20	0.6200	0.383545
20	0.6300	0.378574
20	0.6400	0.373614
20	0.6500	0.368659
20	0.6600	0.363707
20	0.6700	0.358754
20	0.6800	0.353796
20	0.6900	0.348829
20	0.7000	0.343848

Table A. 12. LEFM Analytical – t*p* = 25 mm

t_p (mm)	$2a_i/t_p$	S_R/S_R^C
25	0.5000	0.423387
25	0.5080	0.419307
25	0.5160	0.415259
25	0.5240	0.411242
25	0.5320	0.407253
25	0.5400	0.403291
25	0.5480	0.399353
25	0.5560	0.395438

t_p (mm)	$2a_i/t_p$	S_R/S_R^C
25	0.5640	0.391545
25	0.5720	0.387671
25	0.5800	0.383815
25	0.5880	0.379976
25	0.5960	0.376151
25	0.6040	0.372339
25	0.6120	0.368539
25	0.6200	0.364748
25	0.6280	0.360966
25	0.6360	0.357189
25	0.6440	0.353418
25	0.6520	0.349649
25	0.6600	0.345882

Table A. 13. LEFM J-integral/K-Based – t*p* = 10 mm

t_p (mm)	$2a_i/t_p$	S_R/S_R^C
10	0.5000	0.392054
10	0.5200	0.375757
10	0.5600	0.344351
10	0.5800	0.328905
10	0.6000	0.313696
10	0.6200	0.298703
10	0.6400	0.283906
10	0.6600	0.269302
10	0.6800	0.254887
10	0.7000	0.240655
10	0.7200	0.226665

t_p (mm)	$2a_i/t_p$	S_R/S_R^C
10	0.7400	0.212888
10	0.7600	0.199318
10	0.7800	0.186026
10	0.8000	0.173081
10	0.8200	0.160593
10	0.8400	0.148710
10	0.8600	0.137679
10	0.8800	0.127829
10	0.9000	0.119506

Table A. 14. LEFM J-integral/K-Based – t*p* = 15 mm

t_p (mm)	$2a_i/t_p$	S_R/S_R^C
15	0.5000	0.366143
15	0.5133	0.356795
15	0.5267	0.347621
15	0.5400	0.338620
15	0.5533	0.329789
15	0.5667	0.321122
15	0.5800	0.312630
15	0.5933	0.304323
15	0.6067	0.296200
15	0.6200	0.288264
15	0.6333	0.280522
15	0.6467	0.272983
15	0.6600	0.265659
15	0.6733	0.258562
15	0.6867	0.251707

t_p (mm)	$2a_i/t_p$	S_R/S_R^C
15	0.7000	0.245110
15	0.7133	0.238787
15	0.7267	0.232759
15	0.7400	0.227043
15	0.7533	0.221657
15	0.7667	0.216621

Table A. 15. LEFM J-integral/K-Based – t*p* = 20 mm

t_p (mm)	$2a_i/t_p$	S_R/S_R^C
20	0.5000	0.350953
20	0.5100	0.344756
20	0.5200	0.338673
20	0.5300	0.332703
20	0.5400	0.326846
20	0.5500	0.321104
20	0.5600	0.315477
20	0.5700	0.309968
20	0.5800	0.304578
20	0.5900	0.299305
20	0.6000	0.294157
20	0.6100	0.289137
20	0.6200	0.284246
20	0.6300	0.279490
20	0.6400	0.274870
20	0.6500	0.270392
20	0.6600	0.266059
20	0.6700	0.261875

t_p (mm)	$2a_i/t_p$	S_R/S_R^C
20	0.6800	0.257845
20	0.6900	0.253973
20	0.7000	0.250264

Table A. 16. LEFM J-integral/K-Based – t*p* = 25 mm

t_p (mm)	$2a_i/t_p$	S_R/S_R^C
25	0.5000	0.339539
25	0.5080	0.335030
25	0.5160	0.330598
25	0.5240	0.326242
25	0.5320	0.321963
25	0.5400	0.317761
25	0.5480	0.313637
25	0.5560	0.309591
25	0.5640	0.305625
25	0.5720	0.301738
25	0.5800	0.297932
25	0.5880	0.294208
25	0.5960	0.290568
25	0.6040	0.287012
25	0.6120	0.283541
25	0.6200	0.280157
25	0.6280	0.276862
25	0.6360	0.273657
25	0.6440	0.270543
25	0.6520	0.267521
25	0.6600	0.264594

Appendix B

Database of Fatigue Test Data for Aluminum Welds

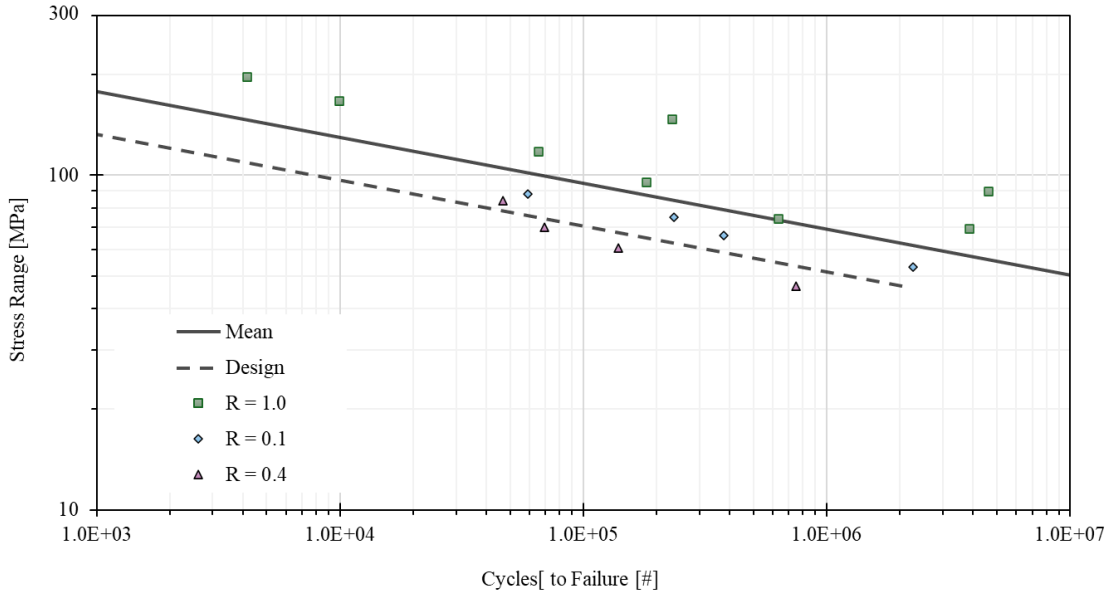

Figure A.1. S-N database for aluminum transverse stiffener welds [3].

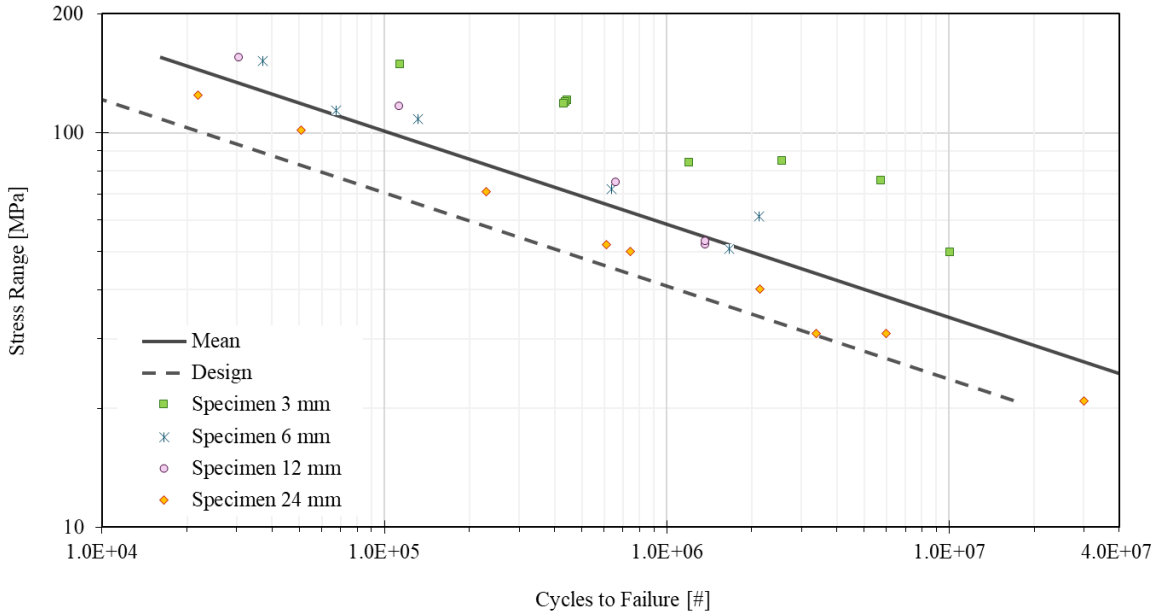

Figure A.2. S-N database for aluminum transverse stiffener welds [57].

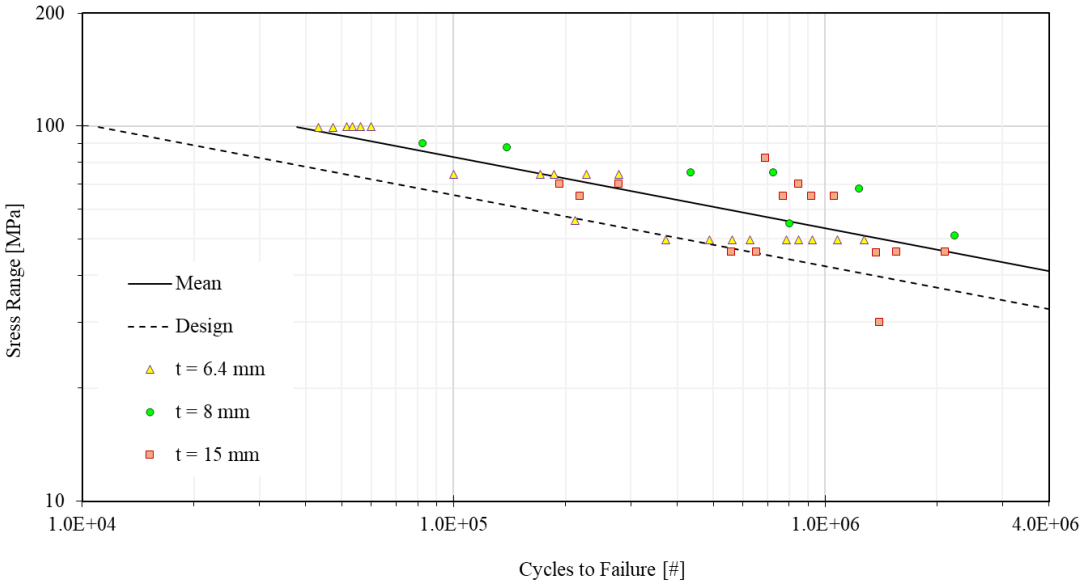

Figure A.3. S-N database for aluminum transverse stiffener welds [1].

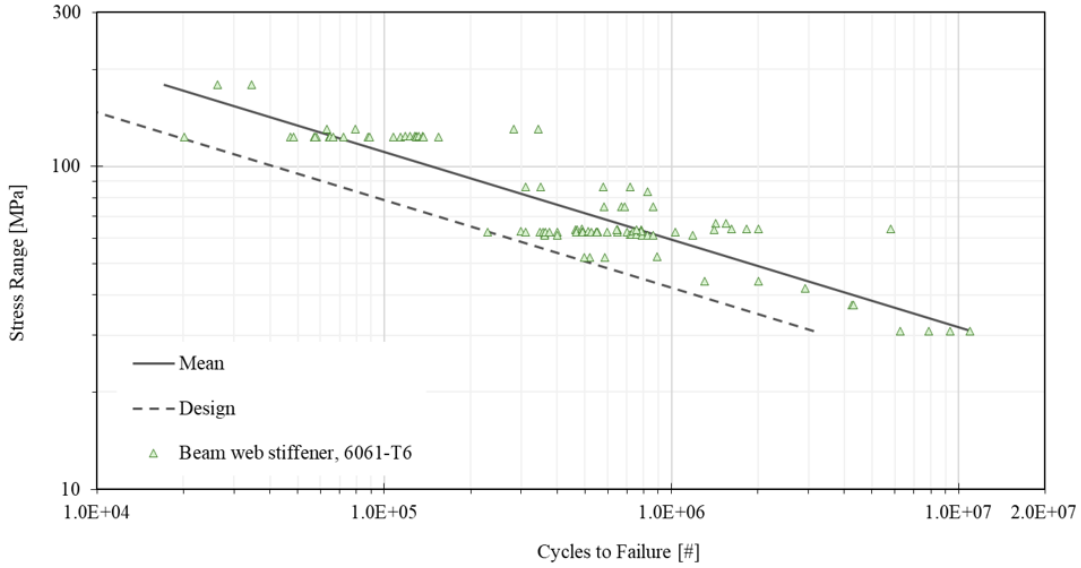

Figure A.4. S-N database for aluminum transverse stiffener welds [16].

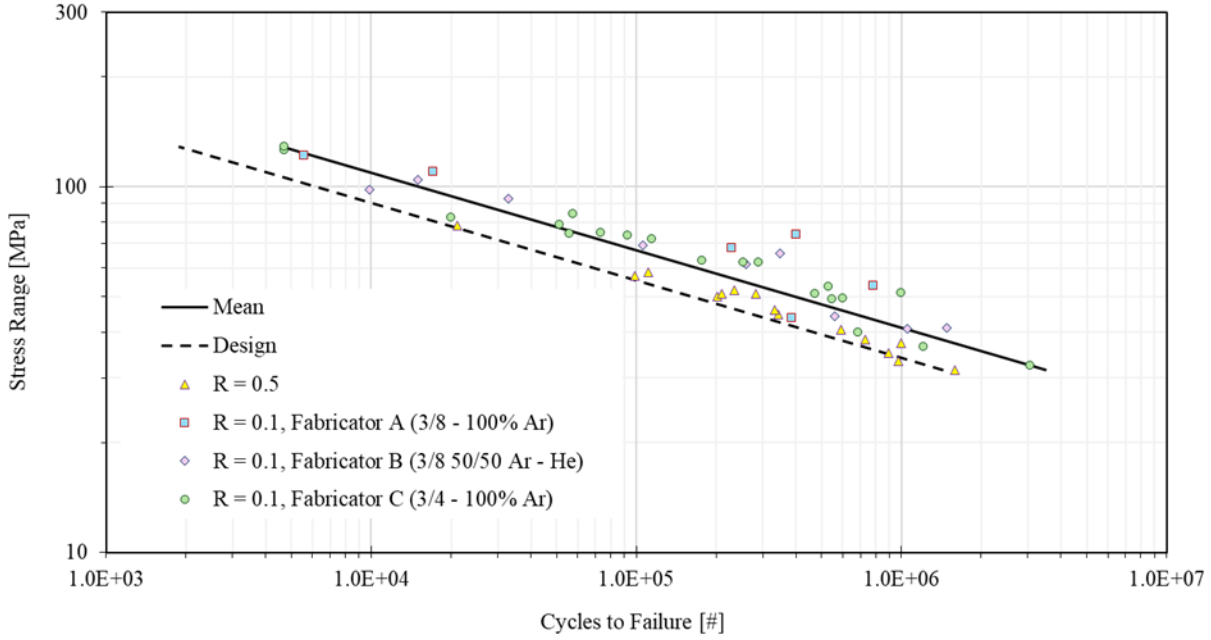

Figure A.5. S-N database for partial joint penetration in aluminum structures [20].

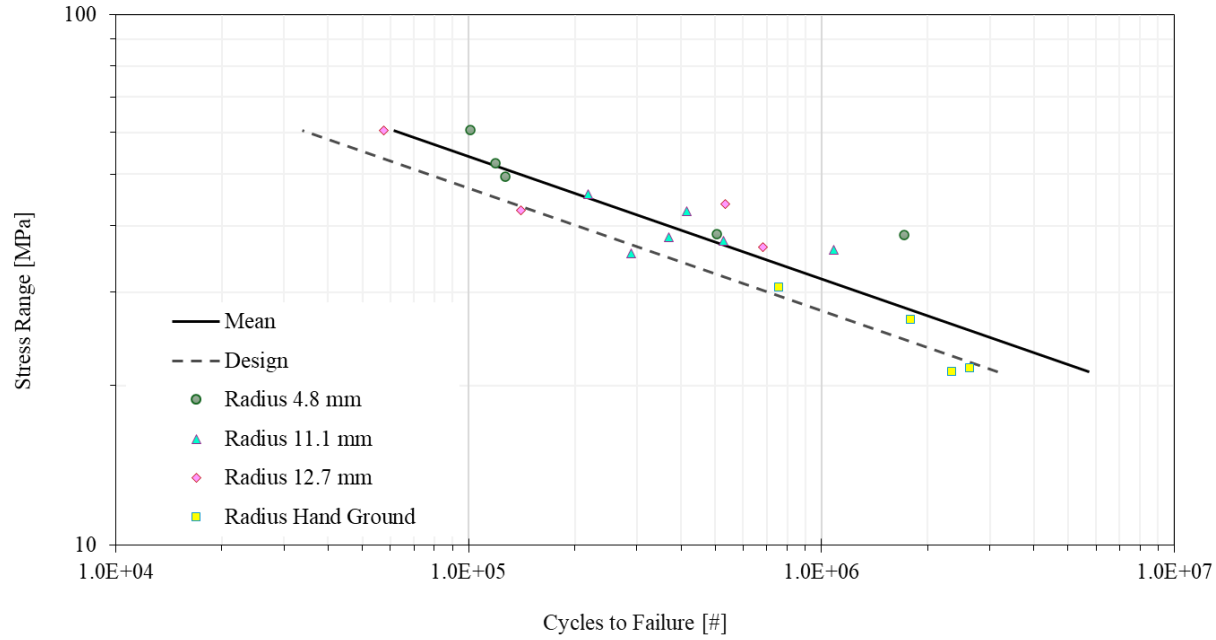

Figure A.6. S-N database for flare-bevel-groove welds in aluminum structures [22].

Table A.1. S-N database for aluminum transverse stiffener welds [3].

Source	Δσ (MPa)	*N* (cycles)	*R* (-)	*t* (mm)	Alloy
[3]	69	3,872,000	-1	9.5	6061-T651
	89	4,631,000			
	118	65,000			
	147	233,000			
	166	10,000			
	197	4,000			
	95	181,000			
	74	633,000			
	53	2,266,000	0.1		
	66	377,000			
	75	236,000			
	88	59,000			
	84	47,000	0.4		
	70	69,000			
	61	139,000			
	47	746,000			

Table A.2. S-N database for partial joint penetration in aluminum structures [20].

Source	Δσ (MPa)	*N* (cycles)	*R* (-)	*t* (mm)	Alloy
[20]	51	283, 000	0.5	9.5	6061-T6
	33	975,000			
	35	891,000			
	38	730,000			
	45	343,000			
	59	111,000			
	37	993,000			
	32	1,592,000			
	41	592,000			
	50	203,000			
	78	21,000			
	46	333,000			
	51	210,000			
	52	233,000			
	57	99,000			
	68	228,000	0.1		
	110	17,000			
	44	386,000			
	74	400,000			
	54	786,000			
	121	6,000			
	98	10,000		19	
	69	106,000			
	41	1,053,000			
	93	33,000			
	66	348,000			
	44	562,000			
	105	15,000			
	62	260,000			
	41	1,477,000			

Table A.2 (continued). S-N database for partial joint penetration in aluminum structures [20].

Source	Δσ (MPa)	*N* (cycles)	*R* (-)	*t* (mm)	Alloy
[20]	84	58,000	0.1	19	6061-T6
	33	305,7000			
	74	93,000			
	63	177,000			
	50	602,000			
	75	56,000			
	75	74,000			
	62	289,000			
	82	20,000			
	51	999,000			
	49	548,000			
	40	687,000			
	62	253,000			
	51	470,000			
	126	5,000			
	72	115,000			
	53	532,000			
	129	5,000			
	37	1,208,000			
	79	51,000			

Table A.3. S-N database for flare-bevel-groove welds in aluminum structures [22].

Source	Δσ (MPa)	*N* (cycles)	Radius (mm)	*R* (-)	*t* (mm)	Alloy
[22]	39	1,715,000	4.8	0.1	6.4	6061-T6
	61	101,000				
	53	119,000				
	50	127,000				
	39	504,000				
	21	2,349,000	Hand Ground (HG)		12.7	
	27	1,789,000				
	22	2,644,000				
	31	759,000				
	38	370,000	11.1		6.4	
	35	289,000				
	37	527,000				
	36	1,082,000				
	46	218,000				
	43	416,000				
	43	141,000	12.7		12.7	
	44	533,000				
	60	57,000				
	37	684,000				